Diss. ETH No. 22429

# Preterm rupture of fetal membranes: mechanical characterization and repair strategies

A thesis submitted to attain the degree of
DOCTOR OF SCIENCE of ETH Zurich

(Dr. sc. ETH Zurich)

presented by

MICHELA PERRINI

MSc in Biomedical Engineering, Politecnico di Torino

born on 11.10.1986

citizen of Italy

accepted on the recommendation of

Prof. Dr. Edoardo Mazza, examiner
Dr. Martin Ehrbar, co-examiner
Prof. Dr. Nicole Ochsenbein-Kölble, co-examiner

2015

*Per mamma*

# Abstract

The fetal membrane is a bilayer tissue surrounding and protecting the fetus during pregnancy. The two main layers, amnion and chorion, are connected by means of an interface layer – referred to as “spongy” – and both composed of an epithelium, a basement membrane and a stromal layer. The membrane is a tissue programmed to rupture at term. It is characterized by morphological changes arising in the area overlying the cervix – referred to as “zone of altered morphology” (ZAM) – as a consequence of a remodeling process preparatory for delivery. The spontaneous preterm premature rupture of the membrane (PPROM) represents a serious complication associated with 30% to 40% of all preterm birth and related to high mortality and morbidity of the newborn. Moreover, the fetal membrane lacks of a healing response, thus leading to a high risk of iatrogenic preterm premature rupture of the membrane (iPPROM) after interventions in the uterine cavity for the diagnosis or treatment of severe fetal pathologies.

This thesis focuses on the experimental evaluation of repeated stretching of the membrane as a risk factor for PPROM and the qualification of repair strategies to prevent iPPROM.

Physiologically relevant testing protocols have been developed in order to assess the effect of repeated loading on the mechanical and microstructural response of the membrane, the latter observed in a multiphoton microscope. The intact membrane and amnion were tested under inflation – which closely reproduces the in vivo multiaxial loading state of the tissue over the cervix – as well as in the uniaxial configuration, representative of the stress state in the vicinity of defects. Cyclic inflation leads to stiffening and reduction of toughness in the intact membrane, associated with alterations of collagen structures in the spongy and fibroblast layer, as well as increased thickness of the amniotic stromal layer. Similarly, the amnion is characterized by high energy dissipation and stiffening when cyclically stretched under biaxial tension, associated with strong but reversible thickness changes. These alterations are comparable with morphological changes characterizing the ZAM, thus suggesting that repeated mechanical loading might initiate a weakening process leading to PPROM when experienced prior to term. Ex vivo and in situ cyclic tests under uniaxial tension showed significant volume reduction due to low energy, unrecoverable in-plane phenomena, i.e. fiber reorientation and lateral contraction. The observed mechanisms might contribute to the toughening of fetal membrane when exposed to repeated loading, thus preventing crack growth and propagation.

Two synthetic catechol-modified glues, cT and cPEG, have been compared and qualified as possible sealants for fetal membrane repair and iPPROM prevention. Defective fetal membranes were repaired with a glue patch with a defined shape. Tests were performed under physiologically relevant environmental and mechanical conditions in order to investigate the sealing performance of the glues, in particular under fast loading and repeated stretching. Both glues seal the fetal membrane during inflation, resisting pressures higher than the intra-uterine baseline, but showing different failure processes. cT withstands high deformations and pressures without breaking, but loses adhesion under shear stresses, thus leading to the rupture of amnion. On the contrary, cPEG ruptures in the defect at a critical level of pressure. The performance of the sealants deteriorates under repeated mechanical load, representative of contractions, as well as under fast and acute deformation of the membrane, representative of impacts. Finite element simulations of inflated synthetic membranes (intact, defective and sealed) were performed in order to compare the performance of cT and cPEG under large deformations, when tightly adherent to the substrate. Sealing with a glue plug leads to a concentration of stresses at the border of the plug, both in the membrane and at the interface, and does not restore the distribution of stresses present in the intact substrate. Overall, cT leads to lower stresses in the substrate and at the interface plug-membrane compared to cPEG. In order to take advantage of the high deformability and toughness of the cT glue in the repair of fetal membranes, the adhesion of the sealant and the shape of the plug should be optimized, thus reducing shear stresses at the interface and matching the deformation behavior of the membrane.

A setup for dynamic culture of amniotic mesenchymal cells (AMCs) was developed in order to test an in vitro amnion model under physiologically relevant biological and mechanical cues, and eventually study fetal membrane healing. Stretching plays an important role in the remodeling of collagen during growth and distention of the membrane, and therefore mechanical stimuli might promote the production of native extracellular matrix components in AMCs, fostering the healing process. A first in vitro amnion model – consisting of AMCs embedded in a polyethylene(glycol)-based (PEG-based) cell-instructive matrix – was developed and preliminary experiments were performed in order to assess the robustness of the model under repeated stretching at different levels of deformation.

This thesis contributes to the research on the human fetal membrane and its premature rupture, providing insights into the effect of repeated mechanical loading on the mechanical and microstructural integrity of the tissue, as well as developing tools for the qualification of repair strategies for iPPROM prevention.

# Riassunto

La membrane fetale è un sottile tessuto a due strati che circonda e protegge il feto durante la gravidanza. I due strati principali, amnios e corion, sono attaccati per mezzo di un interfaccia – definita "strato spugnoso" – e sono entrambi composti da epitelio, membrane basale e stroma. La membrana è programmata per rompersi al termine della gestazione. Il tessuto è caratterizzato dall'insorgenza di cambiamenti morfologici, che si manifestano soprattutto nella zona sovrastante la cervice – detta "zona con morfologia alterata" (ZAM) – come conseguenza di un processo di rimodellamento propedeutico al parto. La rottura pretermine e prematura della membrana (PPROM) è una grave complicazione associata con il 30%-40% delle nascite premature e causa di elevata mortalità nei neonati. In oltre, la mancanza di un processo di guarigione intrinseco nel tessuto determina un elevato rischio di rottura iatrogenica pretermine e prematura della membrana (iPPROM) a seguito di interventi nella cavità uterina per la diagnosi e il trattamento di gravi patologie fetali.

Questa tesi si concentra sulla valutazione del carico ciclico come fattore di rischio per PPROM e la qualificazione di strategie per riparare la membrana e prevenire iPPROM.

Protocolli sperimentali, rappresentativi delle condizioni fisiologiche della membrane, sono stati sviluppati per valutare l'effetto del carico ciclico sulla risposta meccanica e microstrutturale della membrane, quest'ultima osservata in un microscopio a multifotoni. La membrana intatta e l'amnios sono stati testati durante gonfiaggio (inflation) – che meglio rappresenta lo stato di carico multiassiale del tessuto sovrastante la cervice – e in configurazione uniassiale, rappresentativa dello stato di stress intorno a difetti. Il gonfiaggio ciclico determina un aumento di rigidezza e riduzione di tenacità della membrana intatta, associati con alterazioni nelle strutture di collagene dello strato spugnoso e aumento di spessore dello stroma amniotico. Analogamente, l'amnios è caratterizzato da elevata dissipazione di energia, aumento di rigidezza e riduzione reversibile dello spessore quando deformato ripetutamente sotto tensione biassiale. Queste alterazioni risultano simili ai cambiamenti morfologici visibili nella ZAM, confermando che il carico ripetuto della membrana potrebbe determinare l'indebolimento del tessuto e PPROM. Test ciclici uniassiali dell'amnios, sia ex vivo che in situ, hanno mostrato una significativa riduzione del volume dovuta a fenomeni non reversibili nel piano della membrana, i.e. orientamento delle fibre

e contrazione laterale. Questi meccanismi potrebbero contribuire all'aumento di tenacità della membrana in prossimità di defetti, prevenendo la crescita e propagazione di cricche.

Due colle sintetiche catecolo-modificate, cT e cPEG, sono state qualificate come materiali per riparare la membrana fetale e prevenire iPPROM. Campioni di membrane riparati con una placca di colla sono stati testati per valutare la prestazione di cT e cPEG, in particolare durante carico veloce e ripetuto. Durante inflation, entrambe le colle resistono pressioni più alte della pressione intrauterina, ma determinano un diverso processo di rottura della membrana. cT resiste alla deformazione senza rompersi, ma perde adesione favorendo la rottura dell'amnios. Al contrario, la placca di cPEG si rompe nel difetto al raggiungimento della pressione critica. La prestazione delle colle peggiora durante carico ciclico, rappresentativo delle contrazioni, e carico veloce, rappresentativo di impatti. Simulazioni agli elementi finiti di membrane sintetiche inflesse (intatte, con difetto e riparate) sono state realizzate per confrontare l'efficacia di cT e cPEG sotto grandi deformazioni, quando saldamente aderenti al substrato. L'applicazione di una placca di colla provoca concentrazione di stress al bordo della placca stessa, sia nella membrana che all'interfaccia, e non ripristina la distribuzione di stress presente nel substrato intatto. In generale, cT determina stress più bassi nel substrato e all'interfaccia membrana-placca rispetto a cPEG. Per poter trarre vantaggio dall'elevata deformabilità e tenacità di cT nel riparare la membrana fetale, l'adesione della colla e la forma della placca dovrebbero essere ottimizzate, in modo tale da ridurre la concentrazione di stress all'interfaccia e seguire la deformazione della membrana.

Un setup per la cultura dinamica di cellule amniotiche mesenchimali (AMCs) è stato sviluppato per testare un modello in vitro dell'amnios in presenza di stimoli biologici e meccanici fisiologicamente rilevanti. La deformazione della membrana gioca un ruolo importante nel rimodellamento del collagene durante la gravidanza, quindi l'applicazione di stimoli meccanici potrebbe promuovere la produzione di matrice extracellulare in AMCs e favorire il processo di riparazione. Un primo modello in vitro dell'amnios – costituito da AMCs incapsulate in una matrice di polietilenglicole (PEG) – è stato sviluppato. Esperimenti preliminari sono stati condotti per valutare la robustezza del modello durante carico ripetuto a diversi livelli di deformazione.

Questa tesi contribuisce alla ricerca sulla membrane fetale e la sua rottura prematura, fornendo una migliore comprensione dell'effetto di carichi ripetuti sull'integrità meccanica e strutturale del tessuto e sviluppando strumenti per la qualificazione di strategie per riparare la membrana e prevenire iPPROM.

# Contents

**Chapter 1 Introduction ..... 1**

**1.1 Formation and function of the fetal membrane ..... 2**

**1.2 Morphology of fetal membrane ..... 3**

1.2.1 Normal morphology ..... 3

1.2.2 Altered morphology ..... 5

**1.3 Preterm rupture of the fetal membrane ..... 6**

1.3.1 Preterm premature rupture of fetal membrane ..... 6

1.3.2 Iatrogenic preterm premature rupture of fetal membrane and repair strategies ..... 7

**1.4 Mechanical characterization of fetal membrane ..... 8**

**1.5 Objectives and structure of the thesis ..... 10**

**Chapter 2 Physiologically relevant investigation of the mechanical and microstructural response of fetal membrane under repeated loading ..... 11**

**2.1 Introduction ..... 12**

**2.2 Towards a physiologically relevant mechanical test ..... 13**

2.2.1 Physiology of uterine contractions ..... 13

2.2.2 Characteristics of contractions ..... 14

2.2.3 Mechanical tests ..... 15

2.2.4 Inflation device ..... 16

2.2.5 Fetal membrane procurement ..... 17

**2.3 Methods: mechanical study ..... 19**

2.3.1 Samples preparation ..... 19

2.3.2 Experimental protocol ..... 19

2.3.3 Post processing ..... 20

2.3.4 Statistical analysis....23
**2.4 Methods: microstructural study....23**
2.4.1 Samples preparation....23
2.4.2 Cyclic inflation tests....24
2.4.3 In-situ experiments....24
2.4.4 Images processing and parameters extraction....25
2.4.5 Statistical analysis....26
**2.5 Results: mechanical study....26**
2.5.1 Effect of repeated loading on mechanical parameters....26
2.5.2 Cyclic behavior....28
2.5.3 Rupture....29
**2.6 Results: microstructural study....29**
2.6.1 Morphology of fetal membrane....29
2.6.2 Microstructural alterations....30
2.6.3 Microstructure under deformation....32
**2.7 Discussion....33**
**2.8 Conclusion....36**

**Chapter 3 Mechanical and microstructural investigation of the cyclic behavior of human amnion....37**
**3.1 Introduction....38**
**3.2 Methods: mechanical experiments....39**
3.2.1 Sample procurement and preparation....40
3.2.2 Inflation tests....40
3.2.3 Uniaxial tension tests....42
3.2.4 Post processing....42
**3.3 Methods: in situ experiments....45**
3.3.1 Inflation tests....46

3.3.2 Uniaxial tension tests ..... 46
3.3.3 Post processing ..... 47
**3.4 Results ..... 48**
3.4.1 Mechanical experiments ..... 48
3.4.2 In situ experiments ..... 52
**3.5 Discussion ..... 55**
**3.6 Conclusion ..... 58**

**Chapter 4 Towards sealing of fetal membrane ..... 59**
**4.1 Introduction ..... 60**
**4.2 Methods: experiments ..... 61**
4.2.1 Glue preparation and application ..... 61
4.2.2 Inflation device ..... 62
4.2.3 Fetal membrane ..... 63
4.2.4 VHB ..... 65
**4.3 Methods: simulations ..... 66**
**4.4 Results ..... 69**
4.4.1 Sealing of fetal membrane ..... 69
4.4.2 Sealing of VHB ..... 70
4.4.3 Simulations ..... 71
**4.5 Discussion ..... 74**
**4.6 Conclusion ..... 78**

**Chapter 5 Development of an experimental setup for dynamic cell culture ..... 79**
**5.1 Introduction ..... 80**
**5.2 Experimental setup ..... 81**
5.2.1 Requirements ..... 81
5.2.2 Components ..... 82

5.2.3 Validation tests....86

**5.3 Dynamic culture of the in vitro amnion model....87**

5.3.1 Membrane selection and characterization....87

5.3.2 Finite element model....88

5.3.3 Sample preparation....89

**5.4 Preliminary experiments and results....93**

5.4.1 Cells isolation....93

5.4.2 Experimental protocol....93

5.4.3 Immunocytochemistry and microscopy....93

5.4.4 Results....94

**5.5 Discussion....95**

**5.6 Conclusion....96**

**Chapter 6 Conclusions and outlook....97**

**6.1 Contributions of the present work....98**

**6.2 Outlook....100**

**6.3 Closure....102**

**Appendix....103**

**Bibliography....109**

**Curriculum vitae....119**

Chapter 1

# Introduction

## 1.1 Formation and function of the fetal membrane

The placenta and fetal membrane are essential for the embryonic development and assume their function early on, transporting nutrients and waste products to and from the fetus. The membrane is also a barrier against infections ascending from the reproductive tract and protects the fetus from physical impacts [1].

The first cell types specified during embryogenesis are indeed committed to form these extraembryonic structures [2]. The inner cell mass, accumulated in the blastocyst five days after the fertilization, gives rise to the embryo, as well as components of the placenta and the fetal membrane. The trophoblast cells at the periphery of the blastocyst only form extraembryonic structures [3]. Soon after implantation of the blastocyst in the uterine wall, the inner cell mass forms the bilaminar embryonic disc composed of hypoblast and epiblast cells (Figure 1.1a). The amniotic epithelium develops from the epiblast and starts to form a thin membrane (the amnion) enclosing the amniotic cavity within 7-8 days after fertilization (Figure 1.1b). The fibroblast layer develops from the extraembryonic mesoderm, which originates from the hypoblast around 2-3 weeks after fertilization (Figure 1.1c) [4]. Thropoblast cells are responsible for the development of the chorionic sac and chorionic villi covering the whole surface of the conceptus (Figure 1.1d). As the gestational sac enlarges, villi in the lower part of the sac are compressed, reducing the blood supply, and begin to degenerate, thus forming the smooth chorion in 6 to 8 weeks (Figure 1.1e) [4]. The villi associated with the decidua basalis increase in number and enlarge, building up the fetal part of the placenta [5]. With the expansion of the amniotic cavity, amnion and chorion loosely fuse together by 17 to 20 weeks of gestation forming the fetal membrane (Figure 1.1f) [4].

The composition and volume of the amniotic fluid change during pregnancy. The volume increases from 20 ml at 10 weeks to 770 ml at 28 weeks, is stable between 29 and 37 weeks and decreases averaging 515 ml at 41 weeks [6]. Similarly, the fetal membrane and the uterine wall grow and distend during pregnancy in order to accommodate the changing volume of amniotic fluid and development of the fetus. During the last trimester, the growth of the membrane slows down as a consequence of the lower collagen synthesis [7, 8]. As a result, the tissue is stretched in the uterine cavity [9-11].

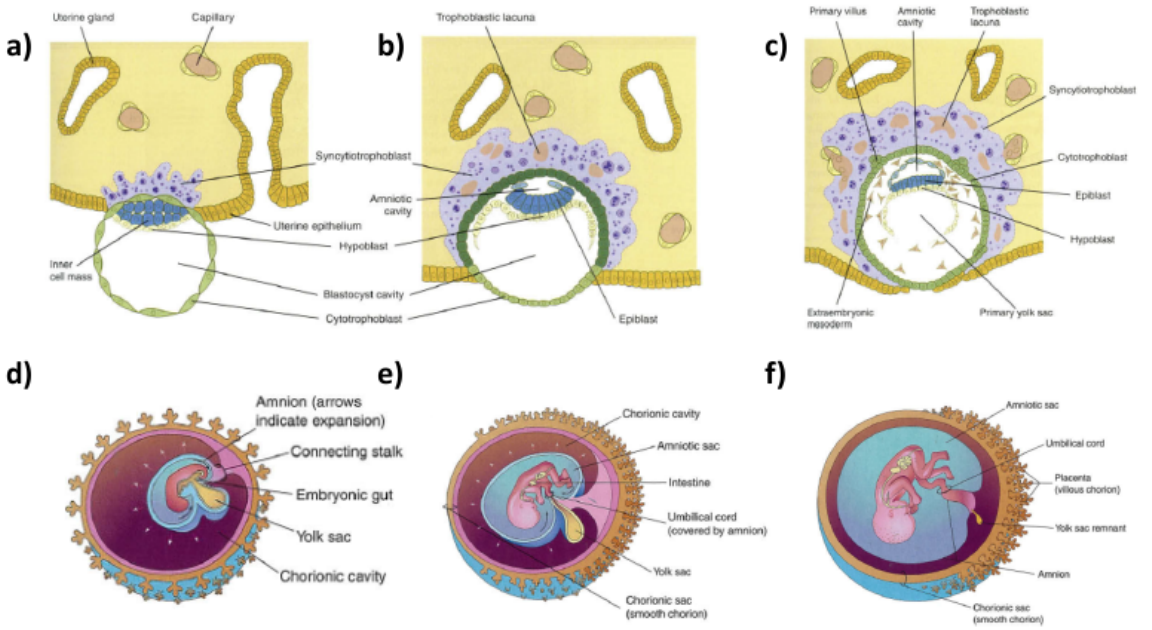


Figure 1.1 Formation of the fetal membrane. a) After implantation, the inner cell mass of the blastocyst forms the bilaminar embryonic disc composed of hypoblast and epiblast cells; b) the amniotic epithelium develops from the epiblast and begins to line the amniotic cavity; c) the fibroblast layer develops from the extraembryonic mesoderm; d) chorionic villi cover the gestational sac at four weeks of gestation; e) the amniotic cavity expands and f) fuses with the chorion at about 17-20 weeks of gestation forming the amniochorionic membrane. Modified and reprinted from Ilancheran et al. (2009) with permission.

## 1.2 Morphology of the fetal membrane

When fully developed, the fetal membrane is a thin (hundreds of µm [12, 13]), avascular tissue enclosing the amniotic fluid and the fetus. The membrane, referred to as “reflected”, is made up of two main layers, the amnion and the chorion, both composed of an epithelium, a basement membrane and a stromal layer [14]. Towards the end of pregnancy, morphological changes arise in the tissue overlying the cervix – referred to as zone of altered morphology (ZAM) – as a consequence of a remodeling process preparatory for delivery [13].

### 1.2.1 Normal morphology

The amnion is the innermost layer, accounts for about 20% of the membrane thickness and consists of five sub-layers [14] (Figure 1.2 and Figure 1.3). The epithelium is in contact with the amniotic fluid and is made of a single layer of epithelial cells [4], which secrete collagen types III and IV and noncollagenenous glycoproteins (laminin, fibronectin, nidogen) forming the basement membrane [1]. Epithelial cells contain an extensive system of intercellular and intracellular

channels making the amnion permeable to fluids and ions [14], and thus a pathway for the regulation of the intramembranous water flow [15]. The basement membrane is a thin layer composed of a network of reticular fibers [14]. The compact layer is almost devoid of cells and mainly consists of a dense network of interstitial collagen (types I and III) organized in parallel bundles and responsible for the mechanical integrity of the amnion [16]. The fibroblast layer is the thickest amniotic layer. It is composed of mesenchymal cells (fibroblasts) embedded in a loose network of collagen types I and III and non-collagenenous glycoproteins [14, 16]. The interface layer (spongy layer) lies between amnion and chorion and originates from the fusion of the two layers (paragraph 1.1). It is made of hydrated proteoglycans and glycoproteins in a mesh of mostly types III and IV collagen [1, 16]. This layer loosely connects the amnion to the chorion, which in turn firmly adheres to the maternal decidua [14].

The chorion consists of three layers resembling a typical epithelial membrane with its polarity towards the decidua [1] (Figure 1.2 and Figure 1.3). The reticular is the thickest layer and consists of a network of different types of collagen, few fibroblasts and proteoglycans [14, 16]. The pseudo-basement membrane is made of fibronectin, laminin and collagen type IV fibers anchoring into the trophoblast [1, 14]. The trophoblast layer consists of 2 to 10 layers of trophoblast cells in contact with the maternal decidua [14]. When the fetal membrane separates from the uterus at delivery, some adherent decidua remains attached to chorion, thus forming the choriodecidua.

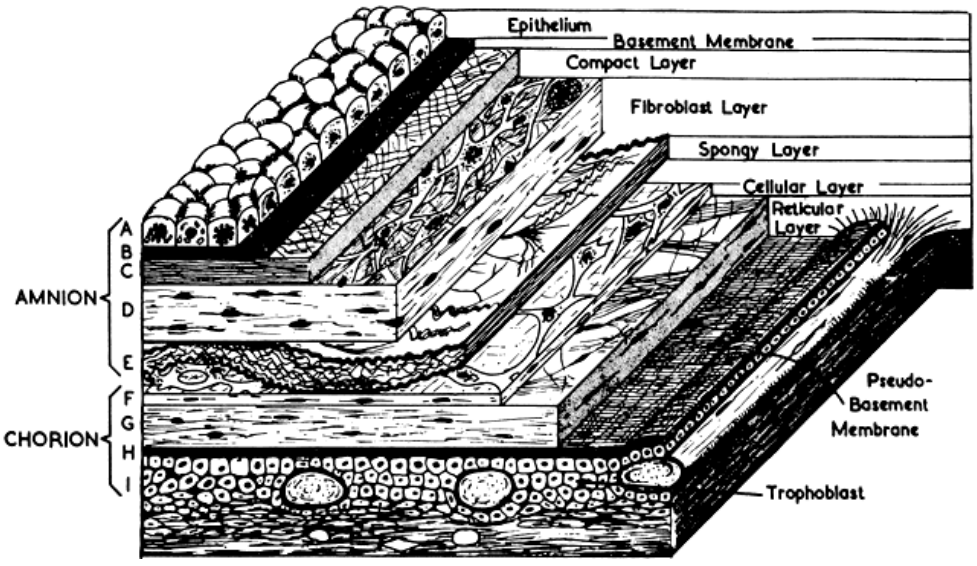


Figure 1.2 Illustration of the layers forming the reflected fetal membrane. Reprinted from Bourne (1962) with permission.

### 1.2.2 Altered morphology

Morphological changes were shown in the part of the membrane overlying the cervix both prior [13] and post labor [17, 18]. The zone of altered morphology is characterized by (i) degradation of the amniotic basement membrane, (ii) swelling and disruption of the amniotic stromal layer, infiltrated by amorphous tissue, (iii) marked thinning of the trophoblast layer and decidua, and (iv) decrease of the total membrane thickness [13, 17-19] (Figure 1.3). After labor, these changes extend over a larger area [18] and a gelatinous substance rich in hyaluronan separates amnion and chorion in the ZAM [20].

These morphological alterations are consistent with extracellular matrix (ECM) degradation, remodeling and cellular apoptosis [21]. Collagen degradation is controlled by matrix metalloproteinases (MMPs). Proforms of MMPs (gelatinase MMP-2 and MMP-9), responsible for the digestion of collagen IV, have been localized in fetal membranes before and after labor [22-24]. The concentration and activity of MMP-9 were shown to be higher in the cervical zone compared to the rest of the membrane before labor [22, 23], whereas both MMPs showed increased activity without regional differences after delivery [23]. MMP-9 is expressed by amniotic epithelial cells, macrophages, trophoblasts and decidual cells [24]. MMPs activation and cellular apoptosis are often correlated. In fact, break-down of the extracellular matrix by MMPs removes structural support for cells, leading to apoptosis, whereas the apoptotic process eliminates cells producing new collagen and activates MMPs [19, 21, 25]. In prelabor fetal membranes, apoptosis of trophoblast cells and PARP cleavage (PolyADP ribose polymerase) were shown to be higher in the ZAM compared to the reflected tissue [22, 26].

This programmed biochemical weakening process of the tissue makes ZAM the site of rupture during labor [19, 21].

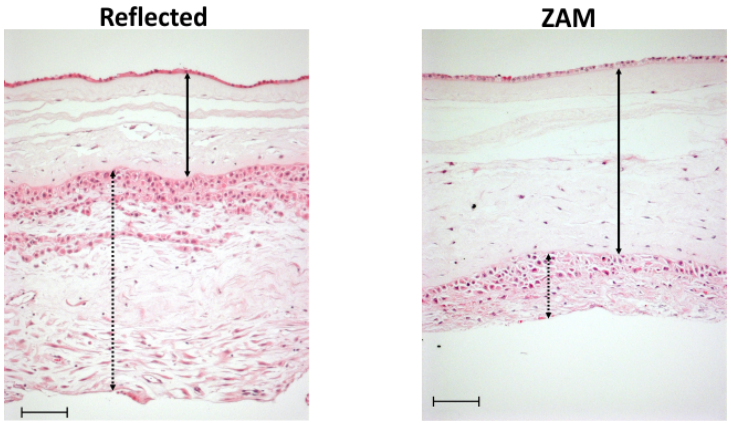


Figure 1.3 Histological sections of reflected and ZAM tissue with hematoxyline and eosine staining (solid arrow: stromal layer, dashed arrow: cellular layer, scale bar: 100 µm).

## 1.3 Preterm rupture of the fetal membrane

The fetal membrane is a tissue programmed to rupture at the end of pregnancy in order to allow the delivery of the fetus. The spontaneous rupture of the membrane (SROM) at term usually occurs during labor. In 8% to 10% of women [1] the premature rupture of the membrane (PROM) occurs and is nearly always followed by the onset of labor [27]. The occurrence of PROM supports the hypothesis that membrane weakening and rupture are not entirely a consequence of physical stresses associated with labor, but they are also strongly related with the biochemically mediated remodeling of the tissue (paragraph 1.2.2) [1].

### 1.3.1 Preterm premature rupture of the fetal membrane

The rupture of fetal membranes prior to 37 completed weeks of gestation is referred to as preterm premature rupture of the membrane (PPROM) [27]. PPROM complicates 1% to 4% of all pregnancies [28] and is associated with 30% to 40% of all preterm births [1], which are the second largest direct cause of deaths in children younger than 5 years [29]. Complications following preterm birth also contribute to lifelong effects on neurodevelopmental functioning, such as increased risk of cerebral palsy, impaired learning, and visual disorders, as well as an increased risk of chronic disease in adulthood [29].

Clinical risk factors for the premature rupture of the fetal membrane (term and preterm) include epidemiological causes (low socioeconomic status, low body mass index, previous preterm birth, infections) and factors with mechanical implications, such as cervical insufficiency and excessive amniotic fluid content (polyhydramnios) [27].

Infections and inflammations of the reproductive tract are among the causes of PPROM [30]. These complications were found to stimulate the production of cell-signaling proteins (cytokines), which govern the activity of matrix-degrading enzymes [1]. Kumar et al. showed that increasing concentrations of TNFα (tumor necrosis factor), IL-1β (interleukin-1 beta) and thrombin cause mechanical and biochemical weakening of the membrane and determine histological changes comparable to those observed in the ZAM [31, 32]. However, the majority of PPROM lack any evidence of inflammation [21].

Over-distention and stretching of the fetal membrane, due to polyhydramnios and early contractions, activate the remodeling of ECM [25], thus increasing the risk of PPROM [1]. El Maradny et al. showed that stretching of the fetal membrane up-regulates the concentration of

MMPs and Interleukin-8, whose concentration in the amniotic fluid usually increases in the third trimester in preparation of labor [33].

*Even though the etiology and sequence of PPROM have not been fully understood yet, these findings suggest that the premature rupture of the membrane, preterm and term, represents an acceleration of the mechanical and biochemical weakening processes leading to the spontaneous rupture during labor.*

### 1.3.2 Iatrogenic preterm premature rupture of the fetal membrane and repair strategies

The preterm rupture of fetal membranes as a consequence of diagnostic or surgical interventions in the uterine cavity is referred to as iatrogenic preterm premature rupture of the membrane (iPPROM) [27]. The incidence of iPPROM varies from 4% to 100% after interventions and largely depends on time of intervention, size of defects and operation techniques [34]. During the last two decades, developments in the fields of fetoscopy and open fetal surgery have resulted in less invasive options for the treatment of numerous pathologies, e.g. twin-to-twin transfusion syndrome (TTTS) and congenital diaphragmatic hernia [34]. However, the high risk of iPPROM severely limits the application of prenatal surgery, its further development and application at earlier gestational ages, when preterm delivery would coincide with fetal death.

iPPROM is a consequence of the formation of local defects in the membrane and lack of healing response in the tissue [28]. Animal studies and a histological investigation of human fetal membranes after fetoscopic interventions showed that the healing potential of the tissue is very limited, probably due to the poor vascularization of the tissue [28]. While the membrane does have the capacity to temporarily seal defects through sliding of amnion over chorion [35], the local or extensive separation of the two layers after surgery (known as chorioamniotic membrane separation) leads to iPPROM in 63% of the cases [36].

In the last decades, attempts have been made to repair the fetal membrane and prevent iPPROM using sealing, healing and plugging techniques [28]. Repair strategies relying on naturally occurring materials, i.e. decellularized human amnion membranes [37, 38], collagen [39] and gelatin sponges [40], fibrin sealants [41], as well as synthetic materials [42-44] have been evaluated in vitro, ex vivo, in animal models, and in patients.

*However, many technical and biological obstacles limit the application in clinical routine and the success of these strategies, e.g. the adhesion of the sealing material in a wet environment, the chemical stability as well as the mechanical compatibility of the sealant and the membrane.*

## 1.4 Mechanical characteristics of the fetal membrane

In the last century, the mechanical behavior of the fetal membrane has been extensively investigated in order to get insight into the mechanisms leading to PPROM. Four types of mechanical test setups, i.e. uniaxial tensile test, puncture test, inflation test and planar biaxial test, were used for the characterization of the tissue, with a main focus on the membrane strength at rupture.

Differences in the rupture strength of the membrane related to the gestational age have been investigated. Some groups found that preterm membranes have a higher rupture strength than term membranes [45-49]. Pressman et al. showed that the tensile strength of the fetal membrane increases up to 20 weeks of gestation, plateaus until 39 weeks and then strongly decreases [49], whereas Oyen et al. found a trend of decreasing force with gestational age, significant for labored membranes [47].

The effect of labor on the mechanical properties of the fetal membrane has been investigated comparing vaginally delivered membranes and tissues from cesarean sections, as well as prematurely and non-prematurely ruptured membranes. Some studies have shown that the process of labor mechanically weakens the membrane [47, 48, 50, 51], in agreement with the increased concentration of hyaluronan and separation of amnion and chorion after labor observed by Meinert et al. [20]. On the contrary, Artal et al. and Polishuk et al. did not find significant differences in the rupture strength of prematurely and non-prematurely ruptured membranes [52, 53].

Overall, inconsistencies in the reported studies might be related to the small number of tested samples and other factors influencing the variability of results, e.g. infections and region of the membrane.

Some works studied the mechanical properties of amnion and chorion separately, showing that amnion is stronger but less deformable than chorion [47, 50, 53-55]. Amnion was also shown to be more affected by the labor process [47, 50]. However, amnion and chorion together are stronger than either layer alone. In fact, Arikat et al. showed that the interaction of the two layers enhances the strength, deformability and toughness of the intact membrane [54].

The ex vivo rupture sequence of the two layers is not consistently documented in literature and strongly depends on the loading configuration and boundary conditions [56]. Some studies state that chorion ruptures first [46, 48, 52, 54], while others show that amnion ruptures first [50, 57, 58]. The separation of amnion and chorion is instead a common feature observed in the rupture process [54, 57, 59].

Only few studies have investigated how local alterations in the microstructure of the fetal membrane influence its mechanical properties. Elkhwad et al. performed puncture tests of tissue from ZAM and reflected membrane. They found that the rupture strength of ZAM is significantly lower compared to the rest of the membrane [22]. However, no differences in the mechanical properties were observed in inflation tests of ZAM and reflected tissue [60]. Bürzle et al. showed that the inconsistency of results might be related to the testing procedure [56]. Using the same puncture setup, the group of J.J. Moore showed that the exposition of fetal membranes to thrombin and cytokine associated with inflammations (TNFα and IL-1β) induces a dose-dependent mechanical and biochemical weakening of the tissue [31, 32].

The time and history-dependent deformation behavior of the fetal membrane has been investigated as well. Lavery et al. characterized the creep and relaxation response of fetal membranes in inflation tests [46, 61], whereas Oyen et al. performed uniaxial and planar biaxial relaxation tests of amnion showing a strain and time-dependent behavior of the material [62, 63]. In a recent study, Mauri et al. analyzed the macroscopic and microstructural time-dependent response of amnion, revealing short-term volume reduction due to water outflow and long-term dissipation without major geometrical changes in the material [64]. Moreover, amnion stiffness, but not rupture strength, was found to increase with increasing strain rate [65].

Toppozada et al. showed that repeated mechanical loading weakens the amnion, in agreement with the clinical observation that the fetal membrane does not rupture during the strongest contraction [66]. Lavery at al. found that repeated inflation reduces the resilience and ability of dissipate stress [51], while Oyen et al. showed a strong energy dissipation in the first loading cycle under uniaxial and biaxial tension [62, 63]. Using a puncture device, Pandey et al. found that cyclic loading paradoxically strengthens the membrane [67].

In a recent study, Buerzle and Mazza investigated the kinematic response of amnion, which showed an extraordinarily large Poisson's ratio and lateral contraction [59].

*In addition to the presence of contradictory results, it is not yet understood how mechanical loading, in particular under repeated stretching, affects the microstructural and mechanical integrity of fetal membrane, thus leading to PPROM.*

## 1.5 Objectives and structure of the thesis

The present thesis contributes to the research on the human fetal membrane and its preterm rupture. The work focuses on the experimental evaluation of repeated stretching of the membrane as a risk factor for PPROM and the qualification of repair strategies to prevent iPPROM. The main objectives of the thesis can be summarized as follows:

**Objective 1** Development of physiologically relevant setups and testing protocols for the characterization of the microstructural and mechanical response of the fetal membrane as well as the evaluation of sealing and healing strategies.
**Objective 2** Investigation of the effect of repeated mechanical loading on the microstructure and mechanical behavior of the fetal membrane and amnion.
**Objective 3** Evaluation of the sealing performance of synthetic glues for fetal membrane repair under physiologically relevant mechanical conditions.

The following chapters provide a comprehensive description of the studies conducted for the fulfillment of the listed objectives.
Chapter 2 describes the development of a physiologically relevant testing protocol representative of the in vivo loading conditions during contractions. The protocol has been used to assess the effect of short-term repeated loading on the rupture and deformation properties of fetal membranes (mechanical study) and long-term cyclic loading on the microstructure of the tissue, imaged in a multiphoton microscope (microstructural study).
Chapter 3 continues with ex vivo and in situ cyclic tests of amnion under biaxial and uniaxial states of tension, providing insights into the microstructural mechanisms determining the history-dependent response of the tissue.
Chapter 4 covers the qualification and comparison of two synthetic glues for fetal membrane repair, with particular focus on the effect of fast loading and repeated stretching on the sealing performance.
Chapter 5 describes the development of an experimental setup for dynamic culture of amniotic cells and an in vitro amnion model, aiming at the study of fetal membrane healing under physiologically relevant biological and mechanical conditions.
Chapter 6 summarizes the main contributions of this thesis and proposes further investigations for a better understanding of fetal membrane preterm rupture and the development of repair strategies.

Chapter 2

# Physiologically relevant investigation of the mechanical and microstructural response of the fetal membrane under repeated loading

## 2.1 Introduction

Towards the end of pregnancy, biochemical and mechanical factors contribute to the weakening of the fetal membrane in order ease its rupture and foster the delivery of the fetus. Stretching of the membrane – associated with distention during fetal growth and contractions – plays an important role in this process, promoting MMPs production [25, 33] and further weakening of the tissue during labor [66]. Over-distention of the membrane and early contractions represent an acceleration of this process before term, thus leading to PPROM [33]. However, it is not clear yet how stretching, in particular under repeated loading, affects the microstructural integrity of the membrane and leads to weakening the tissue.

Some studies investigated the effect of repeated loading on the mechanical properties of the fetal membrane showing contradictory results. Lavery at al. found that repeated inflation at increasing level of pressure stiffens the material and reduces its resilience and ability of dissipate stress [51]. Using a puncture device, Pandey et al. showed an increased stiffness and rupture strength of the fetal membrane already after one cycle, thus concluding that cyclic loading paradoxically strengthen the material [67].

Reflected tissue and ZAM have been imaged so far by using confocal light microscopy [14, 16, 68-70] and electron microscopy [68, 69, 71, 72] in order to identify membrane's sub layers and microstructural changes after labor [17, 18, 20], see paragraph 1.2. However, these techniques do not allow the visualization of the microstructure under deformation due to the fixation of the material.

In this chapter, a mechanical and microstructural study on the effect of repeated loading on the fetal membrane are presented. A physiologically relevant ex vivo mechanical test has been developed in order to reproduce, as closely as possible, in vivo loading conditions. Fetal membranes were tested using a custom-build inflation device, which provides a multiaxial stress state in the tissue. The experimental protocol was designed to be representative of physiological contractions. The effect of cyclic loading on the rupture and deformation properties of the membrane has been investigated comparing cycled and non-cycled samples. Nonlinear optical microscopy, i.e. second harmonic generation (SHG) and multiphoton microscopy, has been used to assess the effect of repeated loading on the microstructure of the membrane. This technique allows the visualization of collagen structures without fixation and staining of the tissue, thus lending itself to investigate the response of extracellular components under deformation [73]. The microstructure of reflected, cycled and ZAM tissues were compared and analyzed in the undeformed state and under uniaxial tension.

The microstructural study has been performed in collaboration with Arabella Mauri (Institute of Mechanical Systems, ETH Zurich), who developed the in situ experiments and performed the data analysis. For completeness, a short description of the image post processing is provided. Parts of paragraphs and figures in this chapter are published in [74] and [75].

## 2.2 Towards a physiologically relevant mechanical test

### 2.2.1 Physiology of uterine contractions

Uterine contractions normally start at the end of pregnancy in order to open the cervix and expel the fetus through the vaginal canal. Contractions are involuntary in nature and initiate in a "pacemaker" region of the uterus, usually in the fundus [76]. With each contraction, there is a progressive shortening of the uterine smooth muscle cells in the upper portion of the uterus, but when relaxation occurs, cells do not return to their original length. The upper active part of the myometrium becomes thicker and pulls up the passive lower segment, which becomes thinner and thinner as labor ensues (Figure 2.1a[1]). This "retraction" process [76] brings about the opening of the ripened cervix in two steps: cervical effacement and cervical dilatation.

The cervical effacement consists in the opening of the internal os as the cervix is gradually pulled up and becomes continues with the lower uterine segment (Figure 2.1b[2]). Then, cervical dilatation occurs when the cervix is pulled back over the fetal head, which is forced against the cervix during contractions (Figure 2.1b[2]). Once the cervix is fully dilated (about 10 cm in diameter), it can no longer act as an impediment to further descent of the fetus.

On the basis of the normal patterns of cervical effacement and dilatation, the labor can be divided into three clinically relevant stages [76]. The first stage of labor is considered to start with the onset of regular contractions that bring about changes in the cervix and ends when the cervix is fully dilated, lasting from 5 to 20 hours. Moreover, Friedman [77] defined two phases in the first stage of labor: the latent phase, which involves cervical effacement and cervical dilatation up to 3 cm, and the active phase, during which the cervix dilates quickly until full dilation is reached. The second stage of labor begins with fully dilated cervix and ends with the delivery of the fetus. The third stage of labor involves the separation and extrusion of the placenta.

Uterine contractions contribute to the spontaneous rupture of the fetal membrane by increasing the intra-uterine pressure in the amniotic cavity. If the membrane is intact at the onset of labor, it usually ruptures during active labor or, more rarely, prior to delivery [76].

[1] Modified from http://midwifethinking.com/2010/08/18/the-effective-labour-contraction/
[2] Modified from http://biobook.nerinxhs.org/bb/systems/reproduction.htm

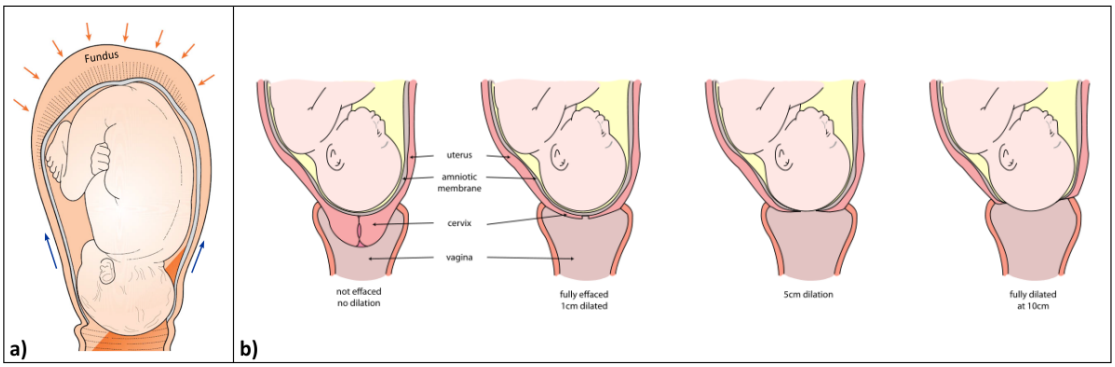


Figure 2.1 Effect of uterine contractions. a) Retraction process: thickening of the upper part of the uterus (orange arrows) and stretching of the lower part (blue arrows); b) cervical effacement and dilatation.

### 2.2.2 Characteristics of contractions

The electrical activity of the myometrium (EMG) is responsible for uterine contractions and is usually monitored during labor by applying electrodes on the abdominal surface of the patient. The intra-uterine pressure can be measured as well by inserting an electronic microtip catheter in the uterine cavity through the vagina (internal tocography). The EMG signal and the tocodynamometry trace show an excellent temporal correspondence [78, 79] and provide important information about the normal and altered uterine activity.

The intra-uterine pressure recorded during contractions has a periodic bell-shape waveform and can be described by using clinically relevant parameters [76, 80] (Figure 2.2):

- amplitude (A): 30 to 60 mmHg;
- baseline pressure (B): 5 to 12 mmHg, without significant changes before and during labor;
- duration (D): 30 to 45 seconds in the latent phase of labor, 60 seconds in the active phase of labor, 90 to 100 seconds in the second stage of labor;
- relaxation time (RT): 2 to 4 minutes in the active phase of labor, 1 to 1.5 minutes in the second stage of labor;
- frequency (number of contractions in 10 minutes): depends on duration and relaxation time.

This simplified description of the intra-uterine pressure and the corresponding values of parameters are representative of a normal, uncomplicated labor and provide information about the magnitude and history of load acting on the fetal membrane in the cervical region after effacement and dilatation.

However, it should be noticed that (i) measurements of intra-uterine pressure reveled marked variability and irregularities in the normal progression of labor among patients [76], (ii) internal tomography provides local measures of pressure which strongly depends on the position of the catheter in the uterine cavity due to the retraction phenomena [76, 78] and (iii) the bell-shape waveform and its parameterization are simplifications of a more complex signal affected by noise and fluctuations of all the parameters in time [80].

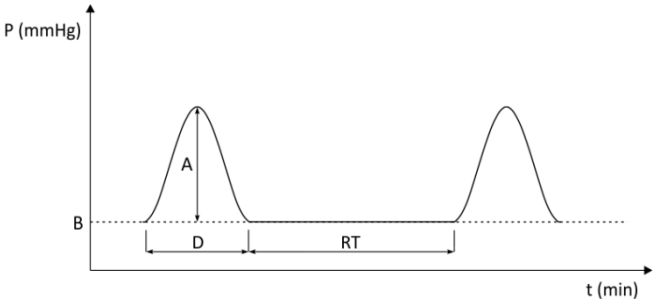


Figure 2.2 Uterine contraction waveform and parameterization.

### 2.2.3 Mechanical tests

Since the second half of the 20$^{th}$ century, the mechanical behavior of the fetal membrane is being studied in order to understand its deformation and fracture properties, as well as investigate clinically relevant conditions (e.g. PPROM, labor, etc.) [27]. Biomechanical tests have been mainly performed using four types of ex vivo mechanical tests:

- uniaxial test (Figure 2.3a): a rectangular strip of material is pulled longitudinally thus creating a uniaxial state of stress, longitudinal elongation and transverse contraction in the central region of the sample;
- planar equibiaxial test (Figure 2.3b): a squared sample is pulled apart on the four sides, thus creating an equibiaxial state of stress, longitudinal and transversal elongation in the central region of the sample;
- inflation test (Figure 2.3c): a circular sample is stretched by fluid pressure acting perpendicular to the surface, thus developing an equibiaxial state of stress, circumferential and radial strains in the central region and a uniaxial state of strain at the boundary;
- puncture test (Figure 2.3d): a circular sample is loaded by a spherical probe, thus developing an equibiaxial state of stress, circumferential and radial strains in the central region.

The fetal membrane is physiologically loaded under a complex multiaxial state of stress due to the geometry of the uterus and the increasing pressure in the uterine cavity during gestation and labor (paragraph 2.2.1). Therefore, the uniaxial test [12, 50, 52, 55] does not provide a physiological testing state. The other presented methodologies provide an equibiaxial stress state for homogeneous membranes, but (i) the planar equibiaxial test [81] presents geometrical and clamping issues to obtain a uniform stress state, (ii) the puncture test [22, 31, 47, 54, 67, 82] is strongly affected by the size of the probe, the friction between the probe and the membrane and the geometry of the clamping [56, 58, 81], and (iii) the inflation test [46, 51, 53, 57, 61, 66, 83, 84] requires large samples and time consuming post processing [21].

Overall, the inflation test better mimics the in vivo loading state of fetal membrane over the dilated cervix and is the best candidate for performing physiologically relevant mechanical tests [22, 81].

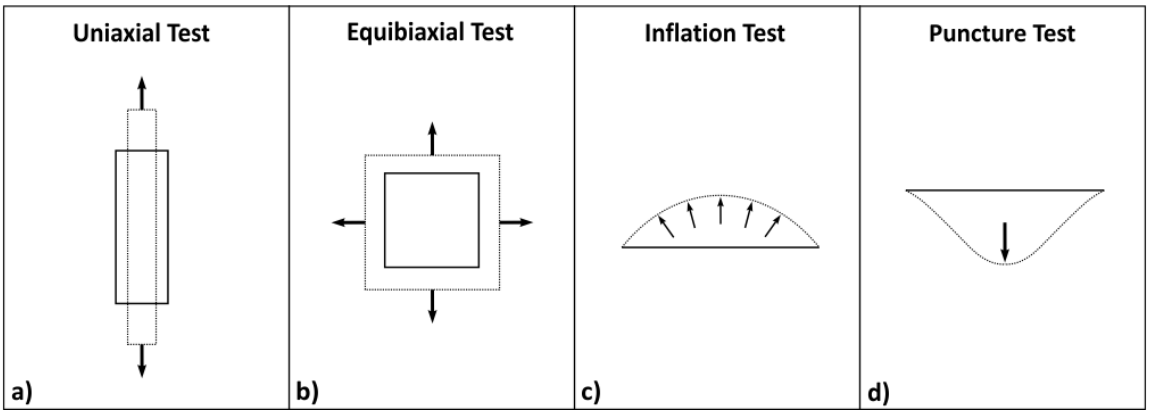


Figure 2.3 Representation of sample's geometry (solid line), loading (arrows) and deformation (dashed lines) in four mechanical tests: a) uniaxial, b) planar equibiaxial, c) inflation, and d) puncture.

### 2.2.4 Inflation device

Fetal membranes were tested using a custom-built inflation device which was previously developed in our laboratory. This device has been used for all the inflation tests performed for this thesis and some components have been modified compared to the first version described in [57] depending on the application. However, the main features characterizing the setup (Figure 2.5) have never been changed (e.g. geometry of the clamping, hardware, etc.).

The key component of the inflation device is an aluminum cylinder with 50 mm inner and 70 mm outer diameter. The sample is positioned on the cylinder (Figure 2.4b), secured with a cover plate with a 50 mm circular opening and clamped by fixing the plate to the frame with six sunk screws (Figure 2.4c). A peristaltic pump (314VBM, Watson-Marlow Ltd, Switzerland) sends fluid into the

cylinder through a plastic tube, while a digital manometer (LEX 1, Keller, Switzerland) measures the pressure in the cylinder. Two CCD cameras (Dragonfly2, resolution 640 x 480, Point Grey, Canada) are respectively positioned above and on one side of the cylinder in order to monitor the deformation of samples during inflation. A red LED backlight (Moritex, MEBL CR7050, Fujifilm AG, Switzerland) is mounted in the frame behind the cylinder in order to improve the contrast in the side pictures (Figure 2.5).

The whole system is controlled by a LabView code (LabView 2008, National Instruments, USA) and the user interface gives access to the parameters necessary for designing experiments and saving data. In particular, inflation tests can be run in:

- manual mode: selecting the voltage (from 0 to 3.8 V), the speed of the pump and the flow rate are defined as input parameters;
- pressure control mode: a pressure profile is designed (e.g. ramp, cyclic tests, etc.), applied and controlled during the experiment by means of PID parameters specific for the tested material.

In both cases, outputs of the experiment are a text file containing the values of measured pressure, top and side pictures saved at the same time intervals.

In order to test fetal membranes under physiologically relevant repeated mechanical loading, a new algorithm to generate a cyclic pressure profile was implemented in Labview. The bell shape of the uterine contraction waveform (Figure 2.2) was approximated with a sinusoidal profile defined in terms of amplitude, baseline, duration, relaxation time and number of cycle (paragraph 2.2.2).

### 2.2.5 Fetal membrane procurement

For all the studies described in this thesis, fetal membranes where collected in the Department of Obstetrics of the University Hospital of Zurich. Patients with single pregnancy were recruited with informed written consent according to the protocol approved by the Ethical Committee of the District of Zurich (study Stv22/2006 and Stv07/07). In order to study the effect of repeated mechanical loading representative of contractions, the selected patients underwent elective cesarean sections between the $38^{th}$ and the $40^{th}$ week of gestation, had no labor contractions prior delivery and preterm rupture of the membrane. Information about pre-labor Braxton-Hicks contractions were not available, but they are normally experienced during gestation as irregular

events not contributing to cervical effacement and dilatation [85]. Moreover, all the patients were negative for diabetes mellitus, streptococcus B, HIV, hepatitis B, chlamydia and cytomegaly.

After the delivery of the baby, the placenta and fetal membrane were taken out of the uterus by gently pulling the umbilical cord, transported to the laboratory and separated by cutting the membrane around the placental border.

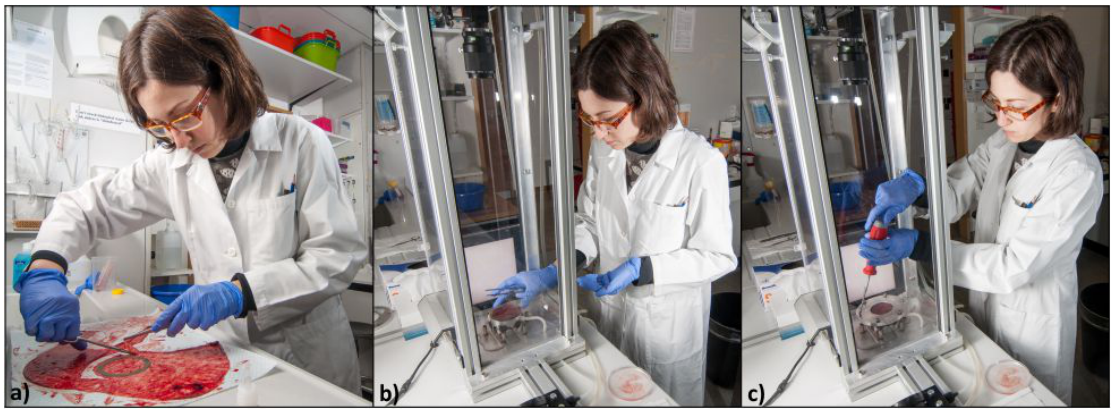


Figure 2.4 Sample preparation and clamping. a) A circular sample is cut with the help of sand paper rings glued on both sides of the membrane; b) the sample is positioned on the cylinder filled with solution; c) the sample is clamped by fixing the cover plate to the frame. Pictures reprinted with the permission of Manfred Maurer.

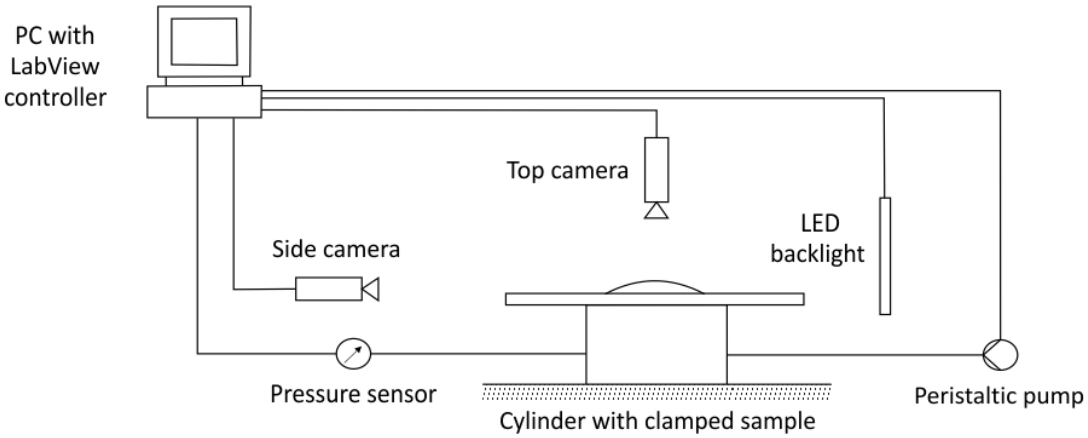


Figure 2.5 Representation of the main components of the inflation device and their connections in the experimental setup.

## 2.3 Methods: mechanical study

### 2.3.1 Sample preparation

Fetal membranes (n=10) were stored in phosphate buffer saline (PBS) solution and tested within 5 hours from the childbirth. Depending on membrane's dimension, from 4 to 8 specimens were cut randomly at least 2 cm far from the placental border. The membrane was spread out on a plastic mat and samples were harvested with the help of sand papers rings (3M wetordry) with ~50 mm inner and 70 mm outer diameter (Figure 2.4a). Rings were glued on both sides of the membrane with the sand against the tissue. The glue (UHU Lasy, Germany) was applied on the outer border and rings were carefully cut with an inner diameter a little bigger than 50 mm in order to avoid the contact of sharp paper tips with the tissue in the inflating area and reduce the friction at the border. Samples were stored at 4°C before preparation and then kept moist with PBS during cutting, gluing and testing.

### 2.3.2 Experimental protocol

Samples from each membrane were divided in two groups and tested with different protocols. The first group of samples was subjected to inflation to burst, with a pressure rate of 0.47 mbar/s. The second group of samples was first cyclically stretched and then inflated to burst (Figure 2.6). Cycles were defined as mentioned in paragraph 2.2.4 and the main parameters were selected to be representative of the first stage of labor (paragraph 2.2.2, Figure 2.6), even though only ten cycles were applied (30 minutes of repeated loading, paragraph 2.2.1). In order to stabilize the pressure control, samples were preloaded at 1 mbar for twenty seconds before each test. The same stabilization phase precedes the inflation to burst after cycles, with smooth transitions between the baseline and the stabilization pressure (Figure 2.6).

Experiments were conducted inflating samples with water and with the amnion facing the fluid. Pressure values, top and side pictures were recorded at 0.5 Hz during cycles and inflation to burst and 0.1 Hz during the relaxation time.

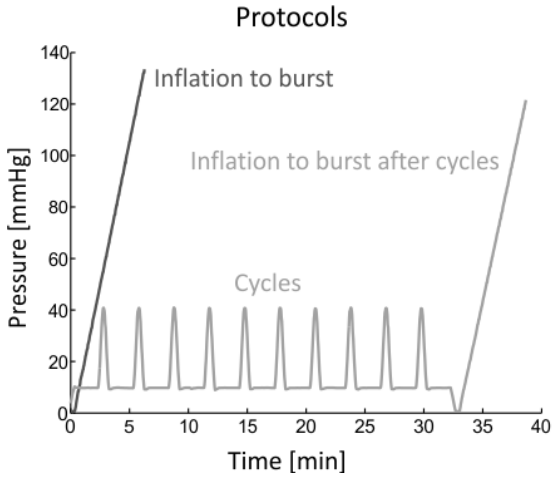


| | |
|---|---|
| Number of cycles | 10 |
| Amplitude [mmHg] | 30 |
| Baseline Pressure [mmHg] | 10 |
| Duration [min] | 1 |
| Relaxation Time [min] | 2 |

Figure 2.6 Mechanical protocols and cycles parameters.

### 2.3.3 Post processing

Experimental data were analyzed as reported in [57] in order to obtain the tension-strain response of the fetal membrane under equibiaxial stress state. As mentioned in paragraph 2.2.3, this loading state is ideally achieved in the center of the sample, thus only the apex region was analyzed. The membrane is considered isotropic in his plane. Being the thickness much smaller than the sample size, a plane stress state is assumed [57]. Moreover, since the fetal membrane is made up of two layer, amnion and chorion, with different mechanical properties and thicknesses [13, 47, 54], the stress distribution is inhomogeneous along the sample thickness and therefore the stress is not a suitable measure of the mechanical properties of the intact membrane. Accordingly, the membrane was characterized as a structure by calculating the Cauchy tension, see equation 1. A finite element approach was used to calculate the in plane biaxial strain at the apex of the sample since a local strain analysis was not performed. In the end, mechanical parameters were extracted from tension-strain curves corresponding to inflation to burst tests (with and without cycles) in order to evaluate the effect of repeated loading on the mechanical properties of the fetal membrane.

*Image analysis*

Side pictures were analyzed in order to measure the apex displacement and the radius of curvature of the inflated sample. The post processing is based on the detection of sample's profile using the MATLAB [86] function "edge" and the Canny method [87]. The apex displacement was obtained by measuring the highest point of the inflated sample with respect to the surface of the cylinder (2 mm under the clamping ring) (Figure 2.7, left). The radius of curvature (R) was

evaluated by fitting the sample profile with a 3rd order polynomial in a range of ±400 pixels around the axis of the cylinder (Figure 2.7, left).

*Reference configuration*

The clamped samples are initially slack, thus affecting the evaluation of the membrane behavior at the beginning of the test. Therefore, it is necessary to establish when the tissue starts to oppose measurable resistance to the increasing pressure and set a reference configuration repeatable for all the experiments. The criteria proposed by Buerzle at al. was used, i.e. the test begins at the time point when the difference between the total measured pressure $P_{tot}$ and the hydrostatic pressure $P_h$ in the cylinder reaches 1 mbar [57]. This threshold value corresponds to the pressure due to the resistance of the membrane ($P_{tot} - P_h = P_{memb}$) and defines a reference configuration at which the sample is slightly preload and stretched. Then, the pressure (P) and apex displacement (d) are referred to the total pressure and the corresponding apex displacement $D_0$ at the reference configuration, respectively (Figure 2.7, left). For the tests including repeated stretching, cycles and the following inflation to burst were analyzed separately. A new reference configuration was defined at the beginning of the inflation to burst after cycles.

*Tension calculation*

The membrane Cauchy tension $T_C$ [N/mm] was defined by the Laplace's law as

$$T_C = \frac{P \cdot R}{2} \quad (1)$$

where P and R are the current pressure and radius of curvature, respectively.

*Stretch model*

Stretch curves describing the relationship between the in plane stretch λ and the apex displacement (d) were calculated based on FE simulations and parameterized with respect to different values of $D_0$

$$\lambda(d, D_0) = 1 + C_1(D_0)d + C_2(D_0)d^2 + C_3(D_0)d^3 \quad (2)$$

Stretch curves were calculated using three different hyperelastic models in order to investigate the sensitivity of results to the selected model. Rubin-Bodner model [88], Ogden model [89] and a

second invariant reduced polynomial model [90] were implemented considering the membrane as isotropic, incompressible and neglecting dissipative effects. Model parameters are reported in [57].

*Mechanical parameters*

The effect of cyclic loading on the mechanical properties of the fetal membrane has been investigated comparing the behavior of cycled and non-cycled samples during inflation to burst. Specifically, the stretch was converted into strain=λ-1 and five parameters were extracted from the tension-strain curves (Figure 2.7, right):

- critical tension: tension at rupture;
- critical deformation: strain at rupture;
- work to rupture: area underneath the tension-strain curve;
- high strain stiffness: tangent stiffness before rupture defined as the slope of the tension-strain curve between 90% and 100% of the critical deformation;
- medium strain stiffness: slope of the tension-strain curve between 60% and 80% of the critical deformation.

Moreover, the critical apex displacement (CD) and the global apex displacement (GD = $D_0$ + CD) at rupture were analyzed.

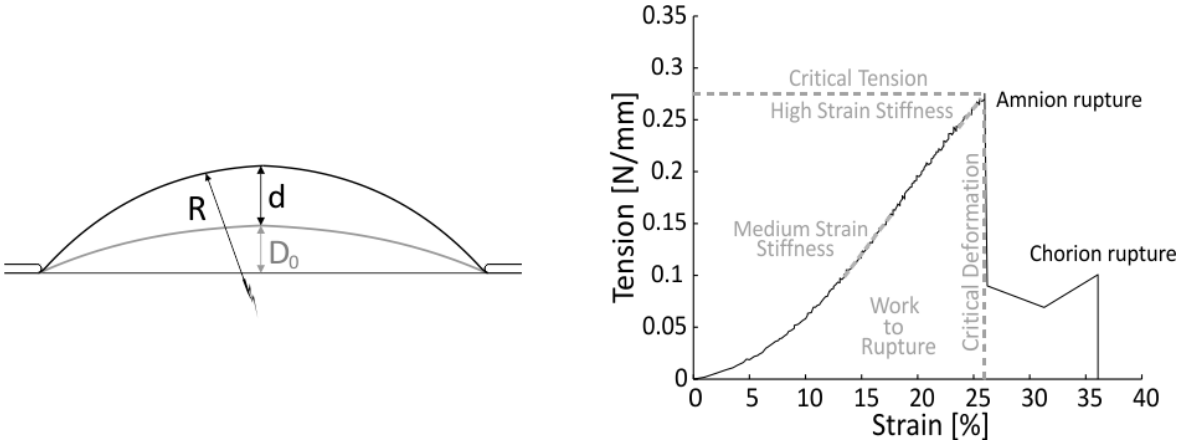


Figure 2.7 Post processing. Left: the apex displacement was obtained by measuring the highest point of the inflated sample with respect to the surface of the cylinder and referred to its value at the reference configuration $D_0$; right: mechanical parameters extracted in a representative tension-strain curve.

*Analysis of the cyclic behavior*

The deformation behavior of the fetal membrane was analyzed and parameters representative of the energy dissipation and irreversible deformation cumulated during cyclic loading were extracted. The hysteresis was calculated as the area between the loading and unloading tension-strain curve for each cycle and normalized with respect to the first cycle. Residual strains at the end of each cycles were extracted and normalized with respect to the maximum strain reached in the first cycle.

*Rupture analysis*

The rupture of the membrane is characterized by a sudden decreased in the pressure value, often corresponding to the failure of one of the two layers, followed by a lower pick of pressure indicating the failure of the second layer [57]. For the extraction of mechanical parameters, the membrane rupture was defined at the time point of the first drop of pressure (tension) (Figure 2.7, right). The rupture sequence was observed during the experiments and samples were carefully inspected to identify the rupture position. Only samples which ruptured far from the clamping were taken into account.

### 2.3.4 Statistical analysis

The statistical analysis was performed in MATLAB [86] in two steps: first the Kolmogorov–Smirnov test [91] was performed for all the described mechanical parameters to confirm their normal distribution; then, parameters were analyzed by two-way analysis of variance (ANOVA) in order to assess the significance of differences between the two groups and the ten membranes ($p < 0.05$ was considered statistically significant).

## 2.4 Methods: microstructural study

### 2.4.1 Sample preparation

Fetal membranes (n=8) were collected as described in paragraph 2.2.5 with the addition of a perioperative procedure to identify the position of ZAM. After the delivery of the baby, the membrane was marked over the internal os with a cotton-tipped applicator dipped in methylene blue and then taken out with the placenta. One sample from the marked area and two samples of reflected membrane were harvested, stored in Ringer's lactate solution (B. Braun, Switzerland),

tested and imaged within 5 hours from the delivery (Figure 2.8a). The Ringer's lactate solution has a composition similar to the amniotic fluid [15] and therefore was more suitable for tests with longer experimental time.

### 2.4.2 Cyclic inflation tests

From each membrane, one sample of reflected tissue was first cyclically stretched in the inflation device and then imaged. Samples were prepared and clamped as shown in paragraph 2.3.1. The tissue was loaded by applying the protocol described in paragraph 2.3.2, with an increased number of cycles (60) and without inflation to burst. The setup was slightly modify in order to keep samples moist during the whole experiment (3 hours): a cylindrical chamber in PMMA (Poly(methyl methacrylate)) was placed on the metal plate, fixed with a heavy ring of steel and filled with 80 ml of Ringer's solution, ensuring the tightness with a silicone ring (Figure 2.8b). After testing, samples were removed from the inflation device and transported in a dish filled with solution to the Center of Microscopy and Image Analysis (University of Zurich).

### 2.4.3 In-situ experiments

Samples from reflected (R), ZAM and cycled tissue (C) were cut in stripes with dimensions 50 mm x 10 mm (corresponding to the central part of the circular inflated samples). Before imaging, specimens were dunked in the nuclear staining DAPI (40 ,6-diamidino-2-phenylindole, dihydrochloride, Invitrogen) for about thirty minutes. DAPI is a DNA-specific probe which can pass through the intact membrane of live and fixed cells and forms a fluorescent complex by attaching the DNA [92]. The fluorescent staining emits in the wavelength range of blue light and it was used to visualize the nuclei in the amniotic epithelium, which defines the beginning of the sample in the transversal direction (Figure 2.9). Specimens were mounted in a custom-built stretching device (placing the amnion upwards) and uniaxially stretched up to 40% of nominal strain by manually moving the two axis (Figure 2.8c). Due to the absence of a force sensor, for this test series the reference configuration was set at the free length of the mounted sample. Tests were performed at room temperature in Ringer's solution and samples were imaged at 0%, 20% and 40% nominal strain with a multiphoton microscope (Fluoview 1000 MPE, Olympus) equipped with a water objective (XLPlan N 25x, NA 1.05) (Figure 2.8c). 3D stacks of the specimens were acquired through the whole thickness every 3 µm (Figure 2.9) using a Ti:Sapphire laser (wavelength 820 nm) with an in-plane resolution of about 363 nm [93]. Second harmonic generation of collagen

was detected with a specific filter (Olympus FV10-MRROPT, BA397-412), whereas the fluorescence of the nuclei (DAPI) was simultaneously detected in a second channel (BA455-490) (Figure 2.9).

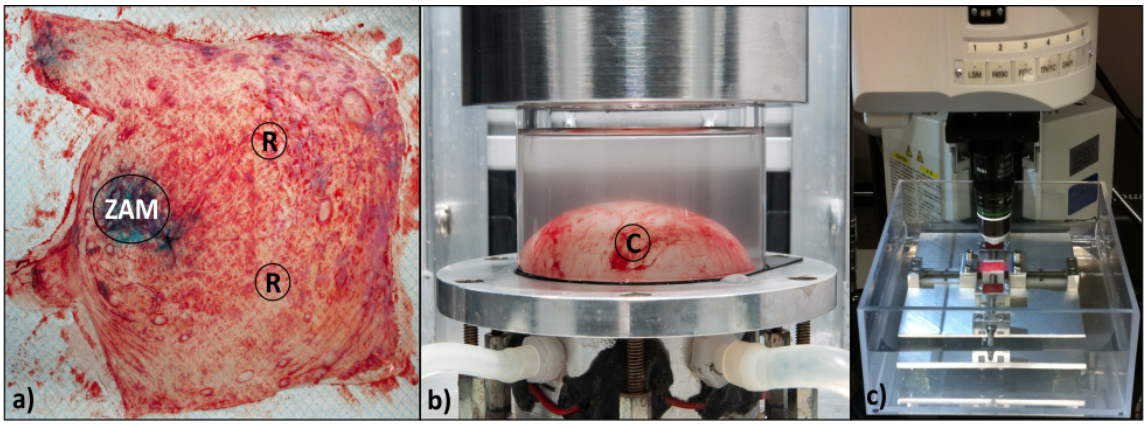


Figure 2.8 Samples selection and testing devices. a) Fetal membrane: samples were harvested from the zone of altered morphology marked during the cesarean section (ZAM) and the reflected membrane (R); b) inflation device with a cyclically inflated sample (C) and chamber filled with Ringer's solution; c) head of the multiphoton microscope and in-situ stretching device with a mounted sample.

### 2.4.4 Images processing and parameters extraction

Image analysis was performed in order to extract some microstructural parameters, i.e. entropy of the spongy layer, thickness of collagenous layers and collagen orientation. 2D images (Figure 2.9) were exported and post processed in MATLAB [86] using custom- written algorithms. Images belonging to different layers were identified by the presence (amniotic epithelium, fibroblast layer, reticular layer) or absence (compact layer, spongy layer) of cellular nuclei.

The image entropy is a statistical measure of randomness based on the intensity histogram, usually used to characterize the texture of images [94]. This parameter was calculated for images of the spongy layer with the MATLAB function "entropy" and it is representative of the damage of collagen structures. The thickness of collagenous layers (compact, fibroblast, spongy and reticular layers) was measured from the intensity of grayscale images in the stack. An intensity factor was defined for each image as the sum of pixels intensity normalized for its dimensions and grey scale. A threshold value of the intensity was set to define the beginning and the end of the sample. The thickness was computed for each sample 16 times over quadratic regions (32 x 32 $mm^2$) and averaged.

The collagen orientation was identified by using the principal direction analysis [95]. Images containing only the SHG signal of collagen were first converted to grayscale and filtered with an

average filter. Successively, the angular orientation for each sub-region was extracted in a 2 x 2 $mm^2$ region and fitted with a truncated normal distribution. The standard deviation ($\sigma$) of this distribution is representative of the dispersion of the collagen. A reduction of $\sigma$ during deformation indicates an increased alignment of collagen structures in the loading direction.

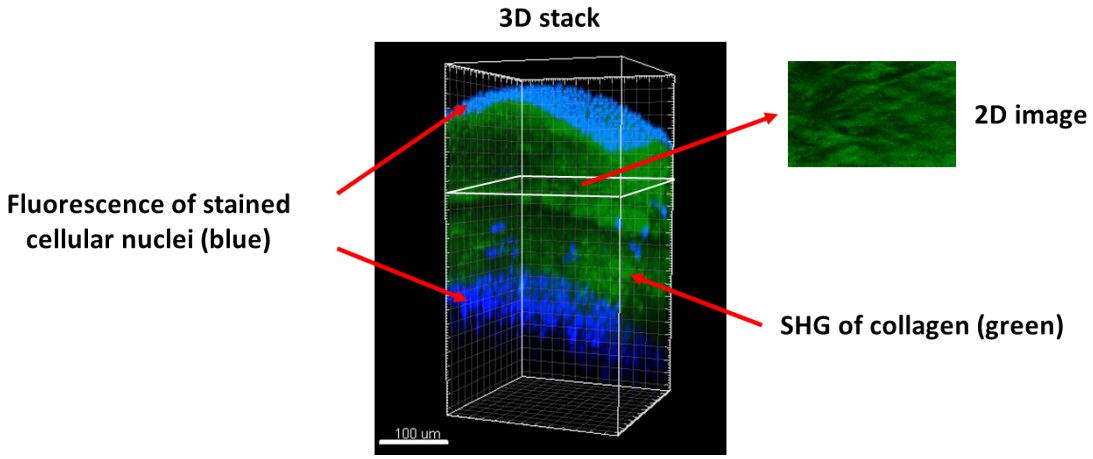


Figure 2.9 3D stack of a representative sample of the fetal membrane showing collagen structures (SHG in green) and stained cellular nuclei (fluorescence in blue). For the post processing, 2D images were exported and analyzed.

### 2.4.5 Statistical analysis

The statistical analysis of the investigated parameters was performed in R: A Language and Environment for Statistical Computing (Open Source Software 2013). A linear mixed effect model was implemented to compare entropy and thickness values of R, ZAM, C samples and values of $\sigma$ at 0%, 20% and 40% of deformation for the three groups ($p < 0.05$ was considered statistically significant). The eight different membranes were included in the model as a random factor which only interacts with the sample's group.

## 2.5 Results: mechanical study

### 2.5.1 Effect of repeated loading on mechanical parameters

On the average, cyclic loading does not affect the critical tension and high strain stiffness, while the medium strain stiffness significantly increases after cycles (Figure 2.10). Critical strain and work to rupture significantly decrease after cycles (Figure 2.10), in association with a higher $D_0$ (cycled: 11.7 ± 2.9 mm, non-cycled: 10.2 ± 2.6 mm) and a significantly lower critical apex

displacement CD (cycled: 6.7 ± 0.9 mm, non-cycled: 8.3 ± 0.9 mm), see Figure 2.11. It should be noted that the global apex displacement at rupture (GD = $D_0$ + CD, Figure 2.11) does not change significantly (cycled: 18.4 ± 2.7 mm, non-cycled: 18.5 ± 2.4 mm), while the critical pressure slightly increases after cyclic loading (cycled: 127.9 ± 29.8 mbar, non-cycled: 138 ± 40.3 mbar).

Differences between the two groups are not influenced by the model formulation used to extract the stretch curves. Even though absolute values of critical deformation change from model to model, the ratio between the mean critical deformation of cycled and non-cycled samples does not change significantly (Rubin-Bodner = 82%; Ogden = 79%; second invariant reduced polynomial = 83%) and differences between the two groups remain significant in all cases.

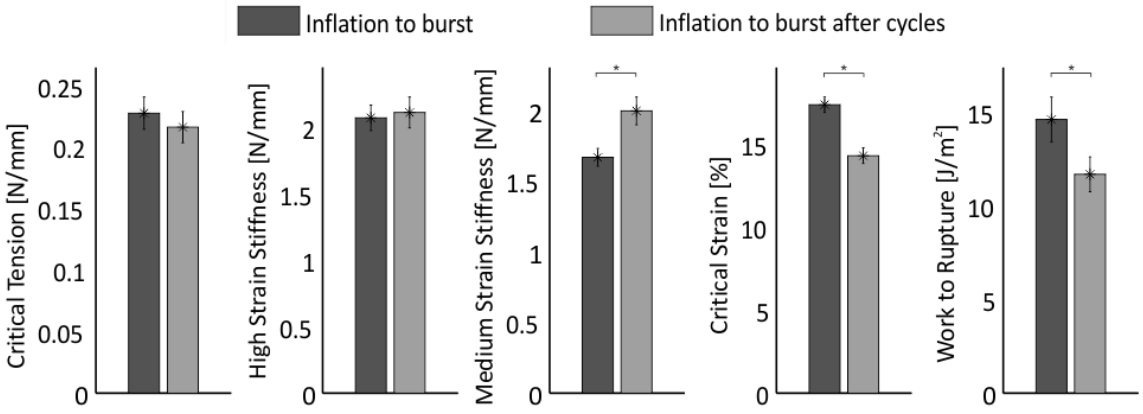


Figure 2.10 Mechanical parameters (calculated using the Rubin-Bodner model). Histograms represent mean ± standard error ($^*p<0.05$) with standard error=standard deviation/√n (inflation to burst: n=26, inflation to burst after cycles n=22).

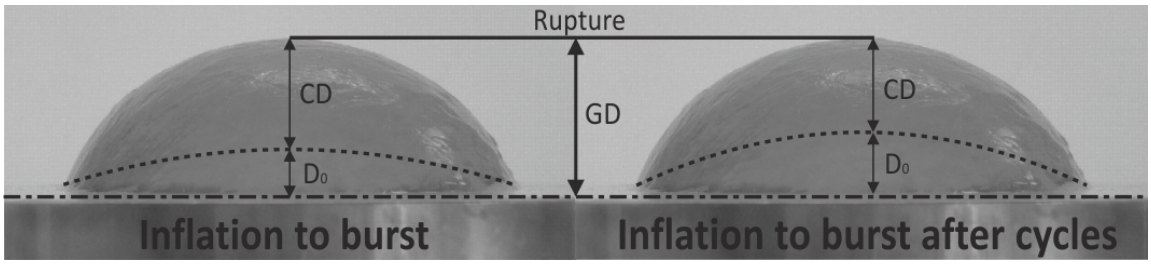


Figure 2.11 Comparison of reference configuration and deformation at rupture between cycled and non-cycled samples. $D_0$: apex displacement at the reference configuration; critical displacement CD: apex displacement from the reference to the rupture configuration; global displacement GD: apex displacement from the undeformed to the rupture configuration (GD = $D_0$ + CD).

### 2.5.2 Cyclic behavior

Fetal membrane exhibits a viscoelastic behavior typical of soft tissues when cyclically stretched in pressure control (Figure 2.12a). The membrane shows a large hysteresis in the first cycle (Figure 2.12a), followed by reduction and stabilization at about 90% of the value in the first cycle (Figure 2.13a). The tissue deforms more and more during repeated loading, cumulating most of the irreversible deformation in the first cycle (residual strain about 30%). Then, the residual strain staidly increases in the following cycles (Figure 2.12a and Figure 2.13b). The gathered irreversible deformation translates into changes of critical strain, work to rupture and $D_0$ at the reference configuration (Figure 2.10, Figure 2.11 and Figure 2.12b). Moreover, inflating samples between 10 and 40 mmHg, the tissue was stretched in the non-linear part of the tension-strain curve (Figure 2.12b), thus affecting the medium strain stiffness (Figure 2.10).

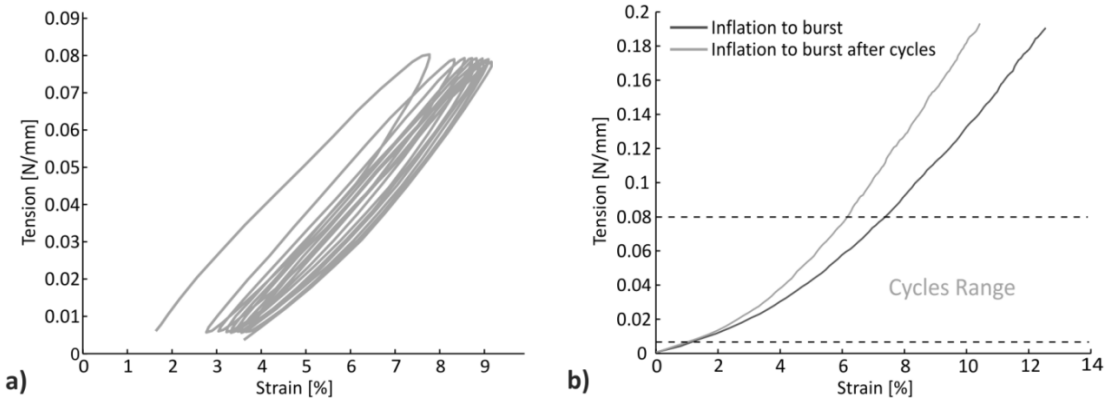


Figure 2.12 Representative tension-strain curves during cyclic loading (a) and inflation to burst (b) (strain calculated using the Rubin-Bodner model).

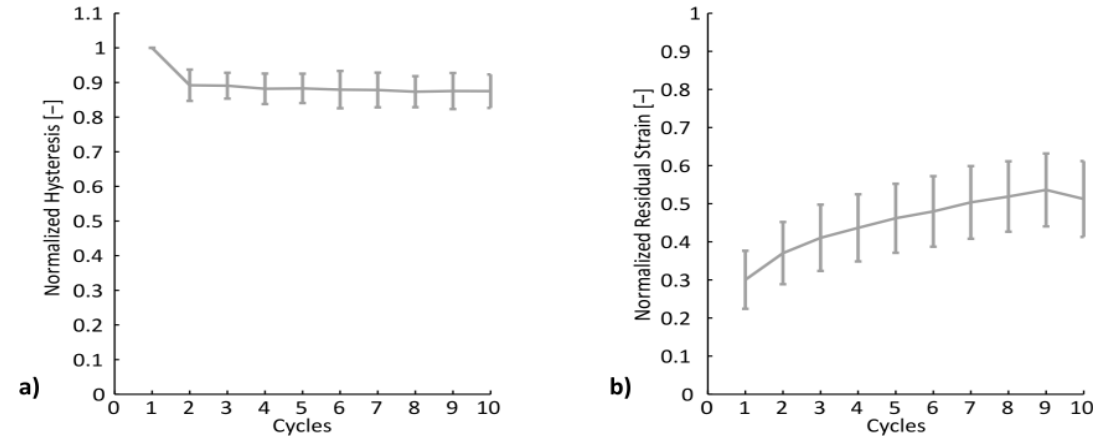


Figure 2.13 Normalized hysteresis (a) and residual strain (b) during cycles (mean ± standard deviation).

### 2.5.3 Rupture

In the 80% of cases and for both groups of samples the sequence of rupture proceeds in the following manner (Figure 2.14): after significant inflation of the membrane, a fracture appears in the amnion radially away from the clamping side (Figure 2.14b), accompanied by an audible “pop” sound and drop of pressure (Figure 2.14b). The chorion, still intact, distends further (Figure 2.14c) until it ruptures in the middle of the sample (Figure 2.14d) at a lower pressure with respect to the amnion (Figure 2.14b). At the end of the test, amnion and chorion appear completely separated over the entire sample (Figure 2.14d). When exceptions occur, amnion and chorion rupture simultaneously at the periphery of the sample.

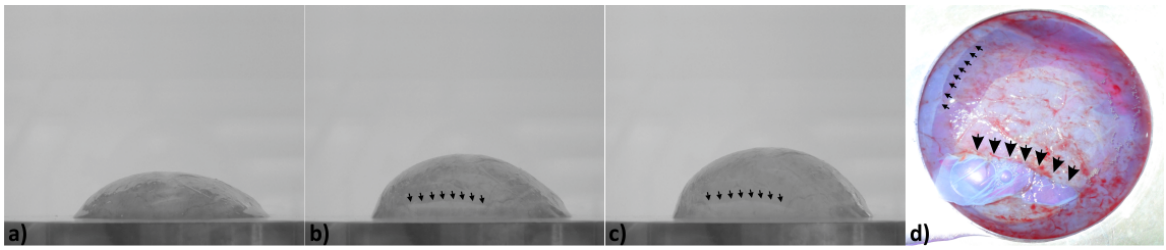


Figure 2.14 Rupture sequence. a) Inflated sample; b) after significant inflation, amnion ruptures (small arrows); c) chorion, still intact, distends further until it ruptures; d) at the end of the test, amnion and chorion are separated (small arrows: amnion rupture; big arrows: chorion rupture; colored water to enhance the visualization of the fractures position).

## 2.6 Results: microstructural study

### 2.6.1 Morphology of the fetal membrane

Nonlinear laser scanning microscopy revealed the microstructure of the fetal membrane and its characteristic layers in the hydrated state (Figure 2.15). For R, ZAM and C tissue, collagenous structures are visible under the amniotic epithelium and different layers can be identified by the presence (amniotic epithelium, fibroblast layer, reticular layer) or absence (compact layer, spongy layer) of cellular nuclei. The amnion is characterized by a homogeneous compact layer of collagen on top of the fibroblast layer. The chorion, mainly composed by trophoblast cells, is connected to the amnion by the interface layer, the spongy.

### 2.6.2 Microstructural alterations

Samples of ZAM and C show the same layered structure of R, although collagen appears altered in the fibroblast and spongy layers. Curly fibre bundles characterize these layers, as opposed to the homogeneous appearance of collagen in R (Figure 2.15). The alteration of the spongy layer in ZAM and C is consistent in all membranes and confirmed by a significantly higher image entropy compared to R (Figure 2.16). The reticular layer seems similarly altered in ZAM, but not in C, while no changes are visible in the microstructure of the compact layer (Figure 2.15).

Moreover, the thickness of collagenous layers is higher in ZAM and in C compared to R, but differences are significant only between ZAM and R (Figure 2.15).

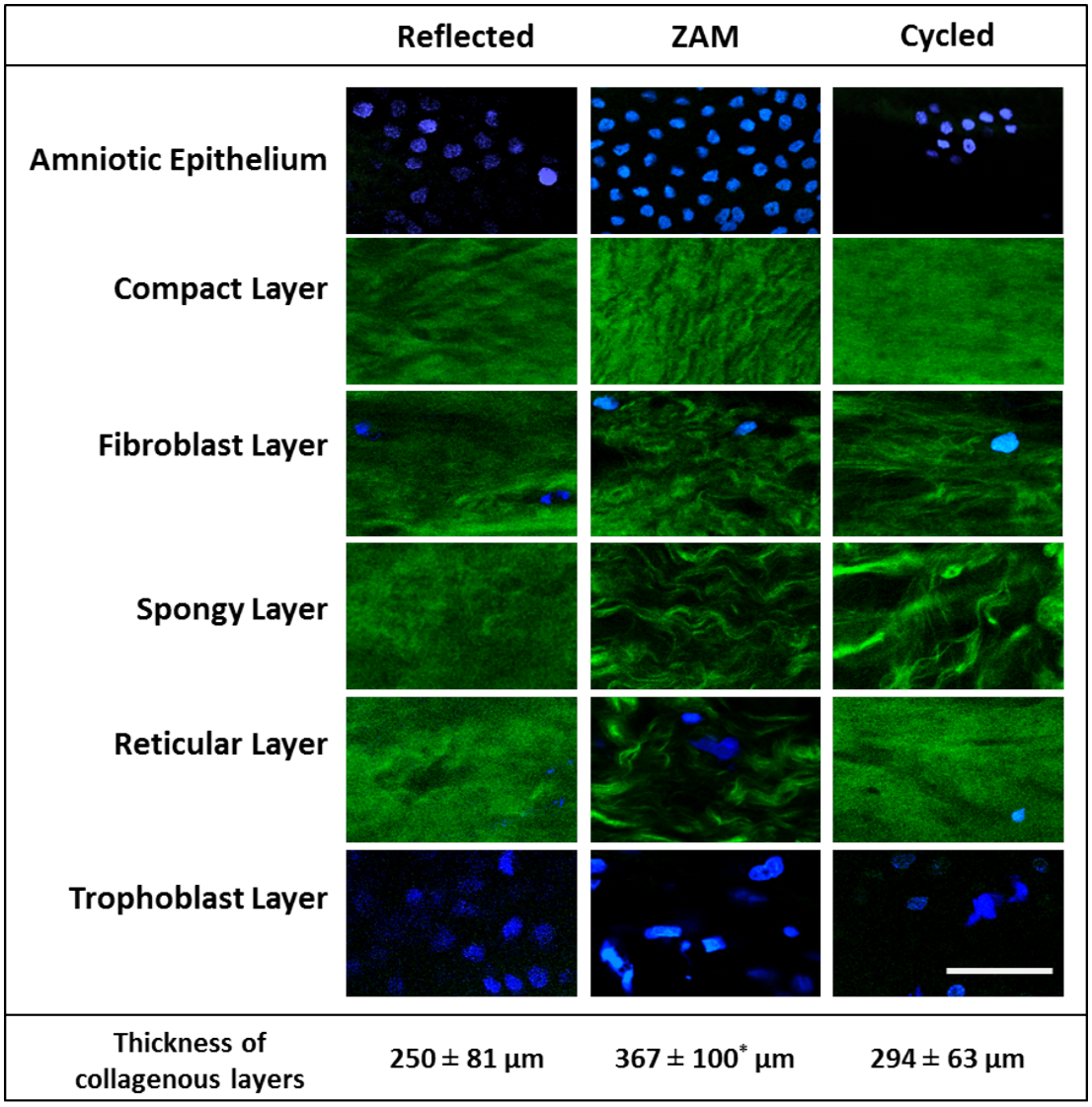


Figure 2.15 Microstructure of a representative R, ZAM and C sample at 0% deformation. A 2D image is shown for each characteristic layer (green: SHG of collagen, blue: fluorescence of nuclei, scale bar: 50 µm). Thickness of collagenous layers is reported as mean ± standard deviation (*$p<0.05$ compared to R).

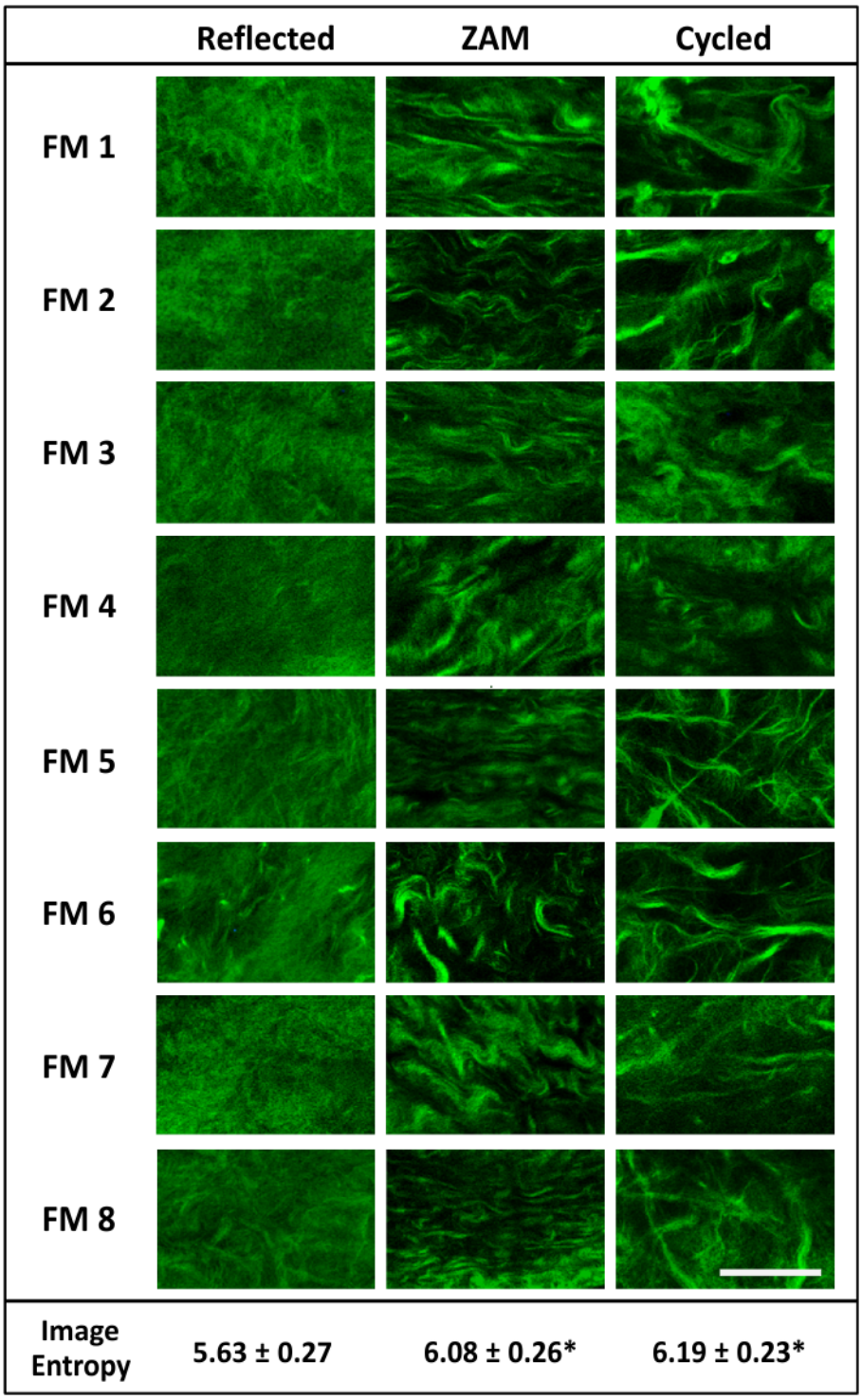


Figure 2.16 Representative images of the spongy layer at 0% deformation in R, ZAM and C samples. A 2D image is shown for each fetal membrane (green: SHG of collagen, scale bar: 50 μm). Image entropy is reported as mean ± standard deviation ($^{*}p<0.05$ compared to R).

### 2.6.3 Microstructure under deformation

Samples of R, ZAM and C have been stretched and imaged at 20% and 40% nominal strain. Both cellular nuclei and collagen were observed to align in the loading direction (Figure 2.17). The standard deviation of the truncated normal distribution, averaged on all the images containing the SHG signal of collagen, decreases significantly from 0% of deformation (R: 139 ± 95, ZAM: 171 ± 111, C: 123 ± 61) to 20% of deformation (R: 77 ± 21, ZAM: 94 ± 35, C: 75 ± 8) for all groups, thus indicating a strong alignment of collagen at moderate deformation. The standard deviation decreases, but not significantly, between 20% and 40% of deformation (R: 69 ± 9, ZAM: 73 ± 26, C: 70 ± 7) and it is not significantly different among groups. However, looking at the specific layers, the fibroblast and spongy layer of ZAM and C show a stronger alignment and reorganization of the curly collagen bundles at 20% deformation compared to the reflected tissue (Figure 2.18).

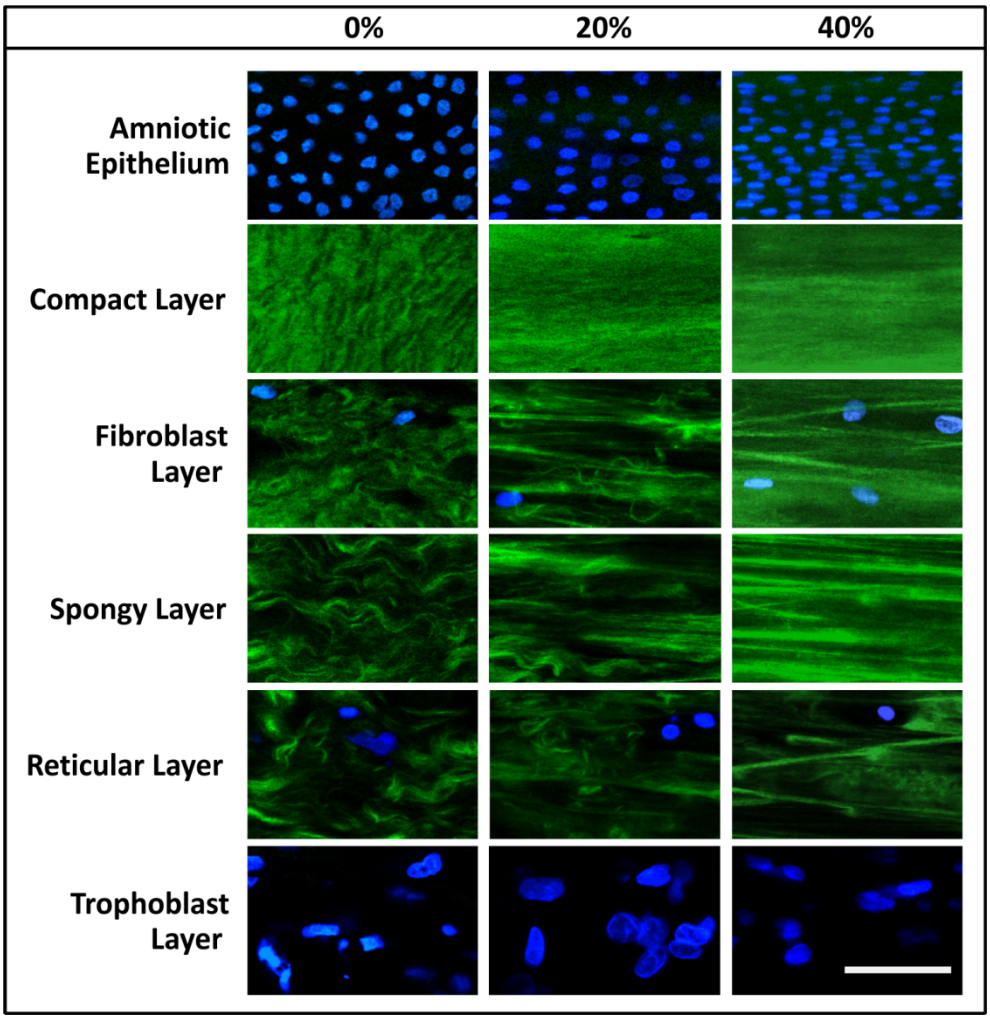


Figure 2.17 Microstructure of a representative ZAM sample at 0%, 20% and 40% deformation. A 2D image is shown for each characteristic layer (green: SHG of collagen, blue: fluorescence of nuclei, scale bar: 50 µm).

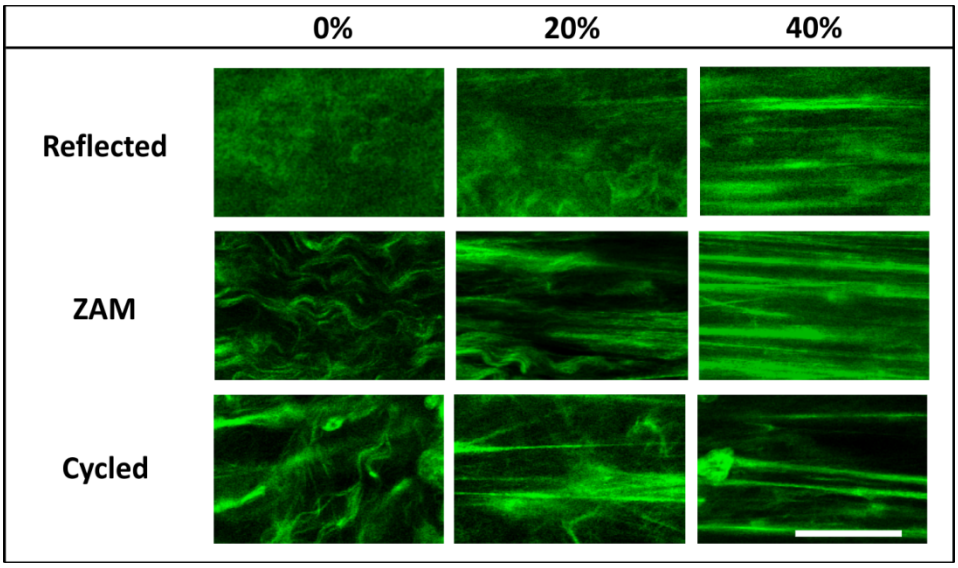


Figure 2.18 Representative 2D images of the spongy layer at 0%, 20% and 40% deformation in R, ZAM and C samples (green: SHG of collagen, scale bar: 50 μm).

## 2.7 Discussion

The objective of these studies was to investigate the effect of repeated mechanical loading on the mechanical behavior and microstructure of the fetal membrane.

The testing protocol was designed to be representative of the in vivo loading conditions of fetal membrane, in particular over the open cervix (paragraph 2.2), therefore (i) fresh membranes with no history of labor were collected after cesarean sections, (ii) samples were cyclically stretched by means of a custom-built inflation device that provides a multiaxial stress state and (iii) the applied pressure profile (cycles shape and parameters) was defined according to the mean physiologic features of contractions. However, it should be noted that the ex vivo model (i) does not include the support of the uterine wall on the membrane, (ii) lacks of the natural variability and increase of the uterine pressure during labor [76, 80] and (iii) is limited to an amount of time not comparable with the duration of labor [76].

The mechanical investigation showed that ten cycles at about 40% of the mean critical membrane tension do affect the deformation behavior and the stiffness of the membrane within the cyclic loading range (Figure 2.12b). The medium strain stiffness significantly increase after cyclic loading and the critical deformation and work to rupture significantly decreased due to the shift of the reference configuration toward a higher apex displacement (Figure 2.11). This phenomenon is a consequence of the cumulated irreversible deformation and the energy dissipated during cycles. The first cycle causes the greatest changes in the material, but smaller gains of residual strains and lower hysteresis steadily last in the following cycles (Figure 2.13). These parameters and their

time history might be slightly affected by the extraction of stretch curves with hyperelastic models neglecting the time-dependent behavior of the material (paragraph 2.3.3). However, Lavery et al. similarly reported loss of resilience and strain-hardening of the membrane as effects of repeated cyclic loading [51].

On the other hand, the global apex displacement (Figure 2.11), the high strain stiffness and the critical tension do not change significantly after cycles (Figure 2.10). This finding disagrees with the strengthening of the membrane after ten cycles at about 50% of the baseline rupture strength reported by Pandey et al. [67]. Differences in results could be related to the use of a different experimental setup: the puncture test, in fact, is affected by stress amplification at the tip of the plunger and slippage of the tissue at the boundary, which might alter the force response of the membrane [56]. As Toppozada et al. and Lavery et al. showed, it is necessary to apply a higher number of cycles or increased pressure to generate a significant weakening in terms of tension at rupture [51, 66].

Cyclic loading does not affect the ex vivo rupture process of fetal membrane, which resulted highly repeatable (Figure 2.14). In 80% of tests, amnion ruptures first and chorion ruptures at a lower pressure after additional distention. The amnion fails in the region under uniaxial strain state (at the periphery of the sample) rather than in the area under biaxial stress state (in the middle of the sample). The chorion, on the contrary, ruptures in the middle of the sample. The separation of amnion and chorion is a critical event which usually occurs during the in vivo rupture process [20], but the ex vivo sequence of layers rupture might be different from the in vivo one and strongly depends on the type of mechanical test. In fact, some studies state that chorion ruptures first [46, 48, 52, 54], while other state that amnion ruptures first [50, 57, 58]. This question has been assessed in a recent study comparing puncture and inflation experiments [56]. It should be noted that values of critical tension and deformation, as well as the observed rupture process, are in line with the results reported by Buerzle at al. using the same setup [57].

In this study, differences between membranes are significant in the critical tension but not in the critical deformation, suggesting that rupture is determined by the level of deformation of the tissue rather than the level of tension. In fact, it is believed that in most cases the membrane spontaneously ruptures over the cervix during the active phase of labor, when full dilation is reached [18, 76]. Even though membranes were stretched for a short time, the mechanical study shows that repeated loading mechanically weakens the fetal membrane leading to the accumulation of irreversible deformation and reduction of toughness. Therefore, it might lead to PPROM when experienced before term.

The effect of cyclic loading on the microstructure of the fetal membrane has been investigated using second harmonic generation microscopy in combination with a custom-built stretching

device placed in the multiphoton microscope. This technique reveals the characteristic collagenous and cellular layers of the fetal membranes described in literature [14, 16, 71] in their physiological hydration and without chemical fixation.

Cycles and ZAM tissue consistently show altered collagen structures in the fibroblast and spongy layer compared to the reflected tissue, corresponding to a significantly higher image entropy. The reticular layer appears similarly altered in ZAM (Figure 2.15). These results indicate that repeated mechanical loading, both ex vivo and in vivo over the cervix, strongly affects the integrity of the interface between amnion and chorion. On the other hand, biochemical factors might mainly cause changes in the reticular layer and swelling of the spongy layer, leading to an increased thickness in ZAM (Figure 2.15). However, it should be noted that cells viability, expression of MMPs and cytokines determining collagen remodeling were not assessed during the study.

Biaxial stretching could not be performed in situ due to limitations of the present setup, but uniaxial stretching provides as well useful information about mechanisms underlying the deformation behaviour of normal and altered fetal membranes (Figure 2.17). Collagen bundles appear randomly oriented in the initial configuration (0%) and aligned in the stretching direction under deformation, with a large recruitment and reorientation already at modest strain. Between 20% and 40% of deformation, collagen is mainly stretched rather than reoriented. Moreover, this mechanism induces asymmetry and compaction of nuclei. It should be noted that the actual local strain might differ from the nominal strain and be affected by the definition of the reference configuration. Values of standard deviation of the truncated normal distribution of fibres angle are not significantly different among the three groups. However, this parameter was averaged on all the images containing the SHG signal of collagen and does not take into account differences among layers. The spongy layer of cycled and ZAM tissue shows a stronger alignment of collagen at 20% deformation compared to the reflected tissue, with curly bundle already stretched in the loading direction (Figure 2.18), thus suggesting that cyclic loading affects the deformation behaviour of collagen structures in the interface layer.

The spongy layer is crucial for the integrity of fetal membrane, allowing the relative sliding of amnion and chorion during growth and distention [9, 71] and contributing to the increased strength of the membrane compared to separated amnion and chorion [54, 96]. Therefore, the alteration of this layer weakens the membrane and might be the main cause of the reduction of toughness observed in the macroscopic investigation. Repeated mechanical loading representative of contractions in the first stage of labor seems to alter collagen structures in the spongy layer, but not to visibly act on the integrity of compact layer and single collagen fibers. The measured irreversible deformation and the increased medium strain stiffness of the cycled tissue might be correlated with microstructural damage in collagen bundles and resulting changes in

collagen recruitment at medium strain levels. Instead, cyclic loading does not affect the response of fetal membrane at high deformation levels (critical tension and high strain stiffness) when collagen fibers are fully stretched and the dense compact layer plays a significant role in the membrane response. It is not clear if the alterations in the spongy layer are mainly due to the first loading cycle or a fatigue effect, since the tissue was only imaged after sixty cycles. The mechanical study suggests that the greatest changes in the tissue happen during the first cycle, but continue in the following cycles. Imaging the tissue during cyclic loading, under biaxial tension and with improved resolution of the second harmonic images might provide these information and reveal microstructural alterations in the compact layer not detectable with the setting used for this study.

## 2.8 Conclusion

A physiologically relevant protocol was developed to investigate the effect of repeated loading on the mechanical and microstructural response of fetal membrane. Mechanical and in situ experiments showed that cyclic loading affects the integrity of collagen structures in the interface layer between amnion and chorion, thus reducing the toughness of the material and altering its deformation behavior. This weakening process might lead to PPROM when experienced before term.

Chapter 3

# Mechanical and microstructural investigation of the cyclic behavior of human amnion

## 3.1 Introduction

The preterm rupture of fetal membranes is considered as a consequence of the acceleration in mechanical and biochemical weakening processes leading to the spontaneous rupture at term [1], see paragraph 1.3. As shown in Chapter 2, early microstructural changes and repeated loading might dangerously affect the integrity of the membrane, thus leading to PPROM and premature birth. Moreover, fetal surgery increases the risk of iPPROM in treated patients [34] due to the introduction of defects and absence of spontaneous healing in the tissue [28].

The structural and mechanical integrity of amnion deserves particular attention, being the load bearing component of the fetal membrane and the most sensitive to mechanical and chemical changes with increasing gestational age [47]. The clinical problem of PPROM motivated the investigation of the mechanical behavior of the fetal membrane [46-55, 57, 61, 67, 74, 83] and amnion [47, 59, 62, 63, 66, 67, 83]. However, only few studies have examined the dependence of the mechanical response of amnion on time and loading history and the associated mechanisms of deformation. Oyen et al. investigated the relaxation and cyclic response of amnion under uniaxial and planar biaxial configurations, showing a strong energy dissipation in the first loading cycle, as well as a strain and time-dependent response [62, 63]. In a recent study Mauri et al. analyzed the macroscopic and microstructural time-dependent response of amnion, revealing a short-term volume reduction due to water outflow and a long-term dissipative behavior without major geometrical changes [64].

In the study described in this chapter, inflation and uniaxial tests were performed in order to compare the cyclic mechanical response of amnion in the two configurations. The inflation test better reproduces the in vivo loading state of the intact fetal membrane in the uterine cavity (paragraph 2.2.3), while the uniaxial configuration is representative of the uniaxial stress state in the vicinity of defects [59]. For the first time, fresh and unfixed amnion was imaged with a multiphoton microscope (MPM) during repeated loading under biaxial and uniaxial tension. In situ experiments allowed for a better understanding of microstructural mechanisms determining the cyclic response of amnion.

The in situ experiments have been performed in collaboration with Arabella Mauri (Institute of Mechanical Systems, ETH Zurich), who developed the in situ experiments and performed the data analysis. For completeness, a short description of the image post processing is provided. Parts of paragraphs and figures in this chapter are included in the submitted manuscript [97].

## 3.2 Methods: mechanical experiments

Inflation (n=7) and uniaxial tension (n=7) experiments were performed in order to investigate the cyclic response of human amnion (without spongy layer). Uniaxial cyclic tests were carried out in displacement control, as common in literature [59, 62, 63]. Inflation tests could not be performed in deformation control due to the permeability of amnion [15] and limitations of the setup in controlling the inflated volume, therefore tests were run in pressure control (paragraph 2.2.4). However, testing protocols were designed to achieve tension and deformation values in the physiological and sub-failure range in both configurations (Figure 3.1, Table 3-1)

Local deformation analysis was performed by tracking the displacement of markers applied on the specimens and tension-stretch curves were analyzed for the loading phase of each cycle.

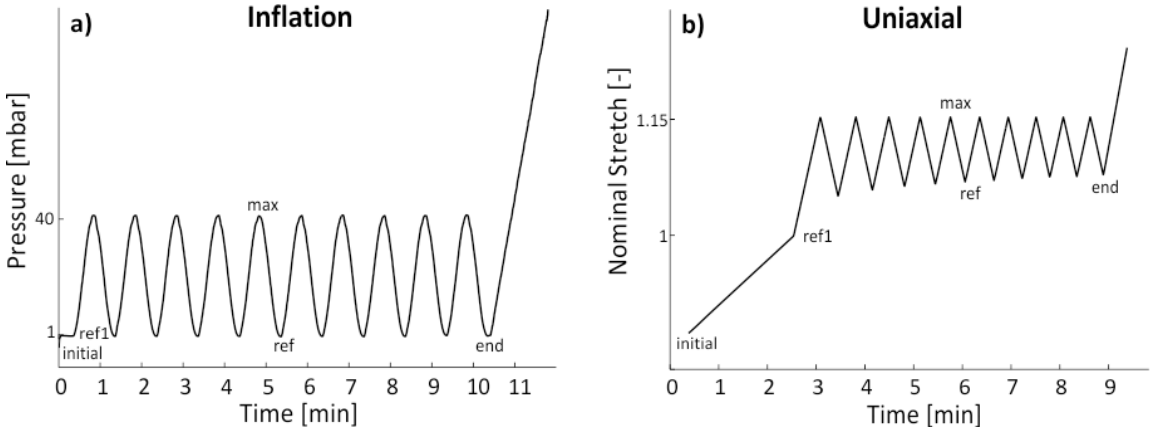


Figure 3.1 Testing protocols. a) Pressure profile applied for cyclic inflation tests; b) nominal stretch profile applied for cyclic uniaxial tests. Initial: slack sample; ref1: reference configuration corresponding to a reference load of 1 mbar (inflation) and 0.01 N (uniaxial) and defining the beginning of the experiment; ref and max: cycles are applied between the reference load and the maximum load/stretch; end: end of the tenth cycle.

Table 3-1 Tension and stretch values reached in the first loafing cycles ($T_C^{max1}$, $\lambda_b^{max1}$ and $\lambda_1^{max1}$) and at rupture ($T_C^{crit}$, $\lambda_b^{crit}$ and $\lambda_1^{crit}$) in inflation and uniaxial tests. Mean ± standard deviation.

| | $T_C^{max1}$ [N/mm] | $\lambda_b^{max1}$ and $\lambda_1^{max1}$ [-] | $T_C^{crit}$ [N/mm] | $\lambda_b^{crit}$ and $\lambda_1^{crit}$ [-] |
|---|---|---|---|---|
| **Inflation** | 0.09 ± 0.01 | 1.07 ± 0.01 | 0.22 ± 0.06 | 1.15 ± 0.02 |
| **Uniaxial** | 0.15 ± 0.05 | 1.12 ± 0.01 | 0.52 ± 0.21 | 1.21 ± 0.05 |

### 3.2.1 Sample procurement and preparation

Fetal membranes (n=10) were collected from patients who underwent elective cesarean section between the 38$^{th}$ and the 40$^{th}$ week of gestation, according to the criteria described in paragraph 2.2.5. Soon after the delivery, the membrane was cut at about 2 cm from the placental border and amnion and chorion where gently separated. The amnion was stored in phosphate buffered saline (PBS) solution at room temperature for about 20 minutes and then spread out on a plastic mat for the harvesting of specimens. For this investigation the ZAM was not marked and specimens were randomly cut far from the placental border, excluding areas of the membrane with visibly damaged amnion or chorion.

Samples for inflation tests were cut and prepared for clamping using sand paper rings with ≈50 mm inner and 70 mm outer diameter glued on both sides of amnion, as described in paragraph 2.3.1 (Figure 3.2a). For uniaxial tests, rectangular specimens 80 mm x 15 mm were excised using a scalpel (Figure 3.2b). The harvested samples were positioned on a plastic sheet and markers were gently applied using a water proof pen (GEOCollege Pigment Liner 0.005) according to the pattern printed on the sheet (Figure 3.2). In both cases, samples were kept moist during preparation, stored in PBS and tested within 8 hours from the collection of the membrane.

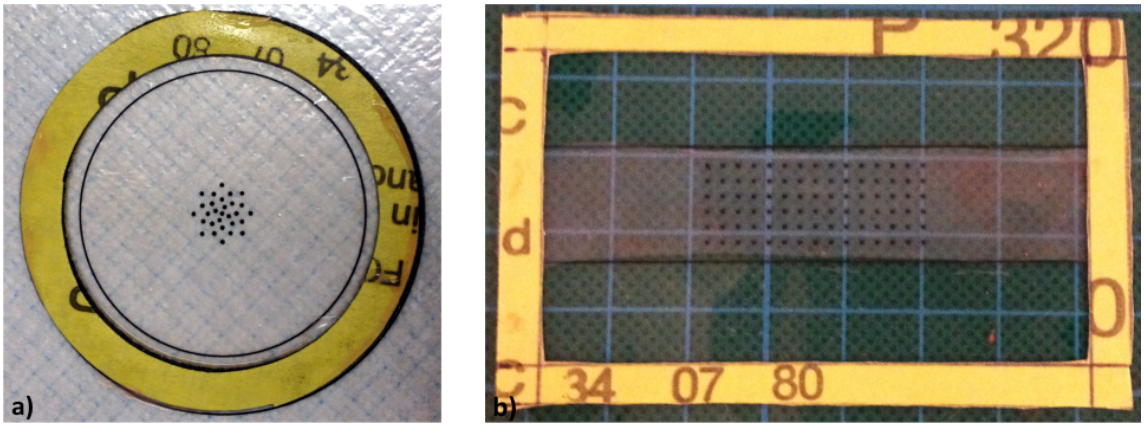


Figure 3.2 Harvested specimens with markers. a) Sample prepared for inflation test; b) samples prepared for uniaxial test.

### 3.2.2 Inflation tests

For this study, major changes were made in the inflation device described in paragraph 2.2.4. The device was equipped with a container, where clamping and testing could be performed in physiological solution (NaCl 0.9%) (Figure 3.4a). In order to transport the device, the clamping

system was reproduced on a movable metal plate positioned in the container. A new inflation cylinder with a transparent plastic base was built and an LED screen was positioned under the container to improve the visibility of markers in the top images (Figure 3.4a).

Inflation experiments were run in pressure control as described in paragraph 2.3.2 and specimens were inflated using physiological solution. The slack amnion (initial configuration) was preloaded to a reference pressure of 1 mbar (ref1) and then stretched applying pressure with sinusoidal profile between 1 mbar (ref) and 40 mbar (max) for 10 cycles of 1 minute each, followed by a monotonic loading till rupture (Figure 3.1a). The reference configuration was defined according to the criteria described in paragraph 2.3.3. In this case, being the tissue immersed in a large container filled with solution, the measured pressure corresponds to the membrane pressure ($p_{memb}$), as shown in Figure 3.3 (Case 2). During testing, pressure values, top and side pictures were acquired at 2 Hz.

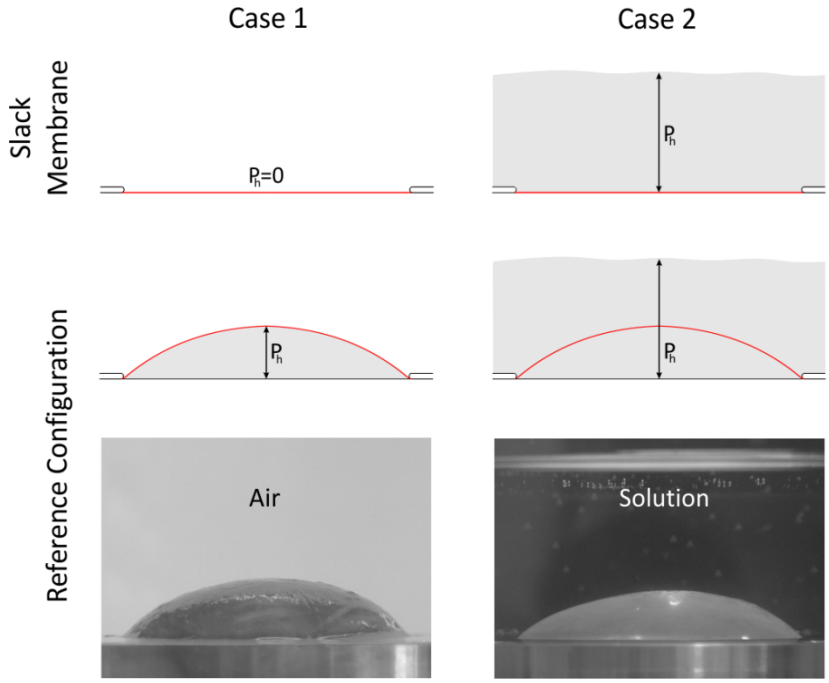


Figure 3.3 Definition of the reference configuration. Case 1: the sample is tested in air and inflated with solution; the measured pressure $P_{tot}$ is set to zero after clamping (slack membrane); during inflation (reference configuration) the hydrostatic pressure generated by the solution within the sample contributes to the measured total pressure together with the pressure generated by the resistance of the membrane ($P_{tot} = P_h + P_{memb}$), as described in Chapter 2. Case 2: the sample is immersed in a large container filled with solution and inflated with the same fluid; after clamping (slack membrane) the measured pressure $P_{tot} = P_h$ is set to zero; during inflation (reference configuration) the height of the fluid column and thus the hydrostatic pressure $P_h$ in the large container does not change; consequently, the only contribution to the measured pressure is due to the resistance of the membrane, $P_{tot} = P_{memb}$. Red line: membrane; blue background: solution.

### 3.2.3 Uniaxial tension tests

Uniaxial tests were performed with our custom-built experimental setup [59], consisting of two hydraulic actuators, two calibrated 20N load cells, a video extensometer system, LED screen and a container filled with physiological solution, where specimens were immersed during testing (Figure 3.4b). Samples were clamped in physiological solution with the help of a sand paper jig and fixed with 60 mm free length (initial configuration). The amnion was preloaded to a reference force of 0.01 N (ref1, corresponding to approximately 0.001 N/mm tension and 0% strain) and then stretched between the reference force (ref) and 1.15 nominal stretch (max) for 10 cycles of 1 minute each, followed by a monotonic loading till rupture (Figure 3.1b). The reference force level was selected to ensure a repeatable loading state at the beginning of each cycle. During testing, force, displacement values and images were acquired at 2 Hz.

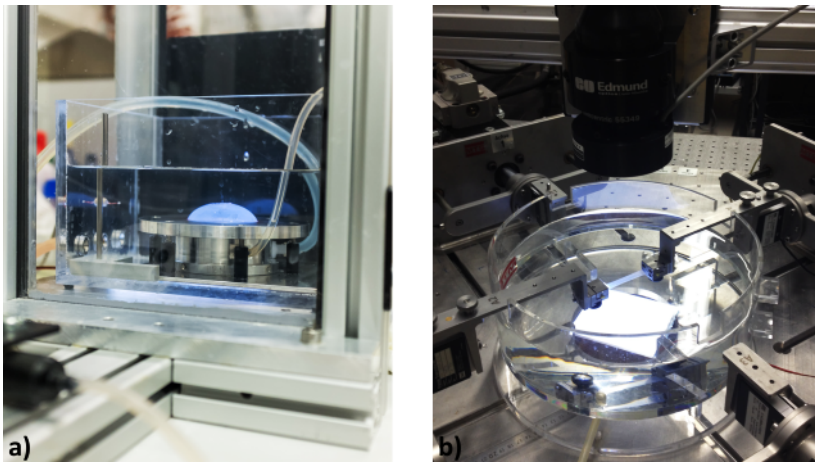


Figure 3.4 Experimental setups. a) Inflation device with inflated amnion samples lighten with the LED screen; b) setup for uniaxial tests with stretched amnion sample.

### 3.2.4 Post processing

*Tension calculation*

As for inflation experiments, the Cauchy tension $T_C$ [N/mm] was calculated as described in paragraph 2.3.3. The Cauchy uniaxial tension $T_C$ was calculated dividing the recorded force by the current width of the specimen. The width was evaluated in the central region of the specimen (30 mm) converting the acquired pictures in black and white and extracting the contour of the specimen.

*Local deformation analysis*

The local deformation analysis was performed using a custom-build algorithm developed by Raoul Hopf and based on functions of the MATLAB Image Analysis toolbox [86].

Since the strain field in inflated samples is not homogeneous, numerical simulations were performed to define a suitable region for the local deformation analysis were an equibiaxial stress strate is expected. Moreover, the curvature of samples inflated at 40 mbar was calculated from side pictures as 1/R (R: radius of curvature, paragraph 2.3.3, Figure 2.7). An axisymmetric model (elements CAX4R) representing a circular sample of amnion (thickness= 0.1 mm, radius= 25 mm) was built in the commercial finite element software ABAQUS 6.10-1 (Abaqus Inc. RI, USA) (Figure 3.5a). The transversally isotropic constitutive model proposed by Buerzle and Mazza [59] was used to describe the mechanical behavior of amnion, while the clamping was modeled as a rigid body with rounded edge (r=1 mm) (Figure 3.5a). Uniform pressure up to 40 mbar was applied on one the underside of the membrane (Figure 3.5a). Circumferential and radial strains were analyzed. The stress field resulted equibiaxial in the center of the sample. The ratio radial/circumferential strain and the curvature change of about 2% and 1% in a circular area with radius equal to 5 mm (20% of the sample's radius), respectively (Figure 3.5b and c). Therefore, analyzing the local deformation in this region provides a good estimation of the average biaxial stretch in the center of the inflated sample with negligible effects of the curvature.

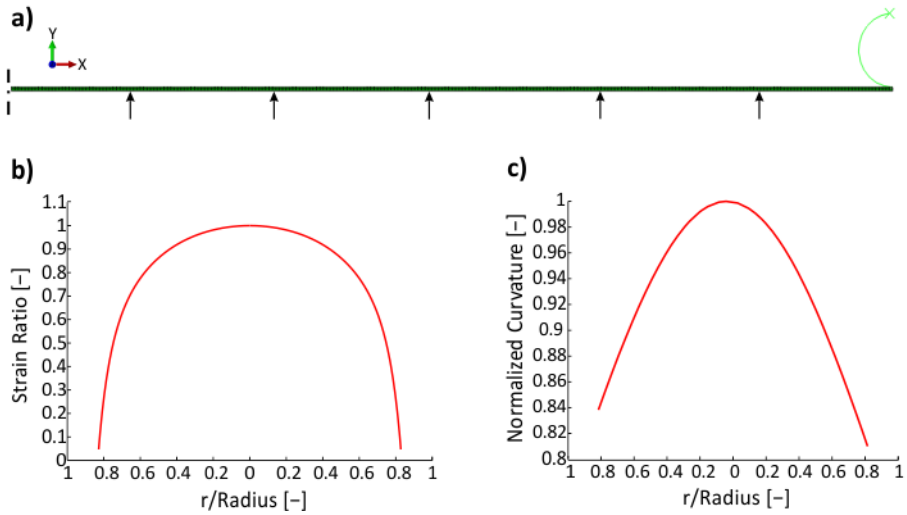


Figure 3.5 Analysis of the strain field in inflation tests. a) Finite element model of inflated amnion (interrupted line: axis of symmetry; arrows: applied pressure); b) Strain Ratio= radial/circumferential strain; c) curvature normalized with respect to the value in the center. r/Radius = position with respect to the radius of the sample (25 mm).

Top images were then analyzed tracing the displacement in the image plane of markers positioned on a circle with radius of 5 mm around the center. The area of the polygon defined by the markers was calculated for each picture and the areal stretch ($A_s$) was defined as current area divided by the area at ref1. The local biaxial stretch was calculated as

$$\lambda_b = \sqrt{A_s} \quad (3)$$

The apex displacement (d) was also measured in each side picture as described in paragraph 2.3.3. The presence of tiny air bubbles forming during clamping affected the tracking of markers, leading to noise in the stretch data. Therefore, stretch values were smoothed by fitting $\lambda_b$-d curves of each loading cycle with a third order polynomial (Figure 3.6).

In the uniaxial tests, the displacement of markers was traced in the central region of the specimen (30 mm) [59]. The local stretch in the loading direction $\lambda_1$ and in the transversal direction $\lambda_2$ were calculated with respect to ref1. The maximum local stretch resulted on the average 20% lower than the maximum nominal stretch due to slippage of specimens in the clamps (Table 3-1).

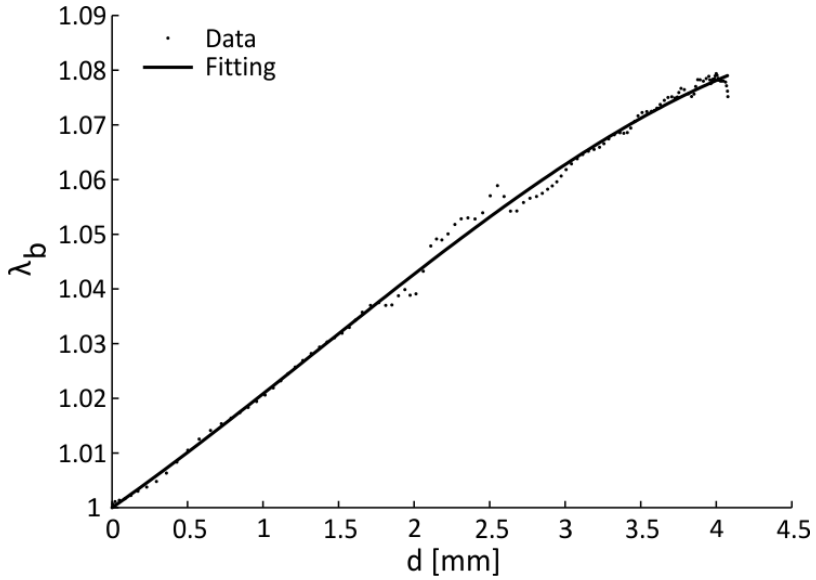


Figure 3.6 Representative $\lambda_b$-d curve of the first loading cycle fitted with a third order polynomial.

*Analysis of the cyclic behavior and mechanical parameters*

Pressure-apex displacement curves (inflation) and force-nominal stretch curves (uniaxial) of the first loading cycle were analyzed and normalized with respect to the maximum apex displacement $d^{max1}$ (inflation) and the maximum force $F^{max1}$ (uniaxial) reached in the first loading. Tension-stretch loading curves were fit with a fourth order polynomial and the first derivative was calculated in order to evaluate the uniaxial and biaxial tangent stiffness K [N/mm]. Residual

stretches at the end of each unloading (ref) were extracted ($\lambda_b^{res}$ and $\lambda_1^{res}$), see Figure 3.7. Normalized residual strains were calculated with respect to the maximum strain reached in the first loading as $\bar{\varepsilon}_b^{res} = (\lambda_b^{res} - 1)/(\lambda_b^{max1} - 1)$ and $\bar{\varepsilon}_1^{res} = (\lambda_1^{res} - 1)/(\lambda_1^{max1} - 1)$. These normalized values hence represent the fraction of the strain at the first maximum that remains after unloading. The dissipated energy ratio (DER) was calculated for each cycle as the total dissipated energy ($E_D$, area between the loading and unloading tension-stretch curves) divided by the energy dissipated during loading ($E_L$, area underneath the loading tension-stretch curve) (Figure 3.7) [63]. Moreover, the kinematic uniaxial response of amnion was investigated in terms of lateral contraction $\lambda_2$ and $\lambda_2$-$\lambda_1$ mean curves were analyzed for the loading phase.

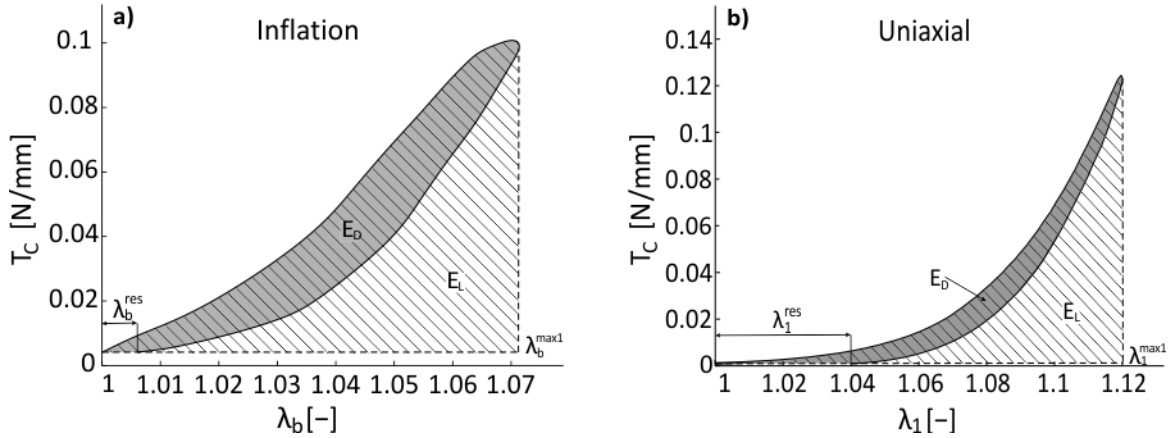


Figure 3.7 Tension-stretch curves of the first cycle of representative inflation (a) and uniaxial (b) tests. $\lambda_b^{max1}$ and $\lambda_1^{max1}$: maximum stretch reached in the first loading; $\lambda_b^{res}$ and $\lambda_1^{res}$: residual stretches; $E_D$: total energy dissipated; $E_L$: energy dissipated during loading.

## 3.3 Methods: in situ experiments

In situ inflation (n=4) and uniaxial (n=3) tests were performed in the multiphoton microscope (Figure 3.8) using the same protocols described in paragraph 3.2.3, excluding the final load to rupture. Before clamping, specimens were stained with the DNA binding dye Hoechst 33342 (2'-[4-ethoxyphenyl]-5-[4-methyl-1-piperazinyl]-202 2,5'-bi-1H-benzimidazole trihydrochloride trihydrate, Invitrogen). Hoechst dye was used in this study since it provides a higher fluorescence signal for live cells compared to DAPI [98]. Staining with DAPI did not always allow the visualization of the whole epithelium (Chapter 2), thus suggesting that cells might still be alive during testing. Second harmonic generation (SHG) of collagen and fluorescence of nuclei were detected using the same setting described in paragraph 2.4.3. 3D stacks were taken in the center of the specimen by collecting images at 2 μm intervals through the whole amnion thickness.

Stacks were acquired in the following loading states: slack (initial), reference configuration (ref1), maximum pressure/stretch in the first (max1), second (max2) and tenth (max10) cycle, beginning of the second (ref2), third (ref3), tenth (ref10) cycle and at the end of the tenth cycle (end). Specimens were imaged from the top with the water objective (Figure 3.8), waiting two minutes after reaching the loading state, in order to let the specimen stabilize and exclude short-term time-dependent effects [64].

### 3.3.1 Inflation tests

Inflation tests were performed in saline solution using the same device, clamping procedure and protocol described in paragraph 3.2.2 (Figure 3.8a), but a different loading method. A large movable reservoir filled with physiological solution was connected to the inflation cylinder through a tube equipped with a valve (Figure 3.9). The reservoir was repetitively moved between two defined heights in order to apply the reference (1 mbar) and maximum (40 mbar) pressure by slowly opening the valve. Pressure values were measured during the experiments with the pressure sensor in the inflation setup (paragraph 2.2.4). The loading rate resulted faster than in the inflation tests outside the microscope, but specimens were let stabilize for two minutes after each loading step, even when not imaged.

### 3.3.2 Uniaxial tension tests

Uniaxial tests were performed with the custom-made stretching device described in [64], consisting of two axes actuated with servo motors, a force sensor and a control box (Figure 3.8b). Samples were clamped and stretched using the same protocol described in paragraph 3.2.3. Also in this case, specimens were let stabilize for two minutes after each loading step.

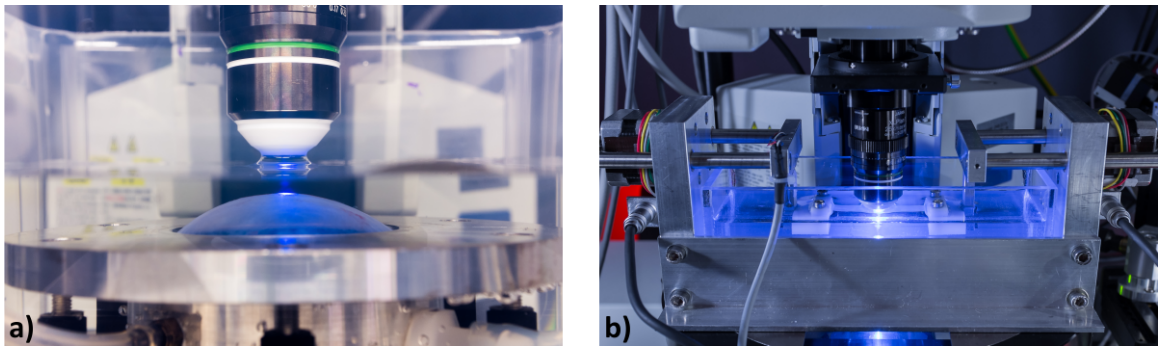


Figure 3.8 Experimental setups for in situ experiments. a) Inflation device in the multiphoton microscope with inflated amnion; b) stretching device in the multiphoton microscope with amnion sample. Pictures reprinted with the permission of Manfred Maurer.

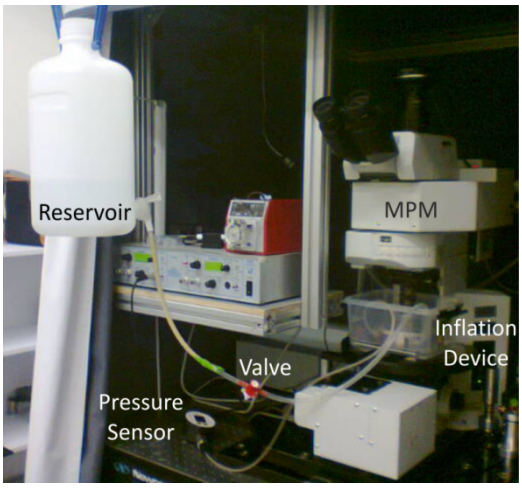


Figure 3.9 Experimental setup for in situ inflation tests.

### 3.3.3 Post processing

Microstructural parameters, i.e. thickness and collagen orientation have been extracted as described in [64]. Briefly, amnion thickness was extracted manually using the software Imaris (Bitplane AG, Switzerland) by drawing seven lines in the transversal section of the specimen perpendicular to the epithelial layer (including cells and excluding the spongy layer in case it was still attached). The thickness was calculated as the mean lines length and the stretch in the thickness direction $\lambda_3$ was defined with respect to ref1. The orientation of collagen bundles was estimated using a custom algorithm based on the multiscale principal components analysis. All the extracted orientation angles from each image were collected through the stack in order to obtain a distribution of angles. The central region (70% of all angles) of the planar distribution of angles was fitted with a normal distribution and the normalized collagen orientation index ($\overline{\mathrm{COI}}$)

was defined as the standard deviation of the distribution ($\sigma$) normalized with respect to its value at ref1.

Combining the macroscopic values of areal stretch ($A_s$), longitudinal and lateral stretch ($\lambda_1$ and $\lambda_2$) with the stretch in the thickness direction ($\lambda_3$) extracted from the microscopic experiments, the volumetric stretch J with respect to ref1 was calculated as $A_s\lambda_3$ for the inflation configuration and $\lambda_1\lambda_2\lambda_3$ for the uniaxial configuration.

## 3.4 Results

### 3.4.1 Mechanical experiments

Amnion was cyclically stretched in the sub-failure deformation range both in inflation and uniaxial configuration (Table 3-1). Inflated samples reach a critical pressure of 133.8 ± 43.7 mbar after cyclic loading. The tissue shows a significant variability in the mechanical response typical of soft tissues (Figure 3.10a and b). However, normalizing the apex displacement (d) with respect to $d^{max1}$ (inflation) and the force (F) with respect to $F^{max1}$ (uniaxial), pressure-apex displacement and force-nominal stretch curves from different specimens collapse in a remarkably small range around the average curve (Figure 3.10c and d).

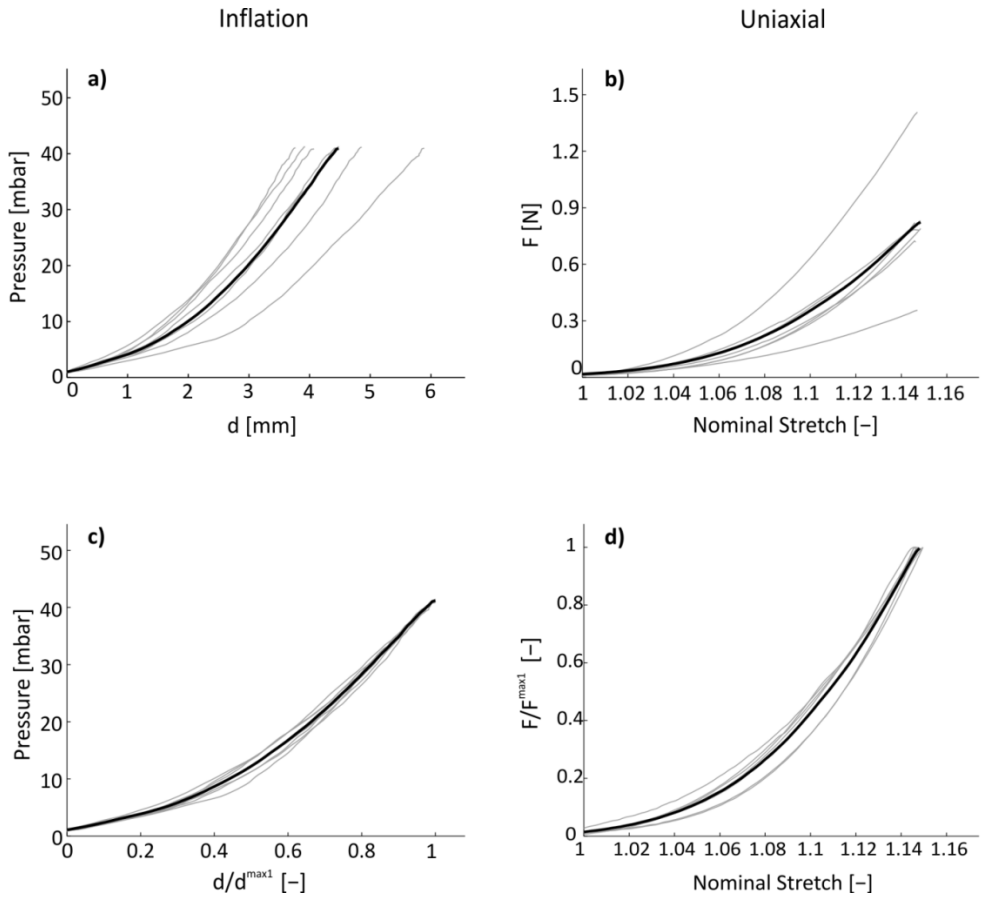


Figure 3.10 Load-deformation curves for inflation (a, c) and uniaxial (b, d) experiments. a) Pressure-apex displacement curves of the first loading cycle; b) force-nominal stretch curves of the first loading cycle; c) pressure-displacement curves normalized with respect to the maximum apex displacement reached in the first loading cycle $d^{max1}$; d) force-nominal stretch curves normalized with respect to the maximum force reached in the first loading cycle $F^{max1}$. Grey lines: curves of the seven tested specimens; black lines: mean curves.

Mean tension-stretch curves of each loading cycle are shown in Figure 3.11a and b. The first cycle determines the most significant changes in the response of the material. Under biaxial tension, the tissue exhibits a stable tension-stretch response during cycles and small residual stretches (Figure 3.11a). Under uniaxial tension, amnion undergoes a strong change in the mechanical response during cycles. The maximum tension decreases by 15% in the second cycle and by 45% in the tenth cycle with respect to the first one (Figure 3.11b). Residual strains are significantly higher than in the inflation tests, reaching 30% of the maximum strain after the first cycle and steadily increasing up to 46% in the tenth cycle (Figure 3.12a).

Both the time history of the applied load (inflation=sinusoidal, uniaxial=triangular) and the testing configuration affect the stiffness of the tissue during cyclic loading. The tangent stiffness changes in line with the sinusoidal pressure history under biaxial loading and reaches the maximum value

when the pressure increases at the highest rate (Figure 3.11c). After the first cycle, the tangent stiffness is initially lower at small stretches, but increases and exceeds the stiffness in the first loading at medium and high stretch levels (Figure 3.11c). On the contrary, the uniaxial tangent stiffness increases nearly exponentially from low to high stretch levels and it is overall lower after the first cycle (Figure 3.11d).

Interestingly, amnion shows higher energy dissipation under biaxial tension compared to the uniaxial configuration. In both cases, the dissipated energy ratio decreases (-20% inflation, -30% uniaxial with respect to the first cycle) and stabilizes after the first cycle (Figure 3.12b).

The kinematic response of amnion is characterized by a high incremental Poisson's ratio ($\nu = \max\left\{-\frac{\partial\lambda_2}{\partial\lambda_1}\right\}$ =6.87 ± 0.52 in the first loading cycle) and a strong lateral contraction, reaching half of its initial lateral dimension at the maximum elongation (Figure 3.13). Similarly to the tension-stretch behavior, the first loading cycle induces the greatest change in the kinematic response, which stabilizes in the following cycles (Figure 3.13). In line with the large $\lambda_1^{res}$, amnion recovers only 50% of the lateral contraction at the end of the first cycle and the slope of the $\lambda_2$ - $\lambda_1$ curve decreases significantly when approaching the reference force (Figure 3.13a). Amnion shows a substantial lateral contraction already during the preload phase (from initial to ref1), resulting in a total (from initial to max1) reduction of its lateral dimension by 70% compared to the initial configuration (Figure 3.13).

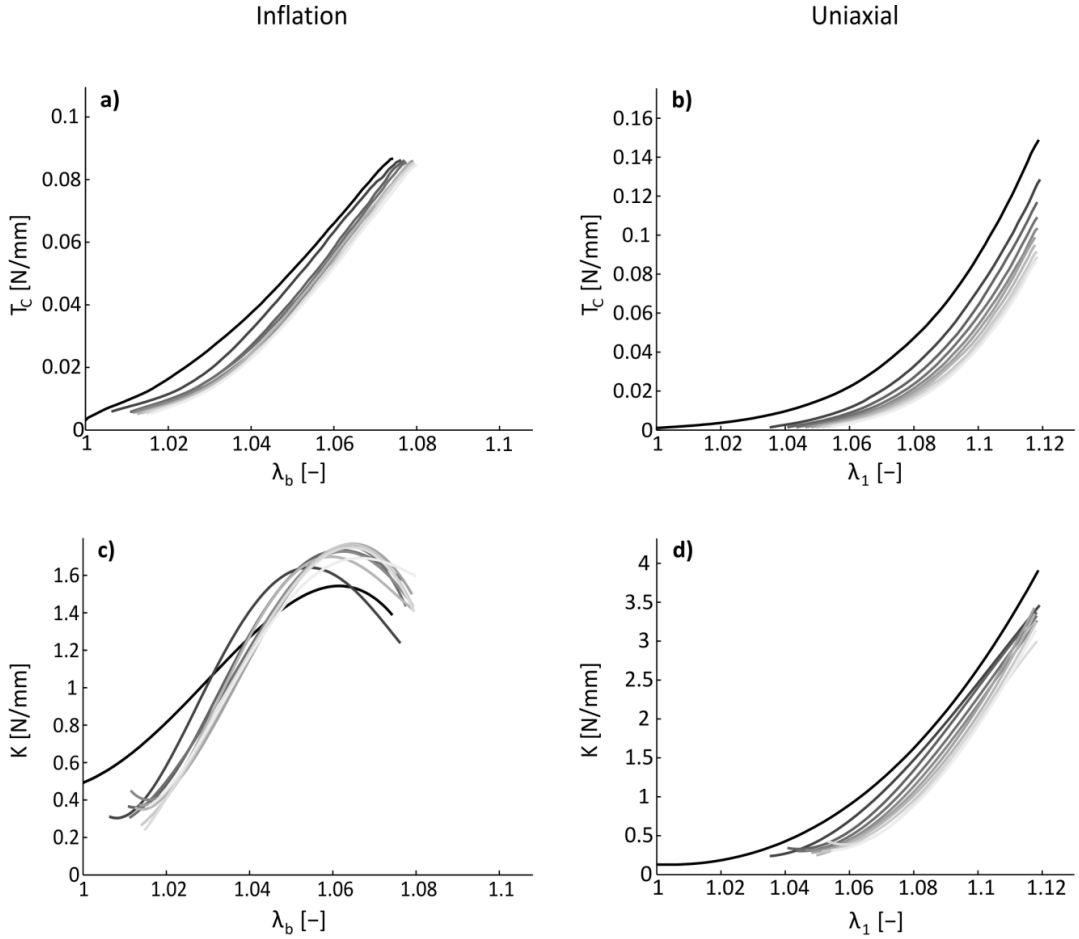


Figure 3.11 Mean tension-stretch loading curves (a,b) and tangent stiffness curves (c,d) from the first (darkest) to the tenth (lightest) loading cycle for inflation (a,c) and uniaxial experiments (b,d).

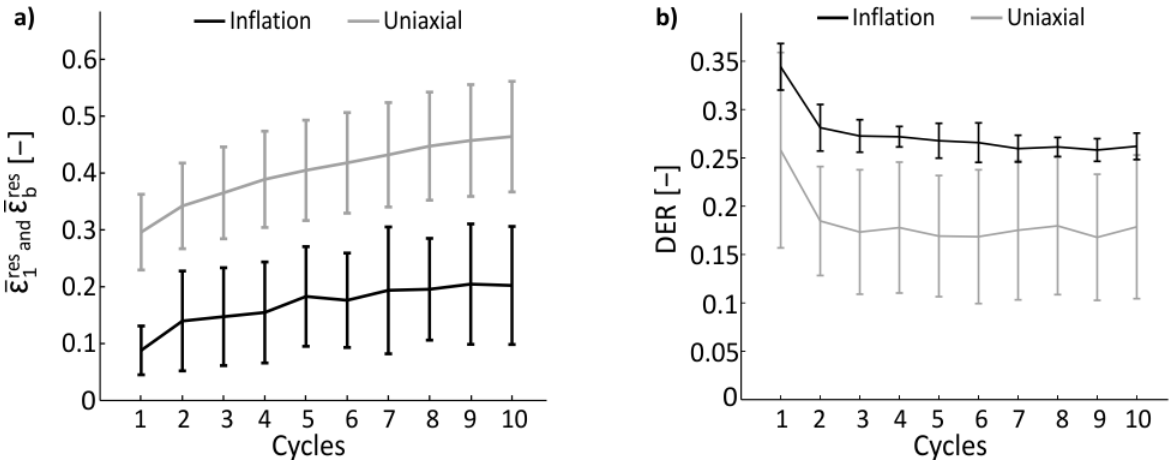


Figure 3.12 Normalized residual strains $\bar{\varepsilon}_b^{res}$ and $\bar{\varepsilon}_1^{res}$ (mean ± standard deviation) (a) and dissipated energy ratio DER (mean ± standard deviation) (b).

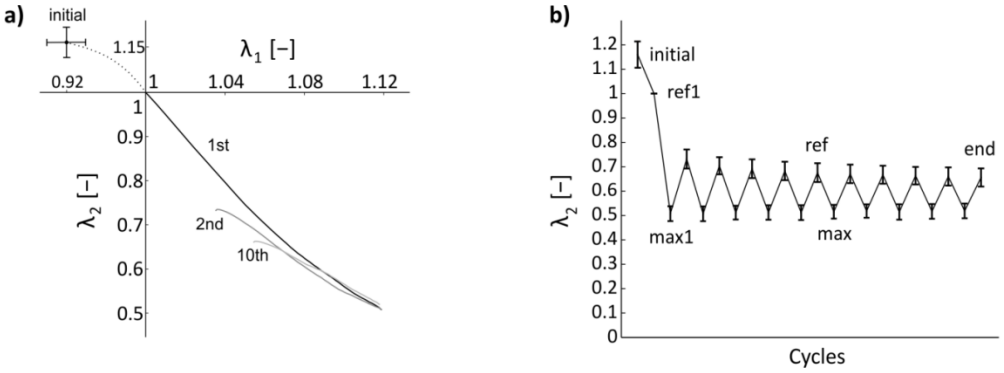


Figure 3.13 Kinematic response of amnion during uniaxial cyclic tests. a) The lateral contraction $\lambda_2$ is plotted against the longitudinal stretch $\lambda_1$ for the initial configuration (mean ± standard deviation), the first (black line), the second (dark grey) and the tenth (light grey) loading cycles (mean curves); b) evolution of the lateral contraction during cycles (mean ± standard deviation). Values are referred to the reference configuration at the beginning of the first cycle (ref1).

### 3.4.2 In situ experiments

Microstructural parameters, i.e. amnion thickness and collagen orientation index, were extracted from images acquired during in situ inflation and uniaxial experiments.

The initial thickness of all the tested specimens resulted 84.1 ± 11.7 µm. Figure 3.14b shows the stretch in the thickness direction $\lambda_3$ calculated with respect to the thickness value at ref1. For inflation and uniaxial in situ experiments, the thickness significantly decreases from the initial configuration to the maximum load (inflation: -70% and uniaxial: -40% of the initial value), with a stronger collapse of the collagenous layers under biaxial tension, in particular during the preload phase (-50% of the initial value) (Figure 3.14a and b). When the tissue is unloaded, the thickness is recovered and for the inflation tests it reaches higher values compared to the reference configuration (Figure 3.14 a and b). The described trend of the thickness remains stable during cycles, with a slight progressive increase and decrease of thickness in the inflation and uniaxial configuration, respectively (Figure 3.14b).

Combining the in-plane deformation data from the mechanical experiments with the stretch in the thickness direction extracted from the in situ experiments, the mean volumetric stretch J was calculated (Figure 3.14c). The volume changes in line with the thickness under biaxial tension and shows the same trend during cycles, with a strong volume reduction during the first loading (-60% of the initial value) and higher volume compared ref1 when unloaded (Figure 3.14c). For the uniaxial configuration, both $\lambda_2$ and $\lambda_3$ strongly contribute to the volumetric changes, determining (i) a strong decrease of volume during the first loading (-80% of the initial value), (ii) incomplete

recovery during the unloading phase due to permanent elongation and lateral contraction (Figure 5), and (iii) a slight progressive decrease of volume during cycles (Figure 3.14c).

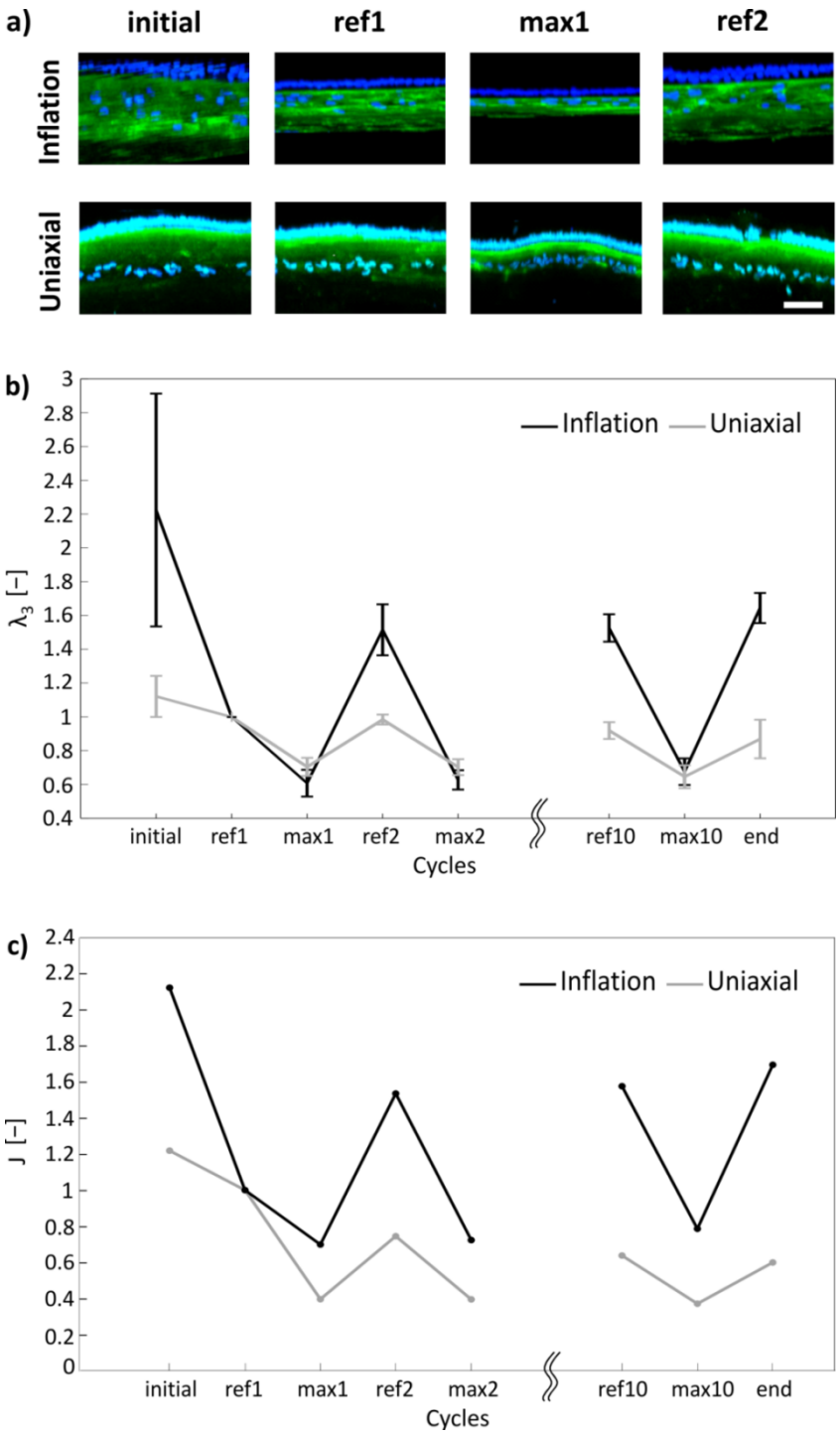


Figure 3.14 Thickness and volume changes during cyclic tests. a) Representative transversal sections of amnion (blue: nuclei, green: SHG of collagen, scale bar = 50 µm) imaged during in situ experiments in different loading states; b) stretch in the thickness direction $\lambda_3$ (mean ± standard deviation); c) estimated volumetric stretch J (mean). Values are referred to the reference configuration at the beginning of the first cycle (ref1).

The orientation of collagen during cyclic loading has been investigated and quantified by the normalized collagen orientation index $\overline{\mathrm{COI}}$, which decreases with stronger orientation of fibers in the loading direction for the uniaxial test (Figure 3.15). Collagen orientation does not change during inflation and the weak increase of $\overline{\mathrm{COI}}$ might be related to the breakup or redistribution of collagen structures (Figure 3.15).

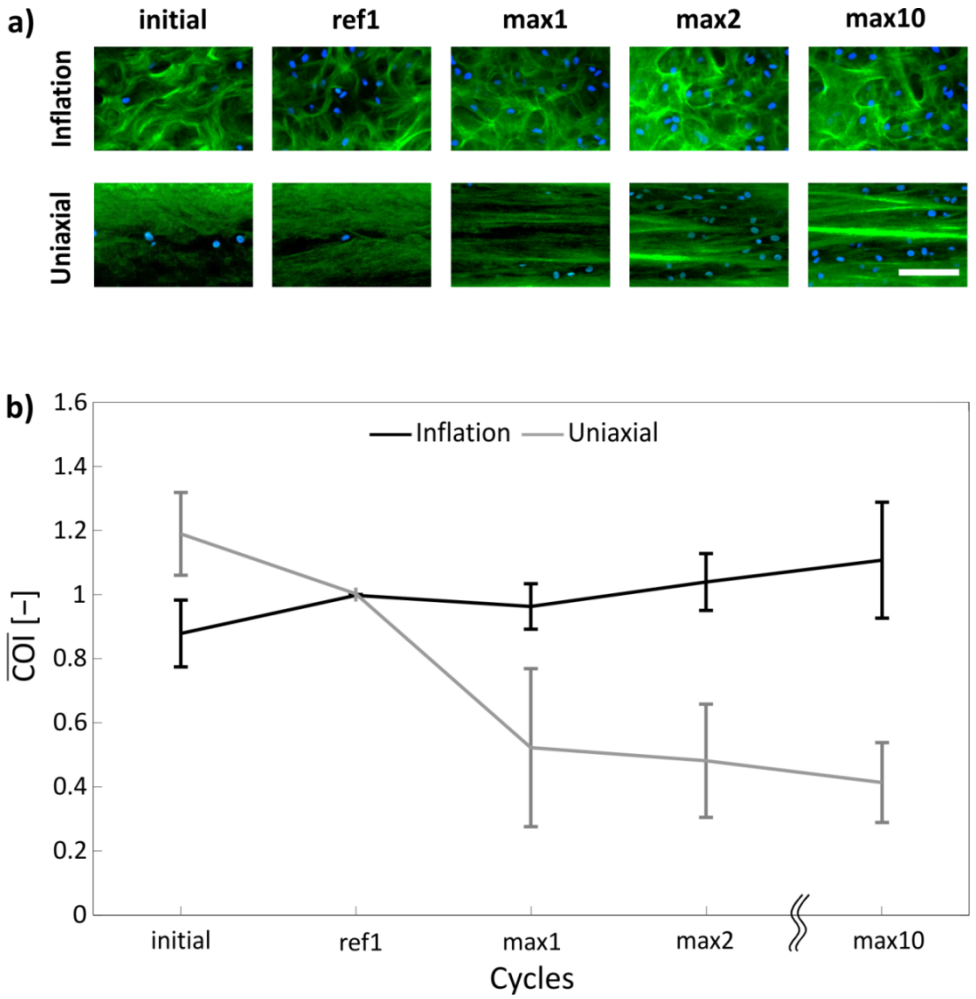


Figure 3.15 Collagen orientation. a) Representative 2D images of the fibroblast layer (blue: nuclei, green: SHG of collagen, scale bar = 100 µm) imaged during in situ experiments in different loading states; b) normalized collagen orientation index $\overline{\mathrm{COI}}$ (mean ± standard deviation).

## 3.5 Discussion

This study provides deeper insights into the mechanical and microstructural response of the human amnion when subjected to cyclic loading. Inflation and uniaxial cyclic tests were combined with in situ experiments and multiphoton microscopy was performed on cyclically inflated and stretched amnion. Testing protocols were designed to test amnion in its physiological loading range (Table 3-1, Figure 3.1) and these conditions were reproduced as closely as possible in the in situ experiments. However, it should be noted that differences in the mechanical behavior observed under biaxial and uniaxial tension might be associated with the different loading mode (pressure and displacement control) and maximum tension levels (Table 3-1).

In both configurations, specimens were preloaded to a reference pressure (inflation) or force (uniaxial) level (ref1) in order to define a well repeatable starting loading state (Figure 3.1). The choice of the reference configuration plays an important role in the detection of deformation mechanisms at low tension. Since in-plane and out-of-plane mechanisms in the amnion resulted activated already at low tension levels, the preload phase was also analyzed.

Amnion shows the typical variability of soft tissues in its mechanical response (Table 3-1), both in pressure controlled biaxial tests (Figure 3.10a) and in displacement controlled uniaxial tests (Figure 3.10b). Similarly to the intact fetal membrane (Chapter 2), cyclic inflation in the sub-failure range does not affect the critical tension of amnion and determines a slight increase of critical pressure, when compared to the values reported by Haller for monotonic inflation tests [96]. These findings might be a consequence of geometrical changes occurring during cyclic loading. In fact, the accumulation of irreversible deformation and increase of apex displacement lead to a smaller radius of curvature, thus requiring higher pressure to achieve the same tension (see Chapter 2, equation 1). The critical uniaxial tension turns to be significantly higher than the one reported by Buerzle and Mazza [59]. Differences might be related to the clamping procedure, the presence of spongy layer in the tested samples and the method used for the extraction of samples' width.

Normalized pressure-apex displacement (inflation) and force-nominal stretch (uniaxial) curves from different samples collapse in a remarkably small range around the average curve (Figure 3.10c and d), as previously shown in relaxation and creep tests [64]. This normalization builds on the idea that once collagen fibers have aligned and become straight, the behavior of different samples is very similar, thus displaying a repeatable deformation mechanism characteristic of the tissue.

The first loading cycle induces the strongest changes in the material response, both under biaxial and uniaxial tension. A similar behavior was observed by Oyen et al. [63] in planar uniaxial and

biaxial cyclic tests of amnion (Figure 3.11). The tension-stretch response of amnion during cyclic inflation (Figure 3.11a) is characterized by smaller residual stretches but higher energy dissipation compared to the uniaxial configuration (Figure 3.12), stiffening at high stretch levels and softening at low stretch after the first cycle (Figure 3.11c). On the contrary, under uniaxial tension the tissue shows a progressive tension softening during cycles (Figure 3.11b), with higher residual stretches but lower dissipated energy (Figure 3.12). The time history of load applied in the two configurations differently affects the stiffness of the tissue, thus confirming the viscoelasticity of amnion [63-65]. Tissue softening at low deformation levels has been also observed in other biological materials as a consequence of microstructural changes during preconditioning both under biaxial and uniaxial loading [99, 100].

Experimental results suggest different deformation and dissipative mechanisms in the two configurations. Fibers recruitment and uncoiling play an import role during biaxial loading yet at small stretch levels, as well as damage of collagen fibers network might occur with increasing deformation in the first cycle, thus leading to higher dissipation. After the first loading cycle, the recruitment of rearranged fibers leads to a faster uncoiling of collagen and stiffening of the tissue. Note that the fiber orientation associated with thickness changes occurring in the biaxial experiments might also contribute to stiffening and energy dissipation. In Chapter 2, the medium strain stiffness of the intact fetal membrane was shown to be similarly affected by repeated cycles under biaxial tension and a rapid uncoil and stretch of collagen bundles was observed in the spongy layer at low strain.

During uniaxial tension tests, low energy but non recoverable phenomena, like fiber orientation and bundling, seem predominant instead. It has been shown that amnion is characterized by an extraordinarily large Poisson's ratio and lateral contraction [59, 64] never observed in other biological materials. The present uniaxial tests confirm this finding, demonstrate the high reproducibility of the kinematic response and show how the lateral contraction evolves during cycles (Figure 3.13). Similarly to the tension-stretch response, the first loading cycle also determines the greatest changes in the lateral contraction, in particular in the cumulated residual lateral stretch and reduction of the incremental Poisson's ratio, which stabilizes in the following cycles (Figure 3.13). Moreover, amnion significantly deforms in the lateral direction already at low tension levels in the preload phase (Figure 3.13). Contraction of amnion seems to be associated with very low deformation energy and is due to water expulsion and collagen fiber bundling.

In situ inflation and uniaxial experiments provide meaningful information about thickness changes associated with water flow during cyclic loading of fresh and unfixed amnion. Amnion thickness was evaluated excluding the spongy layer and its values are consistent with previous studies [13, 27]. Both in the inflation and uniaxial configuration, amnion undergoes a strong thickness and

volume reduction during the first loading cycle, followed by partial recovery and stabilization during cycles (Figure 3.14). In particular, under biaxial tension amnion shows a significant thickness/volume reduction in the preload phase, the collapse of the compact layer at maximum load and an increase in thickness of the fibroblast layer when unloaded to the reference pressure (Figure 3.14). While thickness is retrieved, the volume is not fully recovered under uniaxial loading due to the residual lateral contraction (Figure 3.14c). The reversible collapse of collagen in the thickness direction seems to be the main mechanism activated during inflation, since in-plane collagen rotation and tissue contraction are constrained. On the contrary, collagen alignment and bundling in the membrane plane and collagen collapse in the thickness direction act simultaneously under uniaxial tension. The different in-plane (non-recoverable lateral contraction) and out-of-plane (recoverable thickness) mechanisms confirm that amnion is a transversely isotropic material.

Lake and Barocas [101] have shown that uniaxial stretching of collagen gels determines large volume changes, corresponding to high apparent Poisson's ratios and fibers alignment. Similar phenomena have been observed in fibrin networks, even though associated with different molecular mechanisms [102]. In our previous study on the time-dependent behavior of human amnion, we have shown similar volume reduction during the loading phase and the short-term relaxation phase of amnion, no significant volume change and collagen orientation during the long term relaxation, and recovery of 80% of the volume after unloading [64]. Thickness increase in the deflation phase might be associated with damage of collagen structures in the fibroblast layer, as observed after cyclic inflation of the intact membrane (Chapter 2).

Despite the large scatter, measurements of collagen orientation from SHG images indicated a clear difference between uniaxial and biaxial loading (Figure 3.15). Kinematic constraints allow modest fiber reorientation under biaxial loading, while collagen significantly aligns in the loading direction under uniaxial tension (Figure 3.15). The resolution of the microscope images does not allow to quantify collagen damage and recoil as a consequence of repeated loading and unloading. However, the persistent and progressive alignment of fiber during uniaxial cycles suggests that collagen structures preserve their ability to extend and orient, as observed by Thorpe et al. for tendons [103].

## 3.6 Conclusion

The mechanical behavior of human amnion subjected to cyclic loading in biaxial and uniaxial state of tension has been characterized. In situ experiments provides insights into the microstructural mechanisms determining the history-dependent response of amnion. Repeated inflation leads to significant but reversible changes in the thickness direction associated with water flow and characterized by high energy dissipation. Under uniaxial tension, instead, low energy and unrecoverable in-plane phenomena, i.e. fiber reorientation and lateral contraction, are predominant and lead to a significant volume reduction. These results confirm that biaxial cyclic loading might affect the integrity of amnion, while the fiber reorientation and reduction of volume under uniaxial stress might contribute to the resistance to deformation in the vicinity of defects, and thus to the defect-tolerance of this tissue when exposed to repeated loading.

Chapter 4

# Towards sealing of the fetal membrane

## 4.1 Introduction

The iatrogenic preterm premature rupture of fetal membranes (iPPROM) remains the main complication after invasive interventions into the intra-uterine cavity and limits the application of promising procedures for the treatment of fetal pathologies. In order to overcome the lack of healing response in the fetal membrane and prevent iPPROM, several sealants have been proposed and evaluated for the repair of the tissue in the last decades, e.g. fibrin glue, platelet-rich plasma, commercially available surgical sealants, collagen plugs and biologically inspired sealing materials [28]. However, despite the promising sealing performances observed in ex vivo experiments and animal models, no method for artificial sealing of the membrane after invasive intervention has made it into clinical practice yet [28].

The group of Prof. Messersmith (University of California, Berkeley, USA) has developed a mussel-mimetic tissue adhesive (mussel glue) as a potential candidate for fetal membrane sealing. The glue is based on a branched poly(ethylene glycol) (PEG) functionalized with the 3,4 dihydroxyphenylalanine (DOPA) catechol [104]. This rare amino acid residue is present in high concentration in mussel foot proteins and has both a cohesive (cross-linking under oxidizing conditions) and adhesive function, allowing adhesion to all types of inorganic and organic surfaces in a wet environment [105]. Mussel glue (cPEG) was found to be non-cytotoxic in vitro [106] and stable in presence of collagenase, plasmin and amniotic fluid [42]. Haller et al. showed that mussel glue effectively seals the fetal membrane ex vivo under wet conditions, allowing for burst pressures of the repaired tissue comparable to values measured during normal contractions (48.6 ± 18.4 mbar) [42] (Chapter 2). Mussel glue was also successfully applied for in vivo sealing of fetal membrane defects in a rabbit model [43].

Together with chemical stability and sealing properties, the mechanical compatibility of the sealant and the membrane has to be taken into account in view of the clinical application. The mechanical characteristics of the glue should bring a trade-off between strength, compliance and toughness in order to (i) reduce the stress concentrations at the defect, (ii) follow the deformation of the membrane, thus minimizing shear stresses at the interface and (iii) tolerate repeated and acute stretch [60]. The shape of the glue plug and its adhesion to the tissue also play an important role in this context. The application of a mussel glue patch was shown to reduce stresses at the defect edge [60] and the cPEG glue was found to match the stiffness of fetal membrane at low strain [107]. However, the sealant breaks as a brittle material when a critical state of deformation is reached [60, 107].

The group of Prof. Messersmith has recently developed a new mussel-inspired adhesive, the catechol-modified Tetronic (cT), based on a branched amphiphilic PPO-PEO (poly(propylene

oxide)-poly(ethylene oxide)) block copolymer. cT is characterized by a transition of the PPO domains from hydrophilic to hydrophobic when warmed up from room temperature to 37°C. These structural changes lead to toughening of the polymeric network [108]. Barret et al. showed that cT is significantly more deformable and tougher than cPEG and therefore a promising candidate for fetal membrane sealing [108].

In this work, experiments and finite element simulations have been performed in order to compare and qualify the cT and cPEG glues as possible sealants for fetal membrane repair. A standardized protocol for the application of a glue patch on the membrane was defined. Inflation tests (monotonic and cyclic) were carried out in order to investigate the effect of fast loading and repeated stretching on the sealing performance of the glues. Finite element simulations of inflated synthetic membranes (intact, defective and sealed) were performed in order to compare the performance of cT and cPEG under large deformations, when tightly adherent to the substrate.

This study has been conducted in collaboration with the group of Prof. Messersmith (University of California, Berkeley, USA) and the finite element models were realized in cooperation with Manfred Maurer.

## 4.2 Methods: experiments

A standardized protocol for the application of a glue patch with well-defined dimensions and shape was developed. Monotonic and cyclic inflation tests of fetal membranes repaired with cT and cPEG were performed in order to investigate the effect of fast loading and repeated stretching on the sealing performance of cT and cPEG.

Inflation tests of VHB (very high bonding elastomer, 3M AG, Switzerland) membranes repaired with cT glue were carried out in order to compare the sealing properties of cT to cPEG, which was previously tested on highly deformable membranes by Haller et al. [107]. For this purpose, experiments were performed according to the protocol proposed by Haller et al. for inflation tests of VHB repaired with cPEG glue [107].

### 4.2.1 Glue preparation and application

A mold (round mold) was designed to obtain glue plugs with smooth edges and fixed dimensions (Figure 4.1a). The mold was manufactured in polytetrafluoroethylene, with a central opening allowing the injection of the glue (Figure 4.1a and b). For the application of the glue plug, the

mold was greased and positioned on the specimen aligning the opening with the defect. The glue was prepared according to Table 4-1 by mixing the sodium periodate (in water) and the precursor solution (in 2x PBS with 0.01% wt brilliant blue) with a pipette. 150 µl of mixture were poured in the mold before gelation started and the gel was left to cure and stabilize in a humid environment for 15 (cT) or 10 (cPEG) minutes.

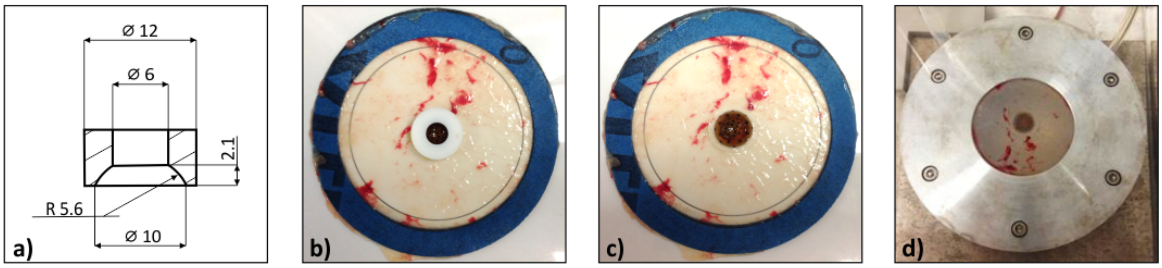


Figure 4.1 Protocol for the application of the glue. a) Mechanical drawing of the mold (round mold); b) mold filled with glue positioned in the center of a defective sample of fetal membrane; c) sample with glue plug after the removal of the mold; d) repaired sample mounted in the inflation device (amnion and plug downwards).

Table 4-1 Amounts and concentrations of the components for the preparation of the cT and cPEG glue.

| Glue | Concentration of precursor (in 2x PBS) | Amount of precursor (in 2x PBS) | Concentration of $NaIO_4$ (in water) | Amount of $NaIO_4$ (in water) |
|---|---|---|---|---|
| **cT 150 mg/ml** | 171.5 mg/ml | 145.8 µl | 32 mg/ml | 20.8 µl |
| **cT 175 mg/ml** | 200 mg/ml | 150 µl | 37.3 mg/ml | 21.4 µl |
| **cPEG 150 mg/ml** | 300 mg/ml | 80 µl | 12 mg/ml | 80 µl |

### 4.2.2 Inflation device

In order to perform inflation tests at physiological temperature (37°C), the inflation device described in Chapter 2 was equipped with a heating system consisting of a pump (Phobya DC12-260 12 Volt Pump), a heating tube and a temperature sensor connected to a control box (Figure 4.2). The system allows for the circulation of heated water in the bath containing the inflation cylinder, as well as the control and steadiness of the temperature. Connecting the tube of the peristaltic pump to the bath, samples could also be inflated with the same warm solution.

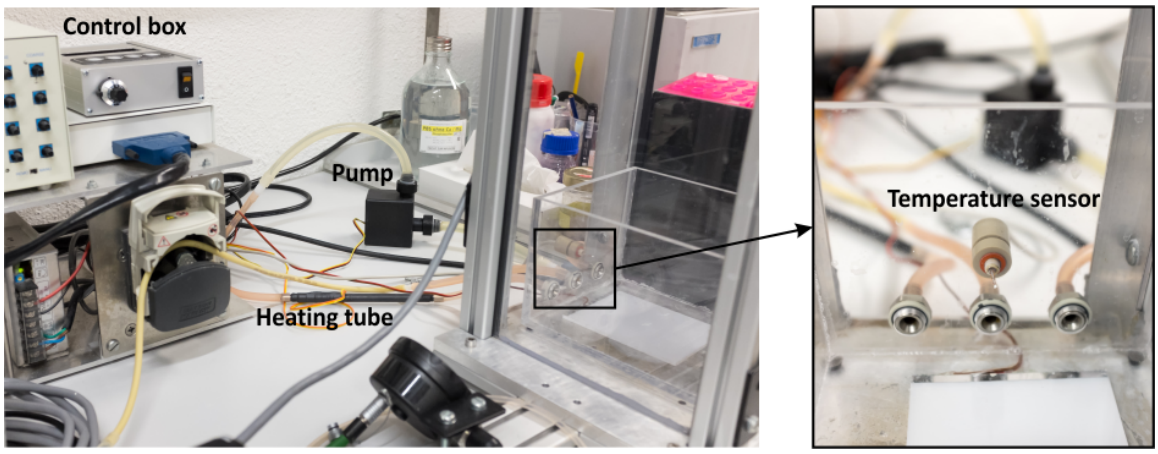


Figure 4.2 Heating system of the inflation device (zoom on the temperature sensor and in/out flow tubes).

### 4.2.3 Fetal membrane

*Sample preparation*

Fetal membranes (n=8) were collected from patients who underwent elective cesarean section between the 38$^{th}$ and the 40$^{th}$ week of gestation, according to the criteria described in paragraph 2.2.5. Soon after the delivery, the membrane was cut at about 2 cm from the placental border and placed on a plastic mat for the harvesting of samples. Specimens were cut using sand paper rings with ≈50 mm inner and 70 mm outer diameter glued on both sides (Figure 4.1b and c) and washed in PBS. Defects were created by placing the samples between the cylinder and the plate of the inflation device (in the bath filled with PBS) and puncturing them in the center with a 3.8 mm trocar. Even if manual, this procedure was repeated consistently by orienting the trocar perpendicular to the tissue and puncturing it as fast as possible. However, the shape and dimension of the defect varies among samples (Figure 4.3). Defective samples were placed on a plastic sheet previously greased with the amnion facing up and dried around the defect. The mold was positioned on the specimen and the glue applied as described in 4.2.1 (Figure 4.1b). After curing, the mold was removed (Figure 4.1c), samples were gently lifted from the plastic sheet and incubated in PBS at 37°C for 1 hour.

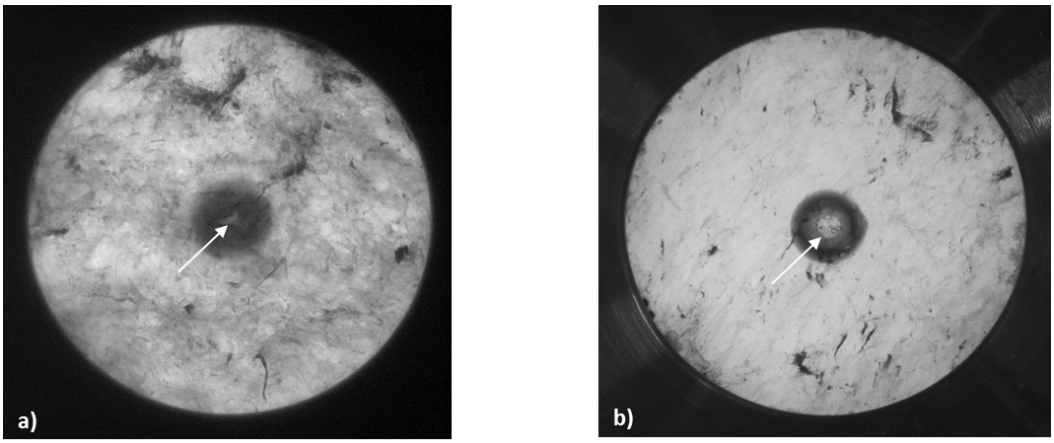


Figure 4.3 Repaired samples of fetal membrane mounted in the inflation device. a) Specimen with a star-shaped defect; b) specimen with elliptical defect. Arrow: defect.

*Inflation tests*

Specimens were clamped in the bath filled with preheated PBS with the amnion (and the glue) facing downwards (Figure 4.1d). Tests were performed according to three different protocols:

- monotonic tests: samples were inflated to rupture at a constant flow rate of about 12 ml/min;
- cyclic tests with low preload pressure (cyclicL): specimens were preloaded to 0.5 mbar in 20 seconds and then cyclically inflated at increasing levels of pressure every five cycles until rupture (Figure 4.4). The maximum pressure was increased by 10 mmHg (starting from 10 mmHg) for each group of cycles, while duration (1 minute) and relaxation time between cycles (2 minutes) were kept constant;
- cyclic tests with high preload pressure (cyclicH): specimens were preloaded to 1 mbar in 20 seconds, thus leading to a higher preload speed, and then cyclically loaded as described above (Figure 4.4).

Pressure values, top and side pictures were acquired at 2 Hz during monotonic tests and 1 Hz during cyclic tests. For each protocol, three samples repaired with cT (concentration of the glue equal to 150 mg/ml for monotonic and cyclicH tests, and 175 mg/ml for cyclicL tests) and cPEG were tested, respectively.

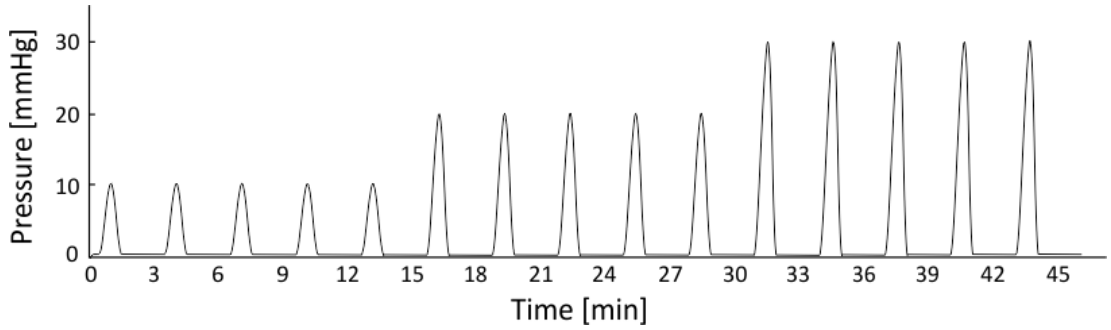


Figure 4.4 Pressure profile applied during cyclic tests.

*Analysis of results*

The sealing performance of the glues and the effect of cyclic loading and preload speed were investigated. The failure of repaired samples was visualized in the top pictures and associated with the rupture of the membrane or the glue. The average critical pressures reached at rupture in the three types of tests (monotonic, cyclicL and cyclicH) were analyzed by two-sample Kolmogorov-Smirnov tests in order to assess the significance of differences between the groups ($p < 0.05$ was considered statistically significant).

### 4.2.4 VHB

*Sample preparation*

Specimens with 70 mm diameter were harvested from VHB membranes of 1 mm thickness, glued on both sides to protective plastic sheets. The top layer was removed and samples were positioned on a plastic mat showing the contour and the center of the specimen. Defects were created in the center of the membrane using a punch device with 3 mm diameter, leaving the protective sheet intact in order to avoid leakage of glue through the defect. The cT glue (150 mg/ml) was applied using the mold described in 4.2.1 (round mold, Figure 4.1a) as well as a cylindrical mold with 10 mm diameter. In both cases, 150 µl of glue were poured into the mold. After 15 minutes of curing, the mold was removed, the protective sheet was gently separated from the VHB membrane and samples were incubated in PBS at 37°C for 1 hour.

*Inflation tests*

Specimens were clamped in the bath filled with preheated PBS with the glue facing upwards. Speed controlled monotonic tests (n=3 for each mold) were performed inflating samples at a constant flow rate of about 12 ml/min until leakage through the defect was observed. Pressure values, top and side pictures were acquired at 2 Hz during testing.

*Analysis of results*

The deformation of the glue in the defect (glue strain) and the plug (plug strain) were evaluated by measuring their diameter (D) in the top and side images recorded right before visible detachment of the plug, respectively (Figure 4.5). The glue strain and the plug strain were calculated as $D/D_0$-1, where $D_0$ is the diameter in the undeformed configuration. Results were compared with the data reported by Haller et al. [107] for 1 mm VHB membranes repaired with cPEG applied with the cylindrical mold.

Strain values were analyzed by two-sample Kolmogorov-Smirnov tests in order to assess the significance of differences between cT plugs with different shapes (round mold and cylindrical mold) and between cT and cPEG ($p < 0.05$ was considered statistically significant).

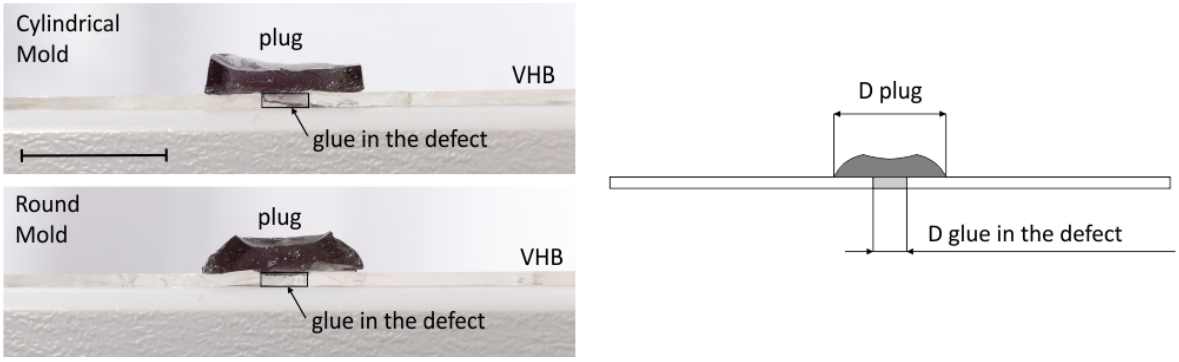


Figure 4.5 Cross-sections of glue plugs applied on defective VHB membranes (left) with the cylindrical mold (top) and the round mold (bottom). Images were taken after testing, therefore the glue results damaged in the defect. The diameter (D) of the plug and the glue in the defect (right) were measured in order to evaluate the plug strain and the glue strain. Scale bar: 10 mm.

## 4.3 Methods: simulations

An axisymmetric model representing a circular sample of VHB (thickness=1 mm, radius=25 mm), intact or with a 3 mm diameter defect, and a glue plug was built in the commercial finite element software ABAQUS 6.10-1 (Abaqus Inc. RI, USA) (Figure 4.7). The geometry of the plug (round mold) was extracted from images of the cross-sections of sealed samples (Figure 4.5, left) and reconstructed in ABAQUS by Tom Reuter (ETH Zurich). The VHB membrane was modeled with the Yeoh hyperelastic formulation proposed by Buerzle [60]. The cT and cPEG glues were modeled with a Mooney-Rivlin formulation, which was found to well describe the material behavior under compression (Figure 4.6). Stress-strain data from compression tests of cT (150 mg/ml) and cPEG were obtained from the laboratory of Prof. Messersmith [108] (Figure 4.6). The resulting material parameters are reported in Figure 4.6.

Both parts were meshed with quadrilateral 8-node axisymmetric hybrid elements (CAX8H), while the clamping ring was modeled as a rigid body with rounded edge (r=1 mm). No relative sliding was allowed between the glue and the membrane (rough tangential contact and hard normal contact), whereas frictionless tangential and hard normal contacts were defined at the clamping. Inflation was simulated by applying uniform pressure on the underside surface of the membrane and the glue (Figure 4.7).

Five configurations were compared at the same pressure level (P=16 mbar):

- intact membrane (Figure 4.7a);
- defective membrane (Figure 4.7b);
- defective membrane sealed with glue in the defect (Figure 4.7c);
- defective membrane sealed with glue in the defect and plug on the top surface (Figure 4.7d),
- defective membrane sealed with glue in the defect and plug on the underside surface (Figure 4.7e).

The diameter of the defect in the repaired membranes (Figure 4.7c, d and e) was compared to the value obtained for the defective membrane at P=16 mbar (Figure 4.7b). The maximum principal stresses were extracted in all the repaired ($\sigma^{r}_{max}$), intact ($\sigma^{i}_{max}$) and defective ($\sigma^{d}_{max}$) membranes. The stresses obtained in the repaired membranes at P=16 mbar were compared to the values in the intact ($k_{intact} = \sigma^{r}_{max}/\sigma^{i}_{max}$) and defective membrane ($k_{defective} = \sigma^{r}_{max}/\sigma^{d}_{max}$), respectively. Values of $k_{intact}$ and $k_{defective} \geq 1$ indicate an increase in maximum principal stresses, whereas $k_{intact}$ and $k_{defective} < 1$ points at a decrease. Moreover, shear stresses at the interface membrane-plug were evaluated for the top and inverted sealing configuration (Figure 4.7d and e).

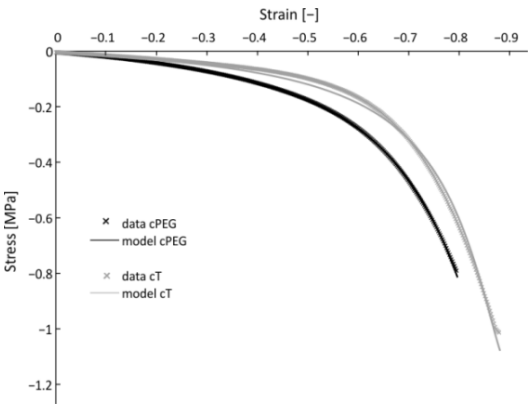


| Mooney-Rivlin model parameters | cT | cPEG |
|---|---|---|
| $C_{10}$ [MPa] | 0.017 | 0.029 |
| $C_{01}$ [MPa] | 0.00108 | 0.00241 |
| $D_1$ [MPa] | 0 | 0 |

Figure 4.6 Stress-strain curves (left) obtained from compression tests of cT and cPEG fitted with the Mooney-Rivlin model (parameters on the right).

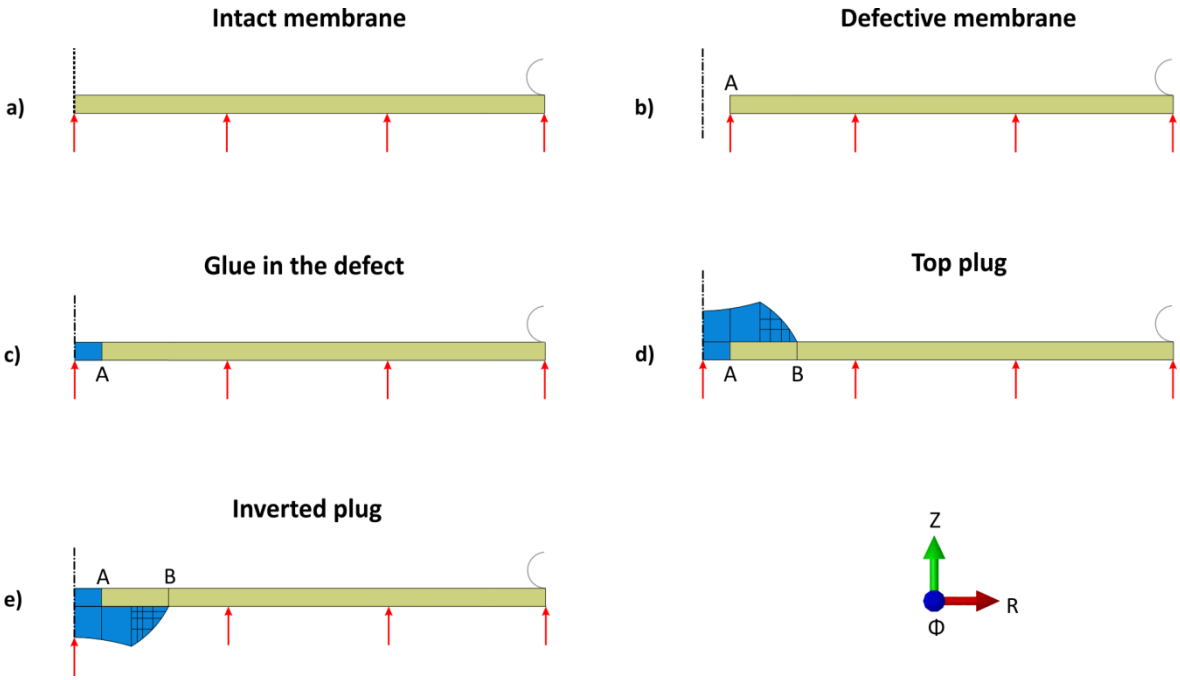


Figure 4.7 Model of intact, defective and repaired membranes (yellow) with a glue plug (blue). a) Intact membrane; b) defective membrane; c) membrane with glue in the defect; d) membrane with glue in the defect and plug on top (geometry of the round mold); e) membrane with glue in the defect and plug on the underside surface (geometry of the round mold). Red arrows: applied pressure; dashed line: axis of symmetry; grey arc: clamping; A: defect edge; B: border of the plug.

## 4.4 Results

### 4.4.1 Sealing of the fetal membrane

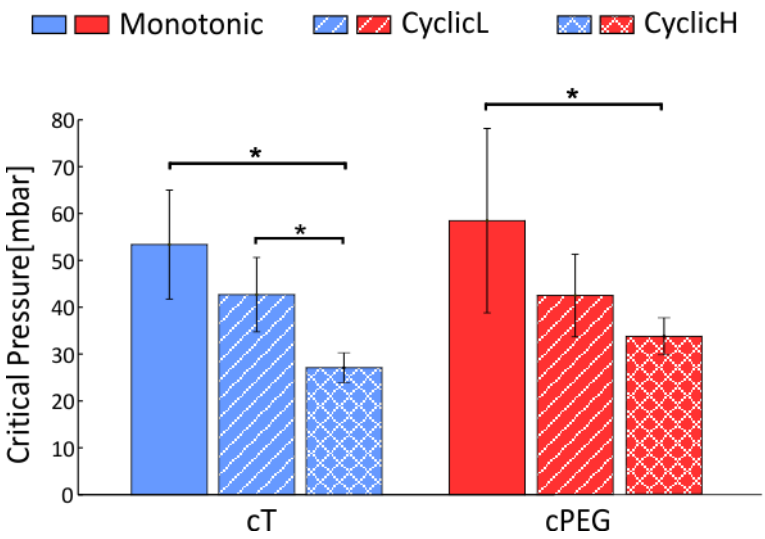


Figure 4.8 Critical pressures archived in monotonic tests (Monotonic), cyclic tests with low preload pressure (CyclicL), cyclic tests with high preload pressure (cyclicH); *p<0.05.

*cT vs cPEG*

Plugs of cT and cPEG glue were applied on the amniotic side of defective fetal membrane samples and their sealing performances were assessed during inflation to burst tests. The glues allow for critical pressures of 54.4 ± 11.6 mbar (cT) and 58.5 ± 19.6 mbar (cPEG) (Figure 4.8, Monotonic), without visible leakage of fluid through the defect during inflation. However, the failure process differs between the two sealants. In specimens sealed with cT glue, a crack propagates in the amnion starting from the defect edge, while the plug stays intact and in contact with chorion, which ruptures after further inflation (Figure 4.9, cT). In samples repaired with cPEG glue, the plug suddenly breaks at the defect, allowing leakage of solution, while amnion and chorion remain attached (Figure 4.9, cPEG).

*Effect of cyclic loading*

Repaired samples of fetal membrane were cyclically inflated in steps of five cycles with increasing amplitude (Figure 4.4). For both glues, the critical pressure decreases under repeated loading (cT: 42.7 ± 7.9 mbar, cPEG: 42.5 ± 8.8 mbar), even though not significantly when compared to monotonic tests (Figure 4.8, cyclicL). The rupture process of the two glues does not change during cyclic tests (Figure 4.9).

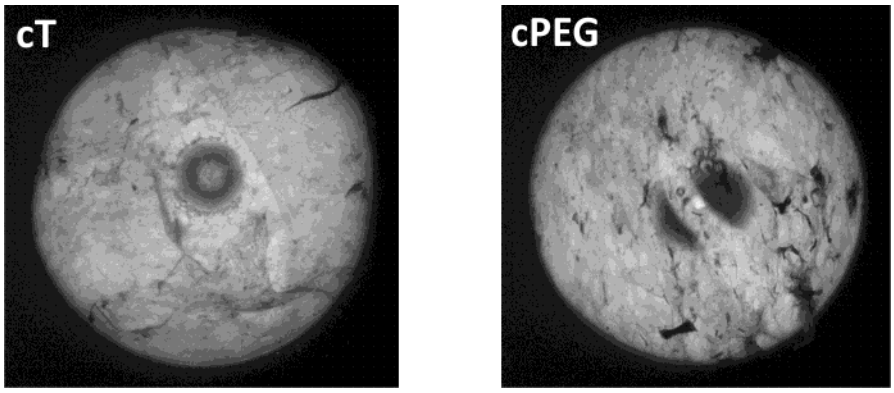


Figure 4.9 Rupture process during monotonic tests of fetal membrane specimens sealed with cT (left) and cPEG (right).

*Effect of preload speed*

Another set of cyclic experiments (cyclicH) was performed preloading the specimens at a higher pressure level (1 mbar) compared to cyclicL (0.5 mbar), but in the same time (20 seconds). The preload speed does affect the sealing performance of the two glues, resulting in a lower critical pressure (cT: 27.3 ± 3.2 mbar, cPEG: 34 ± 4 mbar) compared to monotonic tests ($p<0.05$) and cyclicL tests ($p<0.05$ for cT) (Figure 4.8). Moreover, the failure mode of samples repaired with cPEG changes as a consequence of the faster preload, being similar to the one observed in membranes sealed with cT (Figure 4.9).

### 4.4.2 Sealing of VHB

Inflation tests of punctured and repaired VHB samples were performed in order to assess the sealing performance of the cT glue on a highly deformable membrane and compare it with cPEG (data from [107]). During inflation, the glue in the defect deforms while fully attached through the thickness of the membrane. On the contrary, the plug slowly detaches from the surface of VHB, starting from the border (Figure 4.10c and d). Eventually, PBS solution leaks through the defect because of the complete detachment of the plug. The test does not determine the rupture of the cT glue, while cPEG was shown to rupture through the defect [108]. Therefore the glue strain and plug strain of cT were measured before visible detachment of the plug and compared with the values obtained by Haller et al. before rupture of cPEG. The cT plug deforms significantly less than the cPEG plug (Figure 4.10a and b), independent of the shape and at similar levels of glue strain in the defect (Table 4-2). According to the corresponding finite element simulation (Figure 4.7d, Top plug), the diameter of a strongly adherent plug of cT (round mold) would increase by 107% when the glue in the defect reaches a strain of about 112%.

Table 4-2 Values of glue strain and plug strain obtained for VHB membrane repaired with cT (round and cylindrical mold) and cPEG (cylindrical mold, data from Haller et al. [107]). Mean ± standard deviation; *p<0.05 with respect to cT.

| | **cT Round mold** | **cT Cylindrical mold** | **cT Both molds** | **cPEG Cylindrical mold** |
|---|---|---|---|---|
| **Glue strain [%]** | 112 ± 82 | 75 ± 22 | 93 ± 57 | 87 ± 42 |
| **Plug Strain [%]** | 31 ± 11 | 28 ± 2 | 30 ± 7 | 43 ± 25* |

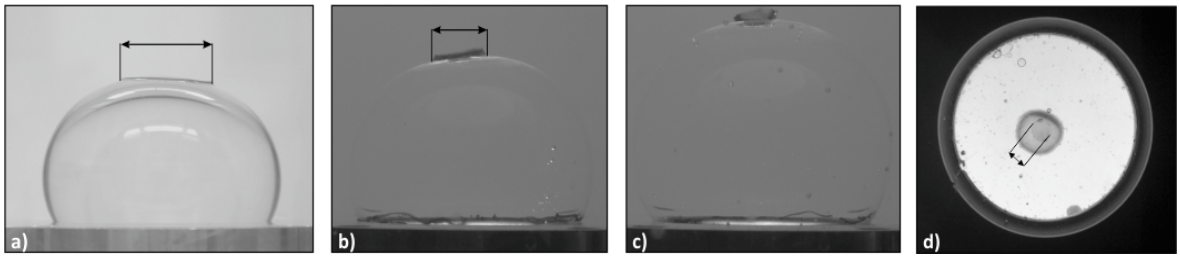


Figure 4.10 Inflated VHB membranes repaired with cPEG (a, before rupture, picture from Claudia Haller) and with cT (b, before detachment). The cT plug detaches from the substrate (c), while the glue in the defect deforms (d). Solid arrow: plug diameter; dashed arrow: defect diameter.

### 4.4.3 Simulations

Finite element simulations of inflated VHB membranes (intact, defective and sealed) were performed in order to compare the effectiveness of the cT and cPEG glue in preventing the opening of the defect and reducing the stress concentration in the membrane, given a perfect adhesion of the glue.

For both glues and all tested geometries, the diameter of repaired defect is smaller compared to the defective membrane without glue (Table 4-3). The presence of a glue plug on the top or the bottom of the membrane better prevents the opening of the defect (diameter about 50% smaller with respect to the defective membrane) compared to the application of the glue only in the defect (diameter about 55% to 60% smaller with respect to the defective membrane) (Table 4-3). , Compared to cT, cPEG reduces the defect size by about 4% more in the top and inverted configuration and 7% more with the glue only in the defect (Table 4-3).

Table 4-3 Ratio between the defect diameter in repaired and defective membranes at P=16 mbar.

| Glue | Glue in the defect | Top Plug | Inverted Plug |
|---|---|---|---|
| **cT** | 58% | 52% | 52% |
| **cPEG** | 54% | 50% | 50% |

In the defective membrane, stresses are concentrated at the edge of the defect (A, Figure 4.7b) and rapidly decrease in the far field (Figure 4.11). Sealing with a glue plug (top and inverted) modifies the distribution of stresses in the membrane, leading to their concentration at the border of the plug (B, Figure 4.7d and e, Figure 4.11), as well as values of $k_{defective} \geq 1$ for both glues (Table 4-4). On the contrary, the application of glue in the defect reduces stresses in the membrane at the defect edge (A, Figure 4.7b and c) by about 60% and 50% for cT and cPEG, respectively (Table 4-4 and Figure 4.11).

In the intact VHB, the maximum principal stress $\sigma^{i}_{max}$ is reached in the center of the membrane (under equibiaxial stress state) (Figure 4.11). Repairing the defective membrane does not restore the stress distribution obtained in the intact substrate, but leads to amplification of stresses (Figure 4.11). Sealing with a glue plug (top and inverted) leads to stress as 170%-190% higher than in the intact membrane (Table 4-5) and concentrated at the border of the plug (B, Figure 4.7d and e, Figure 4.11). The application of glue only in the defect slightly increases the stresses at the defect edge (A, Figure 4.7b and c), with values of $k_{intact}$ of 1.10 for cT and 1.29 for cPEG (Table 4-5).

Table 4-4 Values of $k_{defective} = \sigma^{r}_{max}/\sigma^{d}_{max}$ obtained at P=16 mbar.

| $k_{defective}$ [-] | cT | | | cPEG | | |
|---|---|---|---|---|---|---|
| | **Glue in the defect** | **Top plug** | **Inverted plug** | **Glue in the defect** | **Top plug** | **Inverted plug** |
| | 0.41 | 1.09 | 1.00 | 0.48 | 1.09 | 1.09 |

Table 4-5 Values of $k_{intact} = \sigma^{r}_{max}/\sigma^{i}_{max}$ obtained at P=16 mbar.

| $k_{intact}$ [-] | cT | | | cPEG | | |
|---|---|---|---|---|---|---|
| | **Glue in the defect** | **Top plug** | **Inverted plug** | **Glue in the defect** | **Top plug** | **Inverted plug** |
| | 1.10 | 2.93 | 2.68 | 1.29 | 2.93 | 2.93 |

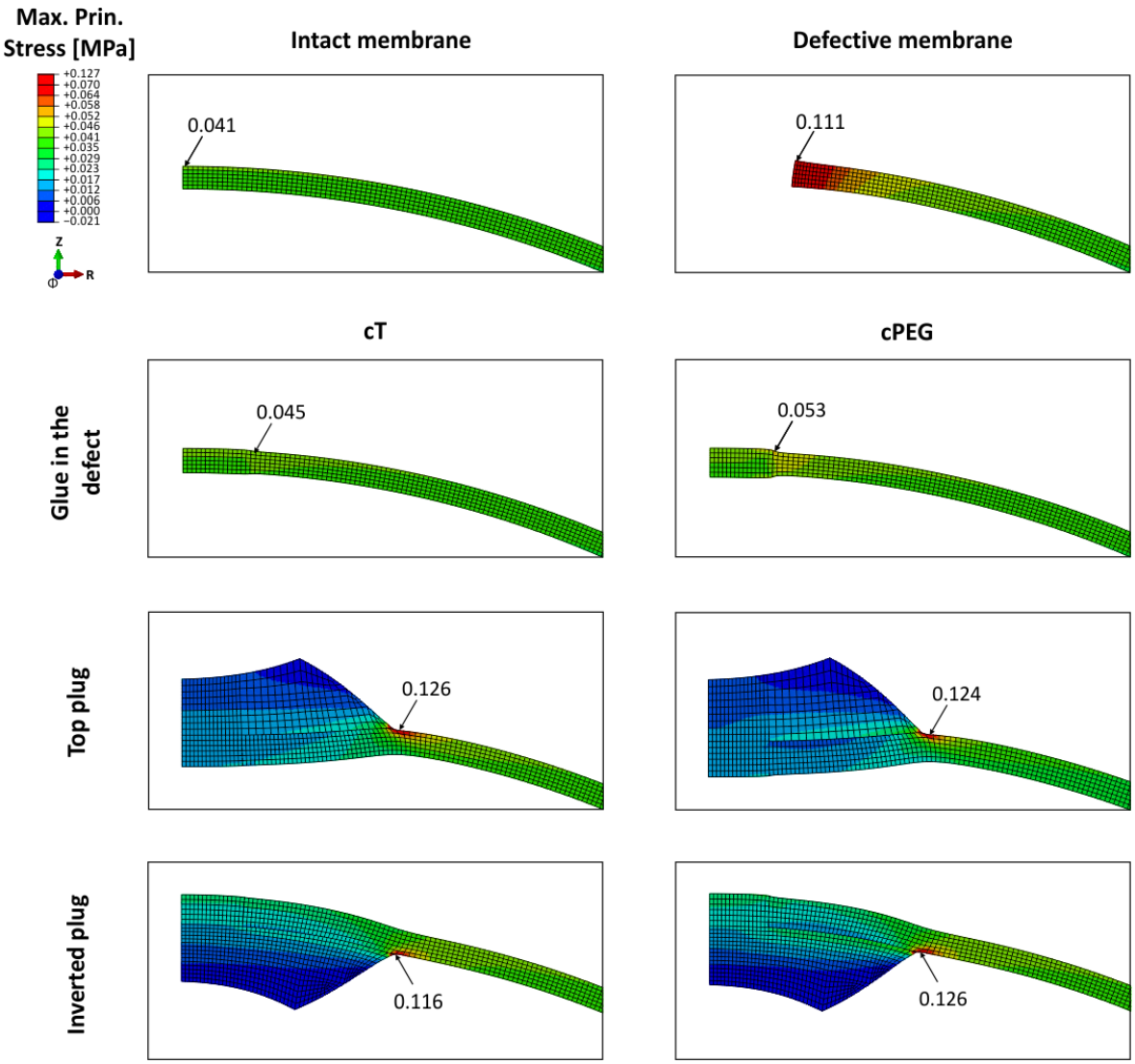


Figure 4.11 Maximum principal stresses in the intact, defective and repaired VHB membranes.

Figure 4.12 shows the distribution of shear stresses at the interface between the membrane and the glue plug in the top and inverted configuration. Shear stresses reach the maximum value at the border of the plug (B, Figure 4.7d and e) and rapidly decrease towards the defect (Figure 4.12). Stresses at the interface are about 15% lower for cT compared to cPEG (Figure 4.12), while the magnitude is similar in the top and inverted configuration for both glues. Overall, shear stresses are about 60% and 50% lower than maximum principal stresses at the border of the plug, for cT and cPEG, respectively.

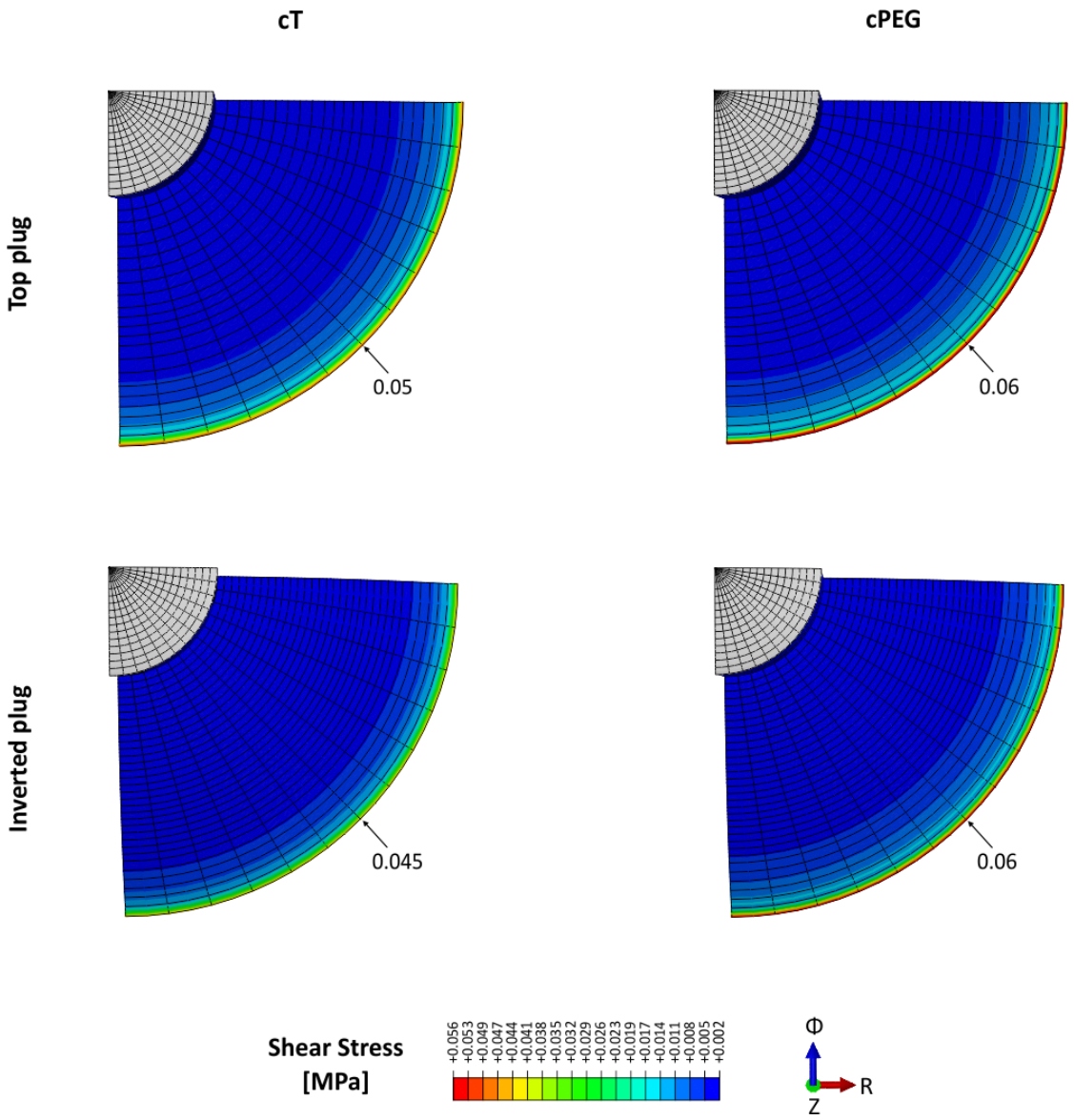


Figure 4.12 Shear stresses at the interface between the glue plug and the VHB membrane.

## 4.5 Discussion

This study aims at qualifying two catechol-modified synthetic glues as possible sealants for fetal membrane repair and offer guidelines for the development of sealing strategies preventing iPPROM.

Ex vivo inflation tests of defective and repaired fetal membranes have been performed in order to compare the sealing performance of the cT and cPEG glue under physiologically relevant environmental (37°C in saline solution) and mechanical (multiaxial stress state) conditions.

Incubation and testing of the cT glue at 37°C was shown to favor the transition of the PPO domains from hydrophilic to hydrophobic, thus toughening the network and improving the

mechanical properties of the glue [108]. On the contrary, the characteristics of the cPEG glue are not affected by temperature [108].

A standardized protocol was developed for the creation of the defect in the membrane and the application of the glue patch, thus allowing for repeatable testing conditions. However, punching the tissue with a star-shaped trocar (similar to the one used in clinical practice), results in the creation of defects with different shapes and dimensions, mainly depending on the thickness of the membrane. In fact, the inspection of punched specimens reveals star-shaped edges in membranes with a thick chorionic layer (Figure 4.3a) and bigger elliptical defects in samples with a thinner chorion (Figure 4.3b). This observation brings to light the role of chorion in the defect-tolerance of the membrane, thus motivating a future systematic investigation of the toughness of the fetal membrane in presence of defects, as well as the study of repair strategies on a more complex system, including the support of the uterine wall, as recently proposed by Mann et al. [44].

Applying the glue with a mold allowed for the creation of plugs with fixed dimensions and the penetration of the sealant through the defect without loss of material. The mold was designed in order to easily apply the glue through the opening and obtain plugs with smooth edges (round mold, Figure 4.1). Despite the standardization of these procedures, manually mixing the precursors might affect the reproducibility of the glue properties. The development of a device ensuring standardized mixing of the two solutions with a constant speed would provide a better control of this procedure.

Monotonic inflation tests reveal that both the cT and the cPEG glue seal the fetal membrane without completely restoring the integrity of the tissue (the critical pressure of the intact membrane was found to be 138 ± 40.3 mbar, Chapter 2) (Figure 4.8). Values of critical pressure are consistent with those reported by Haller et al. for fetal membranes repaired with mussel glue [42], despite the different sealing procedure. Haller et al. applied the glue on the chorion without a defined shape of the plug, but allowing infiltration of the sealant through the defect. The agreement of results suggests that (i) the penetration and integrity of the glue in the defect is essential for the efficacy of the sealing strategy, and (ii) cPEG breaks either at a critical loading state (on the fetal membrane) or at a critical deformation (on the VHB), depending on the stiffness of the substrate [107].

Despite a similar critical pressure, the failure process differs between the two sealants. The cT glue remains intact while a crack propagates in the amnion, starting from the edge of the defect (Figure 4.9, cT). On the contrary, the cPEG glue suddenly breaks at the defect site, while amnion and chorion remain attached (Figure 4.9, cPEG). The described process suggests a loss of adhesion, confirmed by experiments with VHB membranes (Figure 4.10).

Inflation tests of fetal membranes and VHB repaired with cT brought to light a different behavior of the Tetronic glue under normal (in the defect) and shear (at the interface between the plug and the substrate) stresses. The glue in the defect is able to withstand higher deformations than cPEG without breaking, confirming the higher deformability and strength of cT observed by Berret et al. in compression tests [108]. However, the upper portion of the plug detaches from the substrate under the effect of shear stresses. This result seems to be in contradiction with the stronger adhesion on decellularized porcine dermis of cT compared to cPEG reported by Berret et al. [108]. However, the adhesive strength of the glues on the fetal membrane should be investigated and quantified, as well as the level of deformation and shear stresses leading to the detachment of the glue.

Repeated mechanical loading – representative of physiological contractions at increasing amplitude – was shown to slightly reduce the critical pressure retained by membranes repaired with both glues, without changing the failure process (Figure 4.8). Given the high toughness and stability of the cT glue under cyclic compression [108], the decrease in failure pressure might be related with loss of adhesion during repeated loading. Concerning the cPEG glue, cyclic inflation might lead to the accumulation of residual deformation and reduction of toughness in the material.

The increase of loading speed was found to strongly affect the sealing performance, leading to the detachment of the plug for both glues, and thus the propagation of the defect in the amnion and a significant drop in critical pressure (Figure 4.8). According to the values of stretch reached in the intact membrane when preloaded at 1 mbar in 20 seconds (Chapter 3), in this phase the tissue deforms at a strain rate of 0.1%/s. The increase of loading speed was limited to the preload phase, from the slack configuration to the pressure of 1 mbar. In this loading phase (low tension), amnion was shown to undergo strong thickness reduction as well as lateral contraction under uniaxial tension (in the vicinity of the defect) (Chapter 3). These results point out that (i) the adhesion of cT and cPEG is strongly compromised by the fast activation of deformation mechanisms in the membrane and (ii) the definition of a meaningful reference configuration is not only crucial for the characterization of the membrane, but also for the evaluation of the sealing performance of glues. It should be noted that the glue plug was applied in the slack configuration, which differ from the physiological state of the tissue. It is not clear yet whether and by which amount the membrane is stretched in vivo, but it is supported by the uterus following its curvature. Repairing the slack membrane might introduce some artifacts in the behavior of the glue due to geometrical changes and the lack of in vivo residual stresses, released during extraction and preparation of the tissue. Therefore, the sealing performance should be

further investigated on pre-stretched membranes, as well as the effect of the reference configuration.

To summarize, the cT and cPEG are able to seal the fetal membrane, resisting pressures higher than the intra-uterine baseline (10 mmHg, Chapter 2). However, the sealing performance deteriorates under repeated mechanical load, representative of contractions, as well as under fast and acute deformation of the membrane, representative of impacts (e.g. fetus pushing). cPEG ruptures at a critical level of pressure and its adhesion to the substrate is compromised during fast loading. cT is able to withstand high deformations and pressures without failing, but loses adhesion under shear stresses.

It should be noted that the critical pressure provides limited information on the sealing performance of the glues, being affected by the structural integrity and quality of the plug as well as the variability among samples. The experimental investigation should be extended to a larger number of specimens, and the local deformation of the glue should be analyzed in order to evaluate the critical level of strain leading to rupture or detachment.

Fetoscopic interventions are usually performed between the first and the second trimester [34] and the membrane was shown to grow and distend during the following months of gestation [9, 10]. Therefore, the sealant should (i) accommodate the deformation without breaking or detaching, (ii) reduce stress concentrations, and (iii) adhere under shear stresses to a substrate undergoing a significant remodeling process and changes in stiffness (Chapter 1).

Finite element simulations of inflated VHB membranes repaired with cT and cPEG were performed in order to compare the performance of the two glues under large deformations, when tightly adherent to the substrate. Compared to the defective membrane, both glues significantly reduce the increase in size of the defect (Table 4-3). However, sealing with a glue plug (top and inverted, Figure 4.7d and e) leads to a concentration of stresses at the border of the plug, both in the membrane and at the interface, and does not restore the distribution of stresses present in the intact substrate (Figure 4.11). On the contrary, the presence of glue only in the defect (Figure 4.7c) significantly reduces the stresses at the defect edge (Figure 4.11). Being more compliant than cPEG (Figure 4.6), cT leads to lower stresses in the substrate and at the interface plug-membrane. However, despite the lower shear stresses, cT plugs were shown to detach from the surface of VHB during inflation, starting at the border of the plug, i.e. where stresses are concentrated (Figure 4.10).

It should be noted that amnion is stiffer than VHB and displays a different deformation behavior, characterized by an extraordinary lateral contraction in the vicinity of defects (Chapter 3). Therefore, finite element simulations of defective and repaired fetal membranes should be performed in order to evaluate the mechanical compatibility of the sealants and the membrane.

Despite a good knowledge of the constitutive behavior of amnion [59], some important aspects should be better understood in order to compare the sealing performance of cT and cPEG in a finite element model of the fetal membrane, i.e. (i) the effect of the reference configuration, (ii) the failure of adhesion on the epithelium, and (iii) the interaction between amnion and chorion.

The performed simulations point out that the application of a glue plug might lead to a concentration of stresses in the repaired tissue, thus reducing the benefits of sealing in the prevention of iPPROM. Therefore, the plug shape should be optimized in order to (i) reduce stresses in the membrane and at the interface, (ii) limit the opening of the defect, and (iii) match the deformation behavior of amnion as closely as possible. These aspects should be taken into account when moving from the ex vivo to the in vivo application of the sealant in pregnant women. Moreover, tools compatible with surgical sheaths should be developed in order to mix the precursors in a wet environment (amniotic fluid) and apply the glue on the amniotic side of the membrane with a defined shape.

## 4.6 Conclusion

Two catechol-modified synthetic glues, cT and cPEG, were qualified as possible sealants for fetal membrane repair. Their sealing performance was investigated under physiologically relevant environmental and mechanical conditions. Both glues allow for critical pressures higher than the intra-uterine baseline, but lose effectiveness under repeated mechanical load, representative of contractions, as well as under fast and acute deformation of the membrane, representative of impacts.

The cT glue withstands high deformations and pressures without breaking, but loses adhesion under shear stresses, thus allowing the rupture of amnion. However, when fully adherent, it leads to lower stresses in defective synthetic membranes compared to cPEG. Its higher deformability and toughness make the Tetronic glue (cT) a promising candidate for fetal membrane repair, provided an improved mechanical response and adhesion to the membrane under shear stresses is achieved.

Chapter 5

# Development of an experimental setup for dynamic cell culture

## 5.1 Introduction

The healing potential of the fetal membrane after fetoscopic interventions and amniocentesis was shown to be very limited [28]. However, amnion contains cells within the epithelial and mesenchymal fractions which have large proliferation potential and can give rise to multiple cell types [109]. Cell monolayers obtained from amnion-derived cell lines were found to be capable of repairing a central microsurgical defect [110]. The repair could be stimulated by increasing levels of epidermal growth factor and insulin-like growth factor-I in the culture medium [28]. The repair capacity of these monolayers was found to be dependent on gestational age, with cells obtained at earlier gestational ages showing higher proliferation rates and faster closure of the defect [28]. Therefore, the combination of biomaterials with appropriate in vivo stability and biological signals able to promote amniotic cells recruitment, proliferation and extracellular matrix production would likely promote the healing of fetal membranes, especially in the first half of the pregnancy, when fetoscopic interventions are performed.

Based on the hypothesis that cell-instructive scaffolds can induce healing, many attempts have been made to repair the tissue and prevent iPPROM with strategies relying on naturally occurring materials [28], i.e. decellularized human amnion membranes [37, 38], collagen [39] and fibrin sealants [41]. Although these strategies showed potential for sealing, healing was limited by the poor proteolytic stability of the materials and insufficient mobilization of cells.

A synthetic, polyethylene(glycol)-based (PEG-based) cell-instructive matrix including some properties of the naturally derived extracellular matrix (ECM), i.e. factor XIII (FXIII)-mediated cross-linking and growth factor immobilization, has been developed in the Ehrbar's Lab [111, 112]. Using this PEG-based biomimetic matrices, a recent study showed that amniotic mesenchymal cells (AMCs) can be mobilized, induced to proliferate and supported in maintaining their native extracellular matrix production upon presentation of appropriate biological cues (growth factor and cytokines), thus creating a favorable environment for the healing response [113].

The goal of this study is to eventually establish a physiologically relevant in vitro amnion model to study factors which promote fetal membrane healing. Stretching plays an important role in ECM remodeling during growth and distention of the membrane [25], and therefore mechanical stimuli might promote the production of native extracellular matrix components in AMCs, fostering the healing process.

In this chapter, the development of an experimental setup for dynamic culture of AMCs-seeded PEG matrix and preliminary results are described. This work was conducted in collaboration with Anna-Sofia Kiveliö (Ehrbar's lab, USZ).

## 5.2 Experimental setup

Tissues are characterized by complex 3D architectures with heterogeneous distribution of cells, extracellular matrix components, as well as soluble and immobilized factors that, together with the complex in vivo loading conditions, determine the dynamic behavior of cells.

In the fetal membrane, and in particular in the amnion, mesenchymal cells are embedded in collagenous layers with different thicknesses and density [14], which are subjected to high multiaxial deformation during pregnancy. As discussed in Chapter 2, the inflation technique suitably reproduces the physiological loading state of the membrane. Therefore, the bioreactor for dynamic culture was inspired by the inflation device in order to reproduce the mechanical stimuli experienced in vivo by mesenchymal cells as closely as possible.

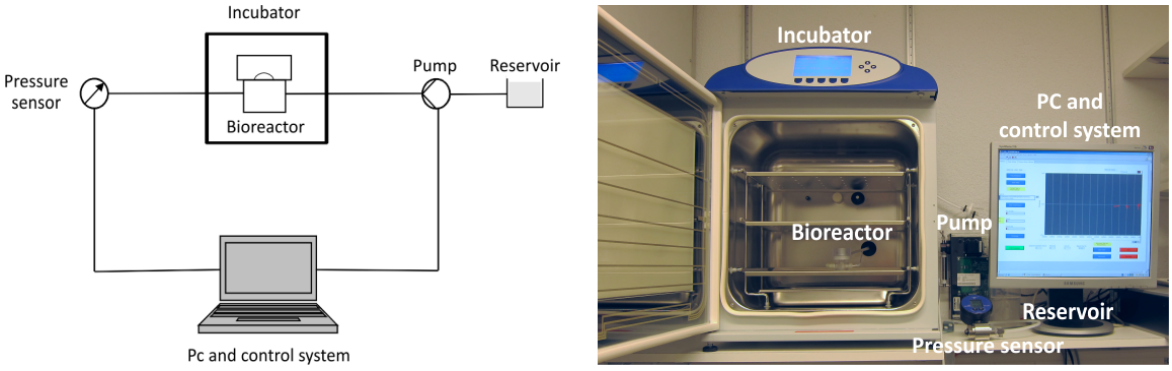


Figure 5.1 Setup for dynamic cell culture: representation of the main components and connections (left) and assembled system (right).

### 5.2.1 Requirements

In order to perform cell culture while applying dynamic loading, different requirements needed to be fulfilled in the development of the bioreactor and setup.

Culture of cells requires (i) the usage of non-toxic and sterilizable materials, (ii) small dimensions of samples to reduce the amount of cells and medium, and (iii) control of temperature and $CO_2$ levels.

The performance of repeated mechanical loading requires (i) the connection of the bioreactor to a pumping system, (ii) well defined boundary conditions for inflation, and (iii) an efficient clamping system and sealing.

The dimensions of the cylinder and the choice of transparent materials are also constrains for the positioning of the device in the microscope and the acquisition of images during experiments,

respectively. In order to apply mechanical load, it is also necessary to support cells with an elastomer membrane with suitable thickness and mechanical properties.

### 5.2.2 Components

The experimental setup for dynamic cell culture has been assembled in our laboratory at the University Hospital of Zurich. The setup consists of a bioreactor, placed in the incubator, connected to a syringe pump and a pressure sensor (Figure 5.1). The system is controlled with a custom-built Labview program (LabView 2008, National Instruments, USA) (Figure 5.1).

*The bioreactor*

The first prototype of the bioreactor has been designed to test one sample at a time and is composed of two parts: the cylinder (Figure 5.2a and b, Figure 5.3a) and the chamber (Figure 5.2c and d, Figure 5.3b). For the design of the cylinder, features of the inflation device presented in Chapter 2 have been reproduced in a smaller scale. The cylinder has an inflating area of 10 mm, is 25 mm tall and has two threaded holes for the connection with the pump and pressure sensor (Figure 5.2a and b, Figure 5.3a). Two small holes on top of the cylinder will host metal pins to guide the positioning and improve the stability of the sample (Figure 5.3a). The chamber has an opening of 16 mm diameter and 15 mm depth to contain the cell culture medium (Figure 5.2c and d, Figure 5.3b). The chamber also allows for the clamping of the sample when screwed on the cylinder (Figure 5.2a and c, Figure 5.3).

Both components of the bioreactor have been machined in polycarbonate (PC), a thermoplastic polymer stable at high temperature, with good optical properties (transparent when polished and non-fluorescent), that can be sterilized with ethanol[3]. The sealing of the system is ensured with a rubber ring positioned between the cylinder and the chamber, while stainless steel washers are used to define the geometry of the sample and the inflating area. The cytotoxicity of the materials has been tested and will be discussed in the next section.

[3] https://www.gordonbrush.com/documents/Cleaning%20Disinfecting%20and%20Sterilizing%20Plastics.pdf

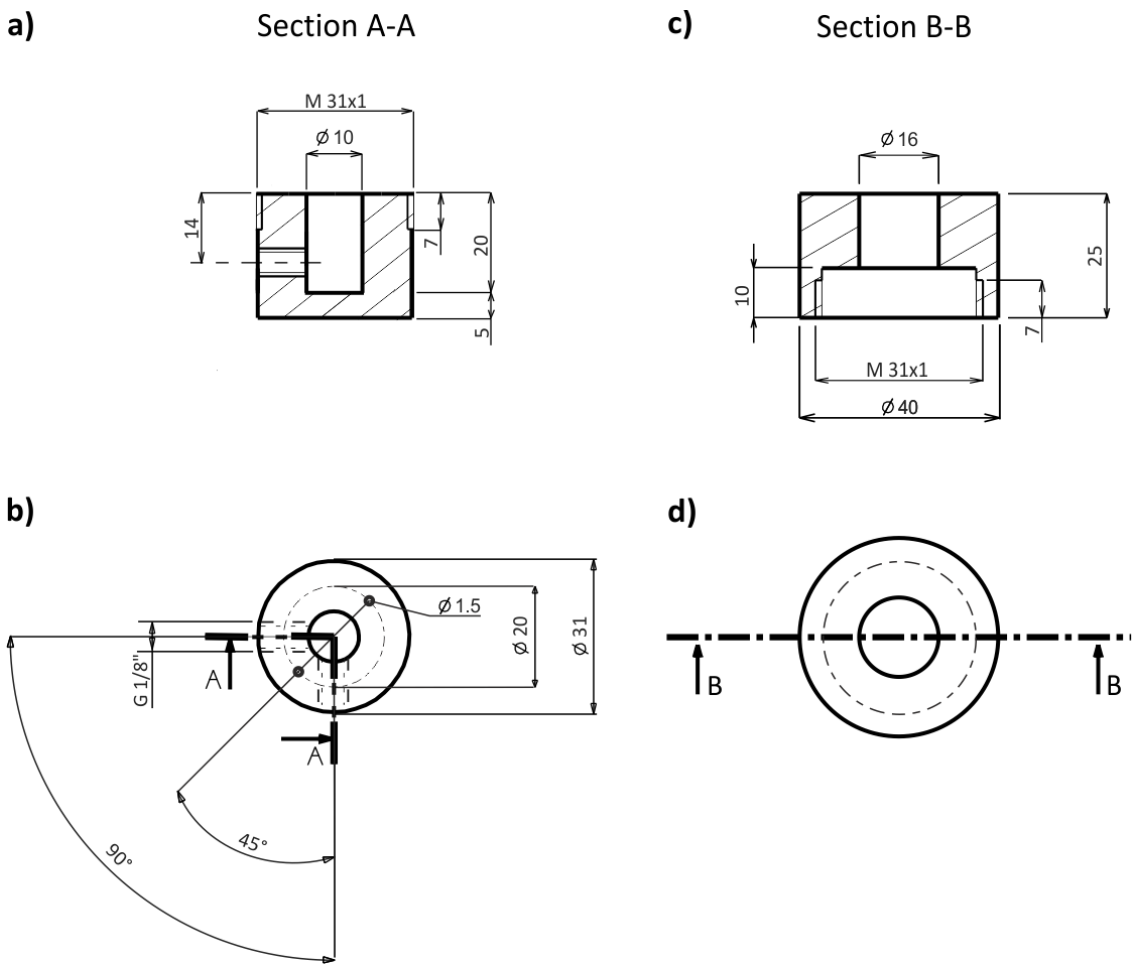


Figure 5.2 Mechanical drawing of the bioreactor. a) Section of the cylinder; b) top view of the cylinder; c) section of the chamber; d) top view of the chamber. Dimension in mm.

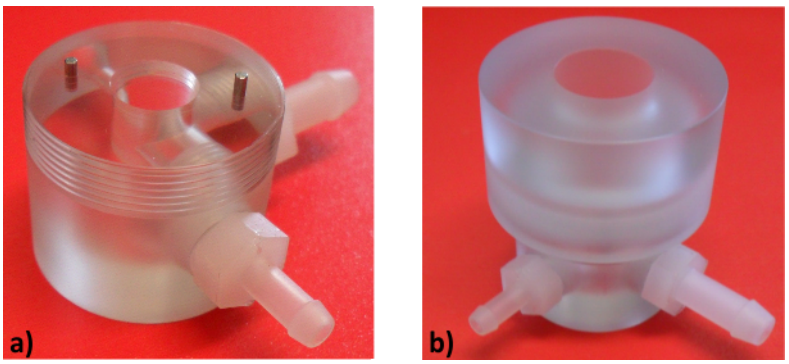


Figure 5.3 Bioreactor. a) Cylinder; b) cylinder and chamber assembled.

*Pump*

A syringe pump was selected in order to control the inflated volume and therefore the applied deformation. The PSD/8 (Precision Syringe Drive/8) syringe pump produced by Hamilton (Bonaduz, Switzerland) is a high precision device (precision of 0.05% of full stroke) controllable with Labview. The pump was completed with a 10 ml syringe and a "Y" valve, connected on one side to the reservoir and on the other to the bioreactor. The selected device allows for forty different speeds of load with volume steps of 3 µl.

*Pressure sensor*

A pressure sensor was introduced in the setup in order to read out the pressure in the cylinder and monitor the progression of the experiment. The Digital Manometer LEO Record (Keller, Switzerland), with a pressure range from -1 to 3 bar and a total error band of 0.1% of the full scale was selected. The interface converter K-114 converts the pressure and temperature signals from the sensor into a USB signal and sends them to the computer allowing for the visualization and saving of the data with Labview (maximum recording frequency of one data point per second).

*Incubator*

The bioreactor is located in the incubator in order to ensure stable environmental conditions suitable for cell culture (37 °C and 5% $CO_2$). The incubator Galaxy 48 R (New Brunswick, USA) is equipped with a 25 mm access port which allows for the insertion of the tubes connecting the cylinder with the pressure sensor and pump.

*Labview control system*

A labview code has been implemented to control the pump as well as read and save pressure data. An intuitive user interface has been designed in collaboration with Giovanni Bianchi (ETH Zurich) in order to access the commands and parameters necessary to run the experiments (Figure 5.4). The following commands are listed in the order they should be selected to run the experiment:

- pump initialization: set the zero position of the syringe;
- insert water: the syringe inserts water in the circuit and the cylinder to remove air bubbles;
- full syringe: fills the syringe with the volume of water selected for the inflation;

- start experiment: the pump starts to cyclically inject water into the bioreactor, while the program saves pressure data in a text file;
- stop pump: stops the pump (if necessary before the last cycle);
- empty the water: the water in the bioreactor, tubes and the syringe is sent back into the reservoir;
- stop: stops the labview program.

The parameters defining the experimental protocol can be selected in the user interface, i.e. number of cycles, speed (speed code from 1 to 40) and volume to inflate (in ml). The program also provides real-time information about the experiment, i.e. expected experimental time, current cycle and elapsed time.


Figure 5.4 Labview user interface.

### 5.2.3 Validation tests

The reliability of the setup was assessed performing cyclic inflation tests of PDMS (Polydimethylsiloxane) membranes prepared in house by Raoul Hopf (10:1 composition and 0.4 mm thickness). Tests were run to prove (i) the efficacy of clamping and sealing of the chamber, (ii) the repeatability of experiments and (iii) the long-term stability of the pump.

Samples (28 mm diameter) were positioned on the water-filled cylinder and fixed with a metal washer 1 mm thick. The chamber was then screwed on the cylinder to clamp the membrane. The inner diameter of the metal washer defines the inflating area and prevents the formation of wrinkles in the membrane during clamping. During inflation neither leakage of water nor slippage of the sample were observed (Figure 5.5a).

PDMS samples were inflated with different volumes of water for five cycles at the slowest flow rate (code 40 corresponding to 0.016 ml/s). Pressure curves from three specimens are shown in Figure 5.5b: curves show a perfect overlap in the loading and unloading phase of the five cycles.

The stability of the inflated volume was verified up to 3600 cycles with 0.2 ml of water inflated at 0.016 ml/s. The recorded pressure data indicate a good short-term and long-term stability of the inflated volume (Figure 5.5b and c).

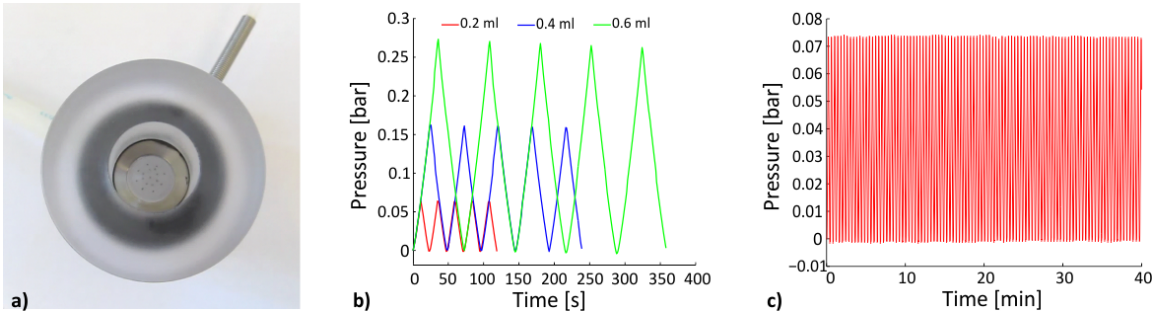


Figure 5.5 Validation of the setup. a) Clamping and sealing; b) repeatability of experiments; c) long term stability of the inflated volume.

## 5.3 Dynamic culture of the in vitro amnion model

A first in vitro amnion model, consisting of AMCs embedded in PEG gel, was developed and cultured under repeated stretching, while supported by a deformable membrane (Figure 5.6).

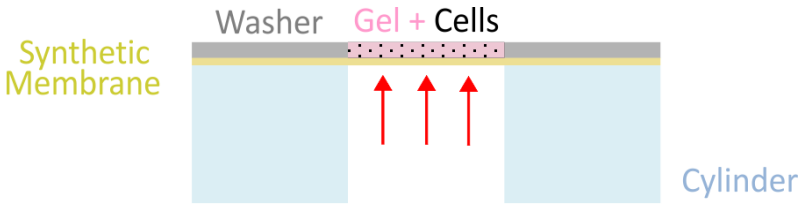


Figure 5.6 Representation of the in vitro amnion model in the bioreactor.

### 5.3.1 Membrane selection and characterization

Supporting the gel with a deformable membrane is essential to perform dynamic culture. In the selection of a synthetic substrate suitable for this application, some requirements were taken into account:

- stable mechanical behavior over thousands of loading cycles;
- uniform thickness and low thickness/inflation size ratio, thus providing equibiaxial stress state in the central part of the sample;
- material stable at high temperature (37°C), sterilizable and non-cytotoxic;
- material optically transparent, thus allowing for imaging with an inverted microscope.

The gloss/gloss non reinforced vulcanized silicone sheets (0.25 mm thickness) produced by SMI (Saginaw, USA) were found to fulfill all the listed requirements. In contrast to in house produced PDMS membranes, the industrial production guarantees uniformity in the thickness and material properties of the sheets.

*Mechanical characterization*

Inflation tests were performed with our custom-built inflation device (Chapter 2) in order to investigate and characterize the mechanical response of the material under repeated biaxial loading. The membrane was stretched applying pressure with a sinusoidal profile up to 35 mbar for 10 cycles of 1 minute each, followed by a monotonic loading. Markers were drawn onto the

membrane for the analysis of the local deformation and stress-biaxial strain curves were obtained as described in paragraphs 2.3.3 and 3.2.4 (stress=tension/thickness).

The membrane shows a non-linear, stable mechanical response during cyclic inflation, with a small and constant hysteresis (Figure 5.7, left). A similar behavior was also observed in pure shear tests over 200.000 cycles at 30% nominal strain performed in our laboratory.

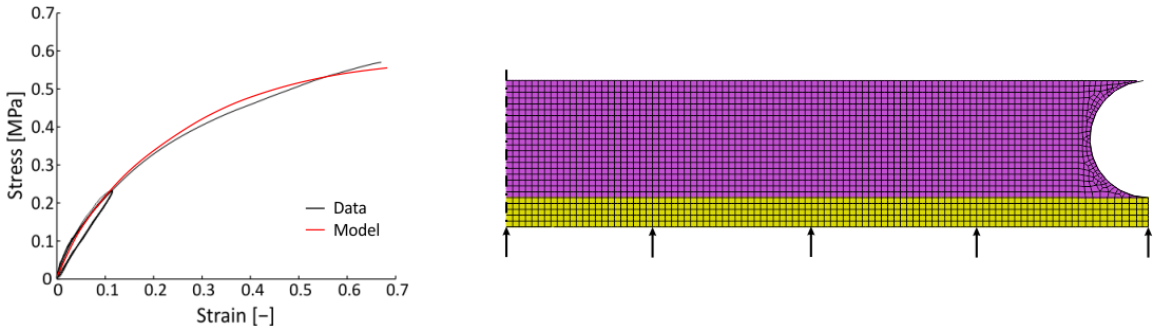


Figure 5.7 Cyclic behavior of the silicone membrane and fitting with the Mooney-Rivlin model (left); finite element model of the PEG gel (pink) supported by the membrane (yellow) (black arrows: applied pressure; dashed line: axis of symmetry; grey arc: clamping) (right).

### 5.3.2 Finite element model

Numerical simulations were performed to estimate the deformation of the gel in dependence of the inflated volume. An axisymmetric model representing a circular sample of PEG gel (thickness=1 mm, radius=5 mm) on top of the silicone membrane (thickness=0.25 mm, radius=5 mm) was built in the commercial finite element software ABAQUS 6.10-1 (Abaqus Inc. RI, USA) (Figure 5.7, right). The gel was assumed incompressible and modeled by a Neo-Hookean material formulation with elastic coefficient $C_{10}$=0.125 kPa, according to the data reported by Ehrbar at al. for 2% degradable PEG gels (shear modulus G=0.25 kPa, [114]). The membrane was described by a Mooney-Rivlin model, the parameters of which ($C_{10}$=0.243 MPa; $C_{01}$=-2.84e-2 MPa, D=0 MPa) were obtained fitting the stress-strain data from the monotonic inflation test. Both parts were meshed with second order axysimmetric elements (CAX8H), while the clamping ring was modeled as a rigid body with rounded edge (r=0.5 mm).

No relative sliding was allowed between the gel and the membrane, whereas penetration of the gel in the clamping was allowed to reduce excessive element distortion, which would lead to convergence problems. Uniform pressure was applied to the underside of the membrane (Figure 5.7, right). In plane coordinates of the nodes at the underside of the membrane were extracted in order to calculate the volume enclosed between the deformed and undeformed membrane.

Convergence of the simulation could be reached up to 0.25 ml of inflated volume. The circumferential and radial strain in the gel (the latter in the direction of membrane curvature) were analyzed at 0.1 ml and 0.2 ml of inflated volume.

During inflation, a strain gradient develops both in thickness and radial direction, with the highest deformation reached in the top-center of the gel (Figure 5.8). Note that in the in vitro amnion model cells randomly distribute in the whole gel.

At 0.1 ml of inflated volume, the circumferential and radial strain decreases from 21% in the top-center to 12% at the interface with the membrane and to about 19% at a radial distance of 2.5 mm from the center (corresponding to half of the radius of the gel). The ratio between the circumferential and radial strain (equal to 1 in case of an equibiaxial stress state) slightly varies in the sample, decreasing from 1 in the center of the gel to 0.96 and 0.8 at radial distance of 2.5 mm from the center, at the top and at the interface with the membrane, respectively.

At 0.2 ml of inflated volume, the circumferential and radial strains decrease from 54% in the top-center to 45% at the interface with the membrane and to about 43% at a radial distance of 2.5 mm from the center. The ratio between the circumferential and radial strain decreases from 1 in the top -center of the gel to 0.98 and 0.9 at radial distance of 2.5 mm from the center, at the top and at the interface with the membrane, respectively.

The gel undergoes a strong compression during inflation, with the thickness in the center reducing by 27% at 0.1 ml and 67% at 0.2 ml of inflated volume.

The strain field in the vicinity of the clamping could not be properly evaluated due to the allowed penetration of the gel into the clamping (Figure 5.8). Nevertheless, preliminary simulations confirmed that the definition of the boundary and contact conditions at the clamping do not affect the strain field in the center of the sample.

### 5.3.3 Sample preparation

A protocol for the preparation of gel disks on the silicone membrane was developed and validated using human bone marrow mesenchymal cells (BMCs).

Membrane samples were cut with a 28 mm diameter die cutter and two holes (3 mm diameter) were created close to the perimeter for the placement on the cylinder (Figure 5.11). Membranes were lain between two metal washers (28 mm outer diameter, 10 mm inner diameter, 1 mm thickness) and placed in a 6 well plate.

Degradable PEG gels containing RGD were formed as described in [111]. Briefly, the covalent cross-linking of 8-arm PEG macromers (PEG-Lys and PEG-Gln) – diluted to 2% concentration in tris

buffer saline (50 mM, pH 7.6) – was performed by addition of 10 U/ml thrombin-activated factor XIIIa in the presence of 50 mM calcium chloride.

Immediately after mixing all components, the cell suspension ($2x10^6$ cells/ml of cell culture medium) was added to the solution and 90 µl of the mixture were pipetted on the membrane. Samples were gently rotated to allow the gel to cover the central part of the membrane and reach the metal border. Gelation occurred within few minutes, but the cross-linking reaction was allowed to proceed for 20 min at 37 °C in a humidified incubator. Samples were incubated in medium (MEMα, Gibco) at 37 °C for 24 hour in order to let cells stabilize in the new environment and then tested.

All the components in contact with cells (membranes, washers, chamber and sealing ring) were sterilized with ethanol and washed with phosphate buffer saline solution (PBS) before the preparation of samples.

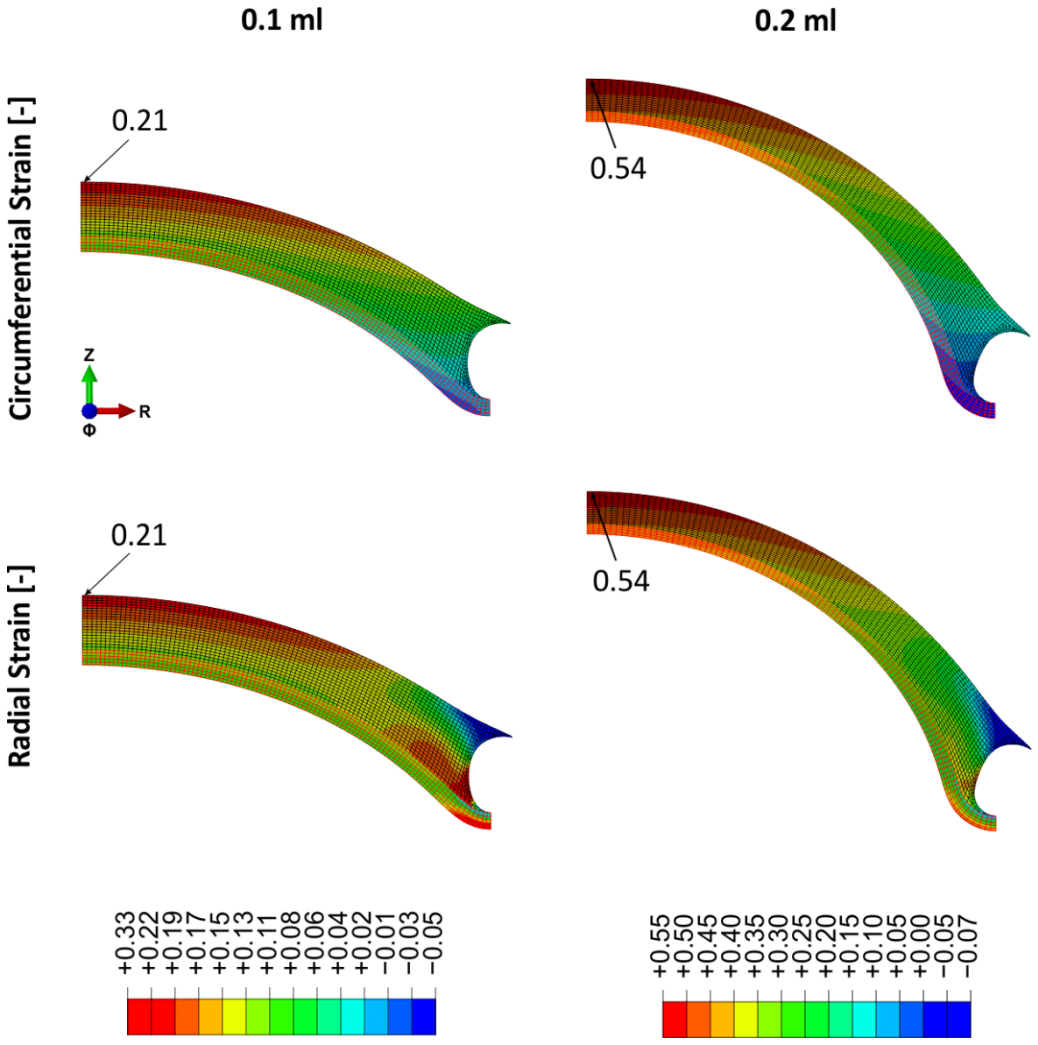


Figure 5.8 Circumferential and radial strain in the gel at 0.1 ml and 0.2 ml of inflated volume. Red mesh grid: membrane, black mesh grid: gel.

### 5.3.4 Validation tests

The cytotoxicity of the materials, the feasibility of dynamic culture and the robustness of the gels were investigated. Sample evaluation was performed by transmitted and epifluorescence microscopy.

*Cytotoxicity test*

Two samples were incubated in MEMα at 37 °C for 24 hours with a ring of polycarbonate (PC) and rubber (sealing ring), respectively. One sample was used as a control for the membrane and the metal washer. LIVE/DEAD® Viability/Cytotoxicity Kit (Molecular Probes, USA) was used to assess the viability of cells. Cells were viable both in the control and in the sample incubated with PC (Figure 5.9), demonstrating the low cytotoxicity of the membrane, the metal washer and polycarbonate. On the contrary, cells died when incubated with the rubber ring. The sealing ring was then exchanged with a PDMS ring, which proved to be non-cytotoxic (Figure 5.9).

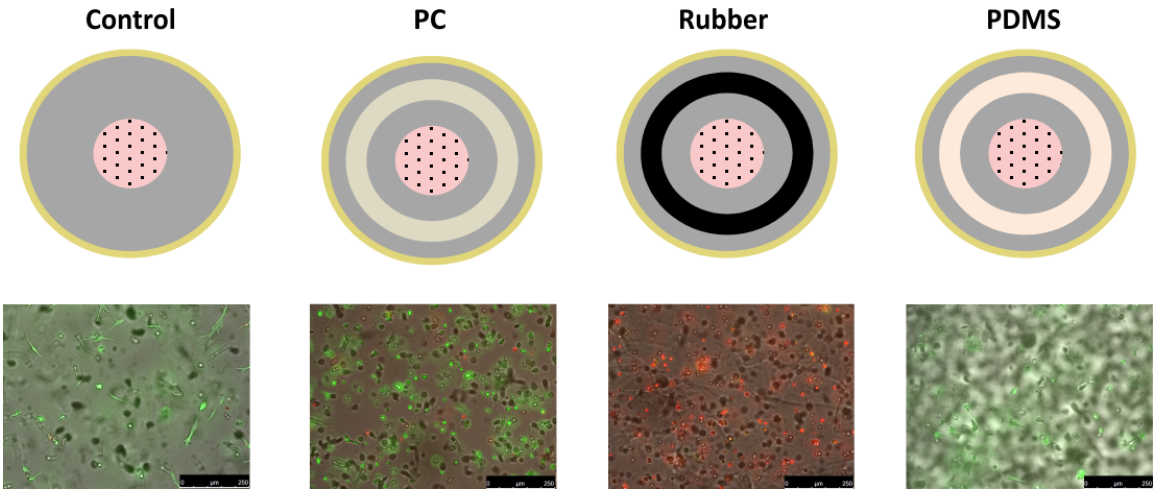


Figure 5.9 Cytotoxicity test. Three samples were incubated with a ring of polycarbonate (PC), rubber (sealing ring) and PDMS. One sample was used as a control. Live/dead staining was performed to assess the viability of cells (green=live, red=dead).

*Feasibility of dynamic culture*

Three specimens were cyclically stretched for 24 hours at a flow rate of 0.016 ml/s, with a low (0.1 ml), medium (0.2 ml) and high (0.4 ml) volume of water respectively. For the mounting in the bioreactor, the lower washer was removed, samples were positioned on the cylinder, the chamber was screwed in and filled with 1 ml of cell culture medium. A plastic lid was then placed on the chamber to avoid evaporation of the medium. After testing, samples were removed from the bioreactor and imaged together with a static control.

Cells appeared viable and spread after 24 hours in the gel. Repeated loading did not affect the viability and morphology of cells in all tested configurations. Cell-cell connectivity looked slightly improved after dynamic culture compared to the static control (Figure 5.10).

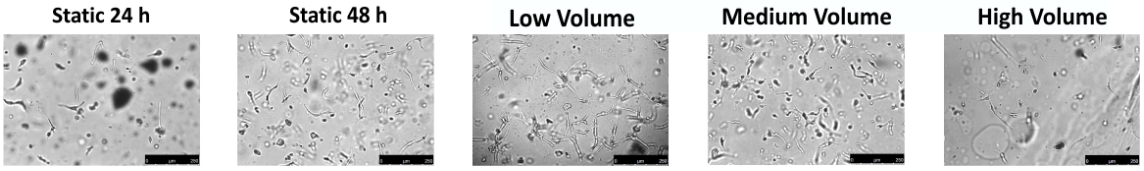


Figure 5.10 BMCs in the PEG gel after static and dynamic culture.

*Robustness of gels*

With the procedure described in paragraph 5.3.3, gels with 10 mm diameter and 1 mm thickness could be formed (Figure 5.11a). The gel strongly attaches to the membrane and the metal washer and no degradation is visible during static and dynamic culture. After repeated stretching at any level of deformation, the gel remains intact and fully attached (Figure 5.11b). When the washer is removed, the outer border of the gel is ripped off by the washer, while the central part stays on the membrane and can be used for further evaluations (Figure 5.11c).

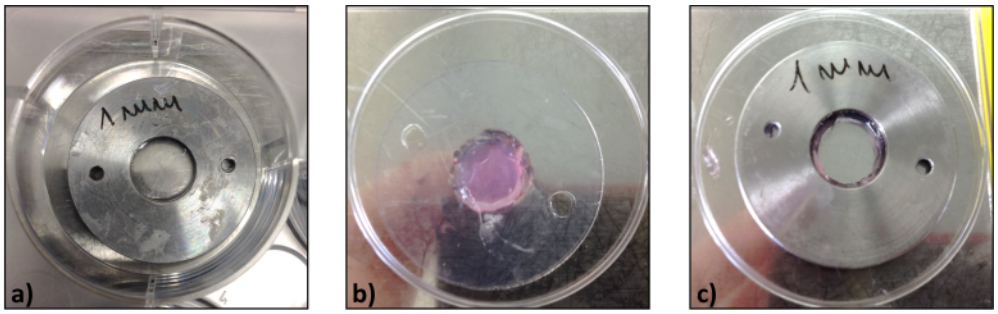


Figure 5.11 Gel before (a) and after stretching (b, c). When the washer is removed, the outer border of the gel is ripped off by the washer (c), while the central part stays on the membrane (b).

## 5.4 Preliminary experiments and results

Preliminary experiments were run to test the behavior of amniotic mesenchymal cells (AMCs) under repeated mechanical loading using the model described in paragraph 5.3.

### 5.4.1 Cells isolation

A fetal membrane was collected as described in paragraph 2.2.5, amnion was gently separated from chorion and washed in PBS. Amniotic epithelial and mesenchymal cells were isolated according to the protocol described by Bilic et al. [115]. In a first step, amnion was incubated for 5 minutes at 37°C in 0.25% trypsin/EDTA (Gibco) solution and washed in PBS. For the isolation of epithelial cells, the tissue was treated with Dispase II (12 U/ml in 1x balanced salt solution HBSS, Roche) for 1 hour at 37°C. Cells were scraped with a rubber policeman, collected and suspended in medium (MEMα). For the isolation of mesenchymal cells, the remaining amnion was cut in small pieces and incubated in collagenase A (Roche) for 2 hours at 37°C. Cells were then collected, suspended in medium and cultured until confluent.

### 5.4.2 Experimental protocol

In order to evaluate the effect of repeated loading on AMCs, three sets of experiments were performed. For each set, two samples were prepared as described in paragraph 5.3.3, with a cell density of $5x10^6$ cells/ml of cell culture medium. After 24 hours of incubation in cell culture medium (MEMα+10% fetal bovine serum) at 37°C, one sample was mounted in the bioreactor and cyclically inflated for 24 hours, while the static control was kept in culture.
The three inflated specimens were stretched with low (0.1 ml), medium (0.2 ml) and high (0.4) volume of water, respectively. Setting a fixed flow rate of 0.016 ml/s, each experiment corresponded to a different number of cycles over 24 hours.

### 5.4.3 Immunocytochemistry and microscopy

After testing, both stretched and control samples were prepared for staining. The metal washer was removed and gels were cut in half. Different pairs of staining were performed on each half in order avoid overlap of fluorescent signals in the same channel: collagen I and actin were stained on one half, while collagen I and fibronectin were stained on the second half. For the staining of

collagen I, the primary antibody (mouse monoclonal anti-collagen I, Abcam, USA) was applied on live cells. The secondary antibody and all the other stainings were applied after fixation of cells with PFA 4% (paraformaldehyde), incubation in 0.1 M glycine and permeabilization with Triton X-100 (0.1% in PBS). Actin was stained with Phalloidin-Alexa fluor 546 (Invitrogen, USA) in PBS with 1% BSA (bovine serum albumin) overnight at 4˚C. Fibronectin was stained with Fn-FITC (Abcam, USA) and DyLight™ 488 Goat anti-mouse IgG (Biolegend, USA) was used as a secondary antibody for staining collagen I. Nuclei were stained with the Hoechst dye (1/1000 in PBS, Invitrogen). Sample evaluation was performed by epifluorescence microscopy.

### 5.4.4 Results

AMCs appeared viable and spread after 48 hours of static culture in the gel and no signs of gel degradation were visible (Figure 5.12, Static control 48 h). However, cells mainly arranged themselves at the interface between the gel and the membrane, in a quasi-2D configuration (Figure 5.12, Static control 48 h). Cell-cell connections started to form after 24 hours and were clearly visible after 48 hours of static culture (Figure 5.12, Static control 48 h).

Cyclic loading did not affect cell viability and connectivity in all the tested configurations and no morphological differences could be detected between stretched and unstretched cells (Figure 5.12, Stretched samples). In all the tested samples, fibronectin and collagen were not detected, except for a weak signal in the gel (Figure 5.12).

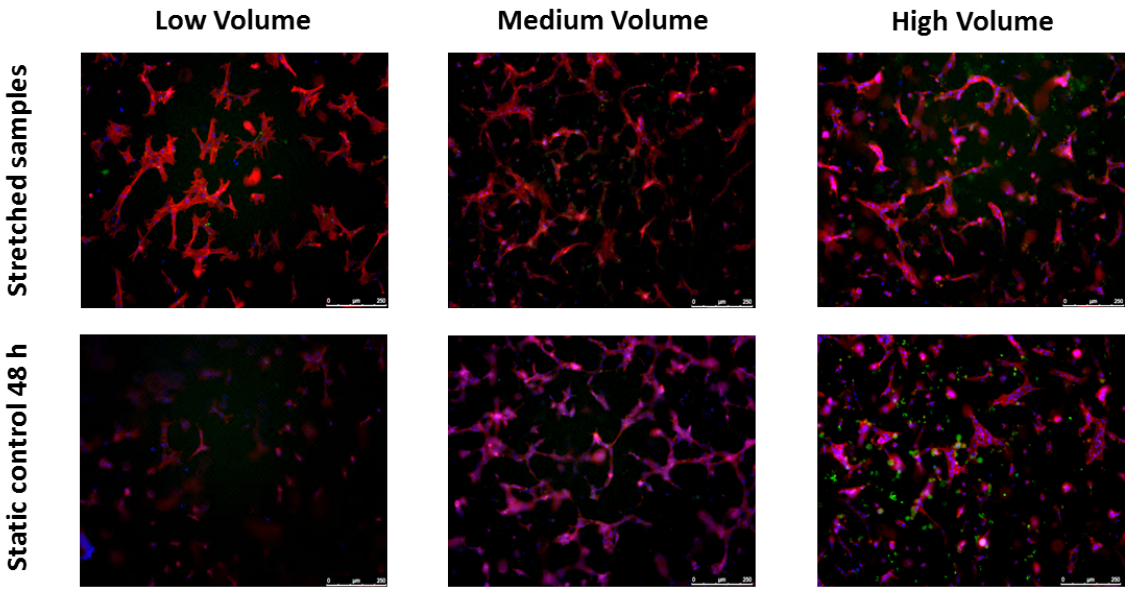


Figure 5.12 AMCs embedded in PEG gel after static and dynamic culture (blue: nuclei, red: actin, green: collagen I).

## 5.5 Discussion

In this chapter, the first steps towards the establishment of an in vitro amnion model for the study of fetal membrane healing have been described.

In order to test the model under physiologically relevant biological and mechanical conditions, a setup for dynamic cell culture has been developed (Figure 5.1). The design of the bioreactor was inspired by the inflation device, scaling down the dimensions of the cylinder and using sterilizable, non-cytotoxic materials (Figure 5.2 and Figure 5.3). The setup was designed to perform long-term experiments in a controlled environment, being stable and reliable over thousands of cycles. The presence of a single bioreactor represented a limitation, allowing for only one test at a time. This could be resolved in the future by connecting together several identical bioreactors.

Similar devices based on the inflation technique have been developed so far, including multiple or single cylinders with different dimensions (inflating area with diameter from 2 to 38 mm) [116-119]. However, they have been used only to perform 2D dynamic culture of cells seeded on a deformable membrane. For the application described here, AMCs extracted from fresh amnion were cultured and exposed to repeated loading in a 3D environment (PEG matrix), recalling physical and mechanical characteristics of the naturally derived extracellular matrix [111, 112].

Stretching of the amnion model in the bioreactor required the employment of a synthetic substrate to support and load the gel, thus transferring mechanical strains to the cells (Figure 5.6). A strong and stable adhesion of the gel to the supporting membrane was essential for this purpose. Indeed, the gel was shown to be unchanged and adherent to the membrane after repeated stretching in all the tested configurations (Figure 5.11). Preliminary experiments with BMCs showed the feasibility of tests at increasing levels of inflated volume and the absence of cellular apoptosis at the clamping location (Figure 5.10).

Finite element simulations showed that inflation of the gel disk (1mm thick) leads to a non-uniform deformation of the material, especially in thickness direction, while equibiaxial stress state is ensured in the central part of the specimen (Figure 5.8). A strain field obtained with more than 0.25 ml inflated volume and in the vicinity of the clamping could not be analyzed due to the excessive element distortion in the soft gel.

It should be noted that the estimated strain field in the gel might be altered by the presence of cells and the formation of cell-matrix adhesions. The deformation experienced by AMCs might differ from the global strain and vary within the cell body. Bell et al. performed equibiaxial cyclic tests of 3D fibroblast-seeded tissue equivalents showing an amplification of cellular and nuclear strains in the direction perpendicular to the cell axis [120]. Overall, inflation of the amnion model closely resembles the in vivo mechanical stimuli transmitted to AMCs embedded in a collagen

network characterized by non-affine and non-homogeneous deformation during growth and stretch of the fetal membrane under a multiaxial stress state.

Preliminary tests were run on three amnion mimicking constructs applying cyclic stretch at different levels of deformation for 24 hours. Experiments showed that AMCs can form a network within 48 hours of culture in the gel and repeated stretching does not affect their viability and ability to form connections (Figure 5.12). Samples were imaged in the center and no preferential orientation of cells was observed. Improvements in cell proliferation and synthesis of ECM matrix components (fibronectin and collagen) were not detected in the stretched samples, compared to the static control after 48 hours (Figure 5.12).

It should be noted that AMCs were cultured in the absence of any biological cue, like growth factors and cytokine. Kiveliö et al. recently showed that AMCs cultured in PEG gels without growth factors can form cell-cell connections which degenerate in about 10 days of culture, and express mRNA levels for collagen I comparable to freshly isolated cells after 4 week of culture [113]. During this study, it was also noted that the ability of AMCs to spread and form a network in the gel varies among donors. Therefore, in order to evaluate the effect of mechanical stimuli and the level of stretch on AMCs proliferation and ECM production, dynamic culture should be performed for a longer period of time.

Further steps towards a safe and clinically relevant model for PPROM treatment should include the development of a bilayer tissue engineered amnion with amniotic epithelial cells seeded on the AMCs-seeded PEG matrix. The setup will also be used to test ex vivo fetal membrane samples puncture and sealing with the instructed matrix in order to test the effect of biological (growth factor) and mechanical (stretching) stimuli on cell recruitment, ECM production and tissue healing. Other types of scaffolds should also be taken in to account, tested and compared with the PEG matrix, e.g. compressed collagen gels, which were found to support the growth of amniotic epithelial cells [121].

## 5.6 Conclusion

A setup for dynamic 3D cell culture was developed in order to eventually study fetal membrane healing under physiologically relevant biological and mechanical conditions. A first in vitro amnion model, consisting of AMCs imbedded in a PEG matrix, was tested under repeated stretching at different levels of deformation, while supported by a synthetic substrate.

Long-term dynamic culture of a more complex amnion model will allow to investigate the effect of biological and mechanical stimuli on cell recruitment and ECM production necessary for the healing process.

Chapter 6

# Conclusions and outlook

## 6.1 Contributions of the present work

**Development of physiologically relevant setups and testing protocols for the characterization of fetal membrane and the evaluation of sealing and healing strategies**

The inflation technique has been exploited in order to test the fetal membrane, intact and repaired, as well as an in vitro amnion model, under a multiaxial stress state representative of the in vivo loading condition.

Significant changes have been made to the existing inflation device, allowing for (i) characterization of the membrane in its hydrated state and in a controlled temperature environment, (ii) local deformation analysis of inflated specimens, and (iii) placement of the device under the multiphoton microscope for in situ experiments.

An inflation protocol was developed in order to investigate the effect of repeated mechanical loading – representative of physiological contractions – on the mechanical and microstructural response of the membrane, as well as on the sealing performance of glues for fetal membrane repair. Ex vivo cyclic tests of amnion were reproduced in situ, allowing for the imaging of the microstructure under biaxial and uniaxial tension, the latter being representative of the stress state in the vicinity of defects.

Inspired by the inflation device, a setup for dynamic culture of amniotic cells was developed in order to test an in vitro amnion model under physiologically relevant biological and mechanical cues, and eventually study fetal membrane healing.

**Effect of repeated mechanical loading on the microstructure and mechanical behavior of the fetal membrane and amnion**

Repeated mechanical loading was shown to affect the mechanical and microstructural response of fetal membrane. Cyclic inflation representative of contractions leads to stiffening of the tissue and reduction of toughness, associated with alterations of collagen structures in the spongy and fibroblast layer and an increased thickness of the membrane. These alterations are comparable with morphological changes observed in the ZAM, thus suggesting that repeated mechanical loading might initiate a weakening process leading to PPROM when experienced prior to term.

Ex vivo and in situ cyclic inflation tests of amnion showed similar effects compared to the intact fetal membrane, i.e. high energy dissipation and stiffening of the tissue, associated with strong but reversible thickness changes, as well as collagen rearrangement without significant orientation. Repeated stretching under uniaxial tension showed, instead, significant volume

reduction due to low energy, unrecoverable in-plane phenomena, i.e. fiber orientation and lateral contraction. The tension state in the near-field of defects being predominantly uniaxial, the observed mechanisms might contribute to the toughening of fetal membrane when exposed to repeated loading, thus preventing crack growth and propagation.
Moreover, experiments revealed a significant response of the tissue in the preload phase, thus suggesting the activation of in-plane and out-of-plane mechanisms already at low tension levels, below the reference configuration.

**Sealing performance of synthetic glues for fetal membrane repair**

Ex vivo inflation tests of defective and repaired fetal membranes have been performed in order to compare the sealing performance of two catechol-modified synthetic glues, cT and cPEG, under physiologically relevant environmental and mechanical conditions.
Both glues seal the fetal membrane, resisting pressures higher than the intra-uterine baseline, but showing different failure processes. cT withstands high deformations and pressures without breaking, but loses adhesion under shear stresses, while cPEG ruptures at a critical level of pressure. The performance of the sealants deteriorate under repeated mechanical loading, representative of contractions, as well as under fast and acute deformation of the membrane, representative of impacts.
Sealing with a glue plug leads to the concentration of stresses at the border of the plug, both in the membrane and at the interface, and does not restore the distribution of stresses present in the intact substrate. Being more compliant, cT leads to lower stresses in the substrate and at the interface plug-membrane compared to cPEG.
In order to take advantage of the high deformability and toughness of the cT glue in the repair of fetal membrane, the design of the plug, the adhesion and mechanical properties of the sealant should be improved, thus reducing stresses and matching the deformation behavior of the membrane.

## 6.2 Outlook

**Mechanical and microstructural characterization of fetal membrane**

In situ experiments in a multiphoton microscope revealed that repeated mechanical loading leads to microstructural alterations in the reflected fetal membrane, comparable with those occurring in the ZAM as a result of increased MMPs concentration and activity. Performing experiments in a controlled environment (bioreactor), thus ensuring cell viability, would allow for imaging of the microstructure and quantification of MMPs after repeated stretching over a longer period of time. Moreover, cytokines involved in the inflammatory process associated with PPROM were recently shown to reduce membrane strength [122]. A similar setup would allow for the investigation of their effect on the microstructure of the tissue and its mechanisms of deformation.

The interface between amnion and chorion was found to play a crucial role in the retention of the structural and mechanical integrity of the membrane. The spongy layer is, in fact, the most affected by the remodeling process preparatory for delivery. Furthermore, the rupture of the membrane (in vivo and ex vivo) is associated with the separation of amnion and chorion at the interface [20]. Therefore, the microstructural characteristics and mechanical functions of the interface layer should be further investigated with dedicated in situ experiments, both in normal and abnormal conditions potentially leading to PPROM, e.g. overstretching and high concentration of cytokines associated with infections.

Strong and irreversible volume reduction and lateral contraction were shown to characterize the response of amnion under uniaxial tension, thus suggesting a peculiar defect-tolerance of the tissue. In order to better understand the failure behavior of the membrane in presence of defects and develop repair strategies for iPPROM prevention, the following aspects should be further investigated under a physiological loading state: (i) the propagation of cracks in amnion, (ii) the orientation of fibers in the near-field of defects, and (iii) the role of chorion and its interaction with amnion in the defect-tolerance of the membrane.

**Definition of the reference configuration**

Nowadays, little is still known about the in vivo deformation of the fetal membrane during pregnancy. The membrane is attached to the uterine wall through the choriodecidua and follows its growth during pregnancy. Comparing the dimensions of the uterus with the area of harvested membranes, some studies have found values of in vivo areal stretch at term between 1.7 [9] and 2.5 [11]. However, it should be taken into account that the tissue undergoes a continuous

remodeling process during pregnancy, leading to destruction of old and formation of new extracellular matrix, as well as growth of the membrane, as shown by Parry-Jones and Priya [10]. Therefore, it is not the material formed at the beginning of pregnancy being stretched at term, but newly formed tissue in a new reference configuration.

The definition of a reference configuration is necessary for the analysis of the ex vivo mechanical behavior of soft tissues in order to compare data obtained in different loading configurations or reported in literature. The reference state is usually associated with reaching a small threshold of force/pressure, which is, however, affected by the preparation of samples and the release of in vivo residual stresses [123]. The microstructural and mechanical investigations of the deformation behavior of amnion showed significant in plane stretches, thickness and volume reduction below the reference configuration set for inflation (pressure=1 mbar) and uniaxial tests (force=0.1 N). A deeper investigation of the mechanical response of the tissue at low tension levels and the definition of a reference configuration based on the activation of microstructural mechanisms, e.g. a threshold in the lateral contraction, would allow for a more robust description of the mechanical behavior of the tissue from the slack to the highly stretched state. Given the high reproducibility of the kinematic response of amnion, this method might also contribute to reduce the large inter-specimen variability and – together with the normalization proposed by Mauri et al. – provide master curves representative of the deformation behavior of amnion [64].

**Modeling of the fetal membrane**

The findings of the ex vivo and in situ investigations form the basis for the development of constitutive models of amnion, able to describe not only the monotonic response, but also its multiaxial history-dependent behavior. A reliable model should account for the important features of the tissue, i.e. (i) the non-linear tension-stretch curves and increase of residual stretch with cycles, (ii) the difference between loading and unloading path with higher dissipation under biaxial tension, (iii) the increase of biaxial tangent stiffness and decrease of uniaxial tangent stiffness during cyclic loading, with major changes from the first to the second cycle, (iv) the strong in-plane contraction with residual lateral stretch under uniaxial tension, and (vi) the peculiar thickness reduction and recovery. Different approaches, like continuum and random fiber network models, might be able to capture the listed features, together with the time-dependent response of the tissue.

In addition to constitutive equations describing the mechanical behavior of amnion and chorion, the interface between the two layers should be characterized, as well as the interaction of the choriondecidua with the uterine wall. These insights would allow to implement a meaningful

model of the fetal membrane in the uterine environment, as preliminary developed by Paskaleva [124]. Such a model could be used for the simulation of physiological loading conditions, e.g. repeated mechanical loading during labor and optimization of surgical procedures and repair strategies.

**Fetal membrane repair**

Repair strategies have shown serious issues related with the chemical stability as well as mechanical compatibility of glues with the fetal membrane, limiting their application for iPPROM prevention in clinical practice.

Even though not able to spontaneously heal [28], the fetal membrane presents some important characteristics that could be useful and should be taken into account in the development of repair strategies, i.e. (i) the proliferation potential of amniotic mesenchymal cells in earlier gestational ages [28] and (ii) deformation mechanisms of the collagen network in the vicinity of defects preventing cracks growth and propagation.

Given these properties of the membrane, biomaterials combining in vivo stability, compatible mechanical properties, and biological cues (growth factors) for cell recruitment, might seal and support defective membranes, while creating a favorable environment for the healing response and, in a later stage, making way for a regenerated tissue. For this purpose, the setup for dynamic cell culture is a useful system to test different repair strategies on in vitro amniotic models, as well as fetal membrane tissue, under physiologically relevant conditions.

Towards the development of this challenging solution for iPPROM, the mechanical and microstructural response of fetal membrane in the presence of defects should be further investigated, as well as the mechanical properties and recruiting potential of biomimetic sealants.

## 6.3 Closure

The preterm premature rupture of fetal membranes is one of the major causes of preterm birth and perinatal mortality and morbidity. The present thesis aimed at contributing to the research on the human fetal membrane and its premature rupture, providing insights into the effect of repeated mechanical loading on the mechanical and microstructural integrity of the tissue, as well as developing tools for the qualification of repair strategies for iPPROM prevention.

# Appendix

# Dynamic culture of endothelial cells (Zurich Heart project)

## Motivation

The Zurich Heart project aims at the development of a novel biomimetic blood propulsion device based on a highly deformable synthetic substrate, hosting a confluent endothelium and withstanding millions of stretch cycles and shear stresses from fluid flow, without loss of its main biomechanical functionalities. A bioreactor providing fluid flow and substrate deformation represents a valuable model system to study the combined effect of strain and shear stresses on endothelial cells activities relevant to the process of endothelialization.

In this context (i) the setup described in Chapter 5 (Figure 1, Inflation system) has been used to perform dynamic culture of endothelial cells seeded on a deformable membrane and assess the feasibility of the model, (ii) a flow chamber allowing fluid flow on the cells was designed and (iii) a preliminary flow system was assembled and tested (Figure 1, Flow system).

This project was conducted in collaboration with the laboratory of Dr. Ferrari (ETH Zurich) and Prof. Casartelli (HS Lucern).

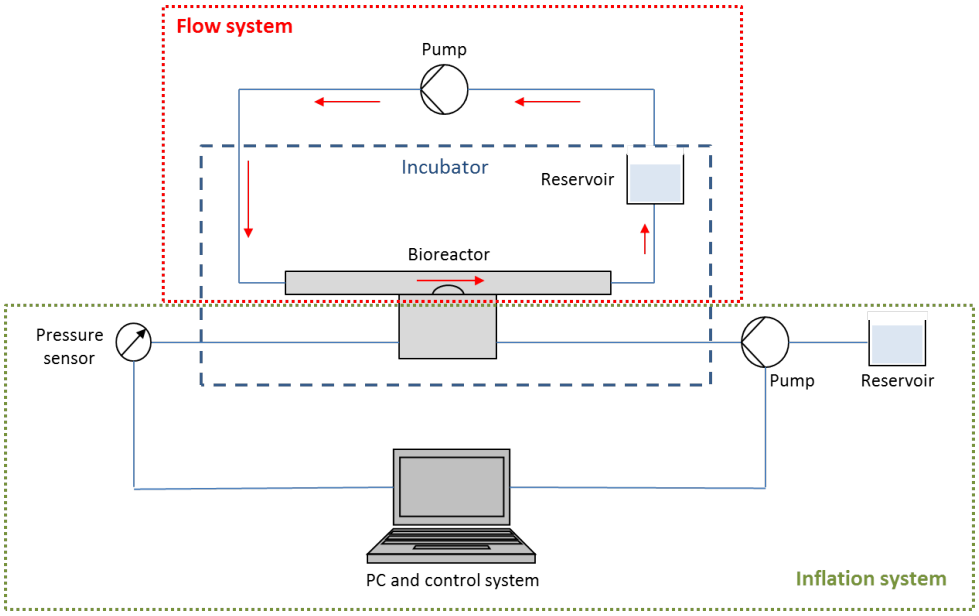


Figure 1 Representation of the main components and their connections in the inflation and flow system.

## Methods and results

*Endotelialization of the membrane*

PDMS (Polydimethylsiloxane) was selected as deformable substrate for dynamic culture of endothelial cells and produced in house. PDMS membranes (0.4 mm thick and composition 10:1) were treated with oxygen plasma (30 seconds at 100 W) and coated with cross-linked gelatin in order to improve di hydrophilicity of the material [125] and the adhesion of cells to the substrate [126].

Human umbilical vein endothelial cells (HUVECs) provided by the laboratory of Dr. Ferrari (ETH Zurich) were thawed, cultured and seeded at the $7^{th}$ or $8^{th}$ passage on PDMS samples with 28 mm diameter (about 80000 cells/$cm^2$). After 72 hours of static culture, HUVECs formed a confluent and connected monolayer on the treated PDMS (Figure 2, Treated PDMS), while a non-homogeneous layer of cells was visible on untreated membranes (Figure 2, Untreated PDMS).

For every test, the integrity of the monolayer was assessed by epifluorescence microscopy, staining actin filaments and cellular nuclei with Phalloidin-Alexa fluor 546 (Invitrogen, Carlsbad, CA, USA) and DAPI (Invitrogen, Carlsbad, CA, USA), respectively.

*Dynamic culture of HUVECs*

An endothelialized PDMS samples was mounted in the bioreactor as described in Chapter 5 and cyclically inflated with 0.4 ml of water for 16 hours at 0.08 Hz, while a static control was left in culture. Endothelial cells appeared viable and strongly adherent to the substrate after acute stretching. Repeated loading did not affect the integrity of the monolayer (Figure 2, Static and Dynamic).

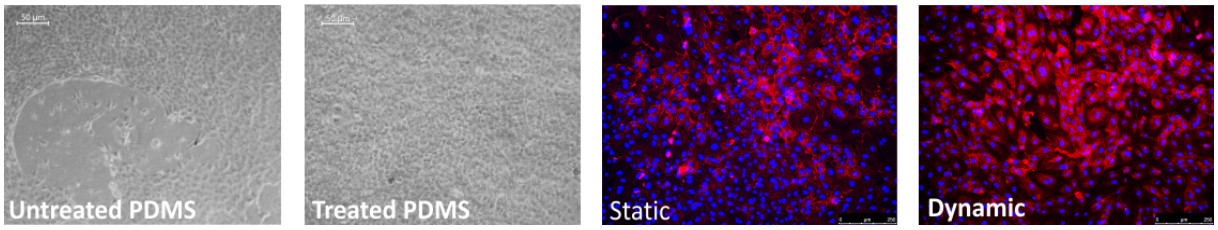


Figure 2 Endothelialization of untreated and treated PDMS membranes (light microscopy) and monolayer of HUVECs after static and dynamic culture of the endothelialized membrane (right, red: actin, blue: nuclei).

*Design of the flow chamber*

In order to apply shear stresses to the endothelialized membrane mounted in the bioreactor, a flow chamber was designed and manufactured according to the following requirements:

- dimensions compatible with the cylinder, the inflating area (10 mm diameter) and the elevation of the membrane;
- minimization of the flow rate and the amount of cell culture medium in the flow system;
- laminar and developed flow in the channel.

The first prototype of the chamber was machined in PMMA (poly(methyl methacrylate) and consists of a cylindrical core screwable on the cylinder and an asymmetric channel (5 mm tall and 12 mm wide), longer on the inlet side to allow the development of the flow (Figure 3).

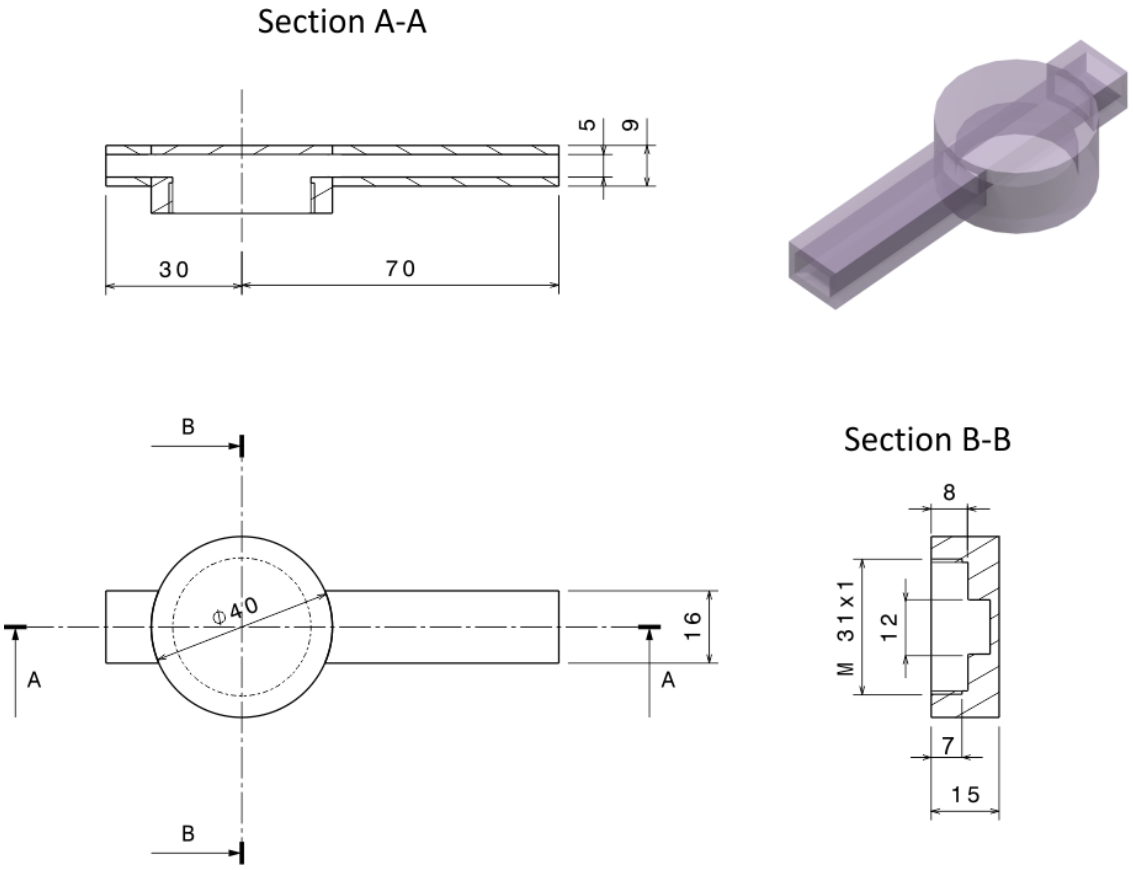


Figure 3 Mechanical drawing and 3D model of the flow chamber.

*Assembly and test of the flow system*

The flow system consists in a closed circuit where a peristaltic pump sucks cell culture medium out of a reservoir, sends it through the flow chamber and back in the container (Figure 1). The selection of the peristaltic pump was based on the possibility to run experiments with a wide range of flow rates, which – given the dimensions of the flow chamber – result in shear stresses on the flat and inflated endothelialized membrane from physiological (o(1) Pa) to super-physiological (o(10) Pa) values [127].

The 520DiN peristaltic pump (Watson Marlow, Switzerland) was selected for preliminary experiments, together with a double 8 mm silicone tube which reduces flow pulsations and vibrations in the circuit. The first flow system was assembled in the laboratory of Dr. Ferrari, positioning the reservoir and the bioreactor in the incubator of the Nikon-Ti microscope (Nikon, Japan) (Figure 4, left). An experiment was run at a flow rate of 1.8 l/min for 16 hours, corresponding to a shear stress of about 1.4 Pa on the flat endothelialized membrane.

After testing, cells in the center of the sample appeared viable, connected and slightly oriented in the direction of flow, while the monolayer was visibly disrupted in the vicinity of the channel wall (Figure 4, right).

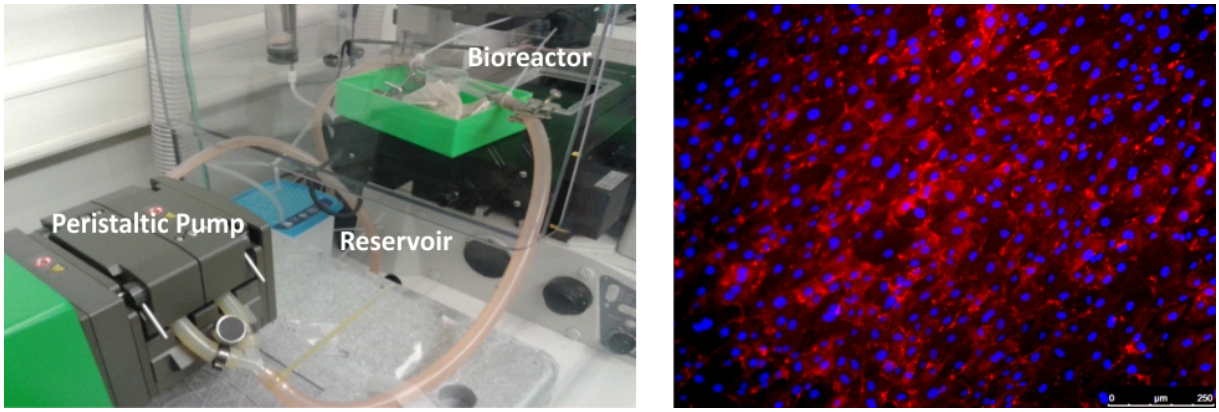


Figure 4 Assembled flow system (left) and HUVECs monolayer after application of shear stresses on the endothelialized membrane (right, red: actin, blue: nuclei).

## Discussion

The preliminary experiments described in this chapter aimed at testing the feasibility of endothelial cells culture under repeated stretching and shear stress. The inflation and flow system will be eventually assemble together, forming a model system to study the combined effect of strain and shear stresses on the endothelialized membrane (Figure 1).

PDMS was selected as deformable substrate, being a biocompatible elastomer widely used for 2D cell culture, with tunable and stable mechanical properties [128]. Treating the surface of the membrane with oxygen plasma and cross-linked gelatin allowed the formation of a homogeneous and connected monolayer of endothelial cells (Figure 2). The integrity and adhesion of the cellular monolayer is, in fact, essential to study the activity of cells during dynamic culture, as well as biological performances of the endothelialized membrane. It should be noted that the plasma treatment stiffens the surface of PDMS and it might affect the mechanical integrity of the material, leading to cracks propagation and failure of the membrane during cyclic loading [128]. Different treatments, as well as materials, should be therefore considered for further development of the biomimetic device.

Testing the endothelialized membrane in the setup for dynamic culture (Chapter 5) showed that acute repeated stretching does not affect the integrity of the monolayer and cells adhesion with the substrate (Figure 2). Given the feasibility of short-term, slow, dynamic culture, tests should be performed to evaluate cells connections, gene expression and adhesion to the membrane under repeated stretching in the physiological range (from 1% to 12% strain in large vessels [129], at the heart beat frequency of about 1 Hz and for high numbers of cycles). Inflation of the membrane determines a non-uniform strain field over the sample (Chapter 5) and the deformation sensed by the cells might differ from the global strain in the substrate [130], therefore a local, multi-scale strain analysis of the stretched membrane should be performed.

A preliminary flow system has been assembled in order to test the effect of shear stress on the endothelialized membrane (Figure 4, left). The geometry of the flow chamber and the peristaltic pump were selected in order to apply shear stresses in the physiological and super-physiological range, compatibly with the dimensions of the existing bioreactor (Figure 3). Applying shear stresses of about 1.4 Pa to the endothelialized membrane, the monolayer resulted intact with a slight orientation of cells in the direction of flow, confirming the findings of Franco et al. [131] (Figure 4, right). Localized cells death and disconnection observed at the periphery of the samples (where the monolayer is squeezed between the cylinder and the chamber) might influence the behavior of live cells and lead to apoptosis in the whole endothelium over a longer period of time.

Therefore, cells seeding should be optimized in order to obtain endothelialization of the substrate only in the inflating area.

The present setup requires a large amount of cell culture medium (400 ml for one experiment) and a bulky, expensive peristaltic pump to produce high flow rates in the chamber. The reshaping of the bioreactor, with a smaller inflating area and elevation of the membrane during inflation would result in the same shear stresses with lower flow rate and volume of medium. Moreover, the shape of the inlet channel should be optimized in order to obtain laminar flow without detachment of the streamline and turbulence behind the inflated membrane.

# Bibliography

[1] Parry S, Strauss JF, 3rd. Premature rupture of the fetal membranes. N Engl J Med 1998;338:663-70.

[2] Cross JC. Formation of the placenta and extraembryonic membranes. Ann N Y Acad Sci 1998;857:23-32.

[3] Carlson BM, Brudon MC. Human embryology and developmental biology: Mosby St. Louis; 1994.

[4] Ilancheran S, Moodley Y, Manuelpillai U. Human fetal membranes: a source of stem cells for tissue regeneration and repair? Placenta 2009;30:2-10.

[5] Moore KL, Persaud TVN, Torchia MG. Before We Are Born: Essentials of Embryology and Birth Defects (with Student Consult Online Access): Elsevier Health Sciences; 2007.

[6] Brace RA, Wolf EJ. Normal amniotic fluid volume changes throughout pregnancy. Am J Obstet Gynecol 1989;161:382-8.

[7] MacDermott RI, Landon CR. The hydroxyproline content of amnion and prelabour rupture of the membranes. Eur J Obstet Gynecol Reprod Biol 2000;92:217-21.

[8] Skinner SJ, Campos GA, Liggins GC. Collagen content of human amniotic membranes: effect of gestation length and premature rupture. Obstet Gynecol 1981;57:487-9.

[9] Millar LK, Stollberg J, DeBuque L, Bryant-Greenwood G. Fetal membrane distention: determination of the intrauterine surface area and distention of the fetal membranes preterm and at term. Am J Obstet Gynecol 2000;182:128-34.

[10] Parry-Jones E, Priya S. A study of the elasticity and tension of fetal membranes and of the relation of the area of the gestational sac to the area of the uterine cavity. Br J Obstet Gynaecol 1976;83:205-12.

[11] Joyce EM. Micromechanical mechanisms of fetal membrane failure: University of Pittsburgh; 2009.

[12] Jabareen M, Mallik AS, Bilic G, Zisch AH, Mazza E. Relation between mechanical properties and microstructure of human fetal membranes: an attempt towards a quantitative analysis. Eur J Obstet Gynecol Reprod Biol 2009;144 Suppl 1:S134-41.

[13] McLaren J, Malak TM, Bell SC. Structural characteristics of term human fetal membranes prior to labour: identification of an area of altered morphology overlying the cervix. Hum Reprod 1999;14:237-41.

[14] Bourne G. The foetal membranes. A review of the anatomy of normal amnion and chorion and some aspects of their function. Postgrad Med J 1962;38:193-201.

[15] Beall MH, van den Wijngaard JP, van Gemert MJ, Ross MG. Amniotic fluid water dynamics. Placenta 2007;28:816-23.

[16] Malak TM, Ockleford CD, Bell SC, Dalgleish R, Bright N, Macvicar J. Confocal immunofluorescence localization of collagen types I, III, IV, V and VI and their ultrastructural organization in term human fetal membranes. Placenta 1993;14:385-406.

[17] Bou-Resli MN, Al-Zaid NS, Ibrahim ME. Full-term and prematurely ruptured fetal membranes. An ultrastructural study. Cell Tissue Res 1981;220:263-78.

[18] Malak TM, Bell SC. Structural characteristics of term human fetal membranes: a novel zone of extreme morphological alteration within the rupture site. Br J Obstet Gynaecol 1994;101:375-86.

[19] Menon R, Fortunato SJ. The role of matrix degrading enzymes and apoptosis in rupture of membranes. J Soc Gynecol Investig 2004;11:427-37.

[20] Meinert M, Malmstrom A, Tufvesson E, Westergren-Thorsson G, Petersen AC, Laurent C, et al. Labour induces increased concentrations of biglycan and hyaluronan in human fetal membranes. Placenta 2007;28:482-6.

[21] Moore RM, Mansour JM, Redline RW, Mercer BM, Moore JJ. The physiology of fetal membrane rupture: insight gained from the determination of physical properties. Placenta 2006;27:1037-51.

[22] El Khwad M, Stetzer B, Moore RM, Kumar D, Mercer B, Arikat S, et al. Term human fetal membranes have a weak zone overlying the lower uterine pole and cervix before onset of labor. Biol Reprod 2005;72:720-6.

[23] McLaren J, Taylor DJ, Bell SC. Increased concentration of pro-matrix metalloproteinase 9 in term fetal membranes overlying the cervix before labor: implications for membrane remodeling and rupture. Am J Obstet Gynecol 2000;182:409-16.

[24] Vadillo-Ortega F, Gonzalez-Avila G, Furth EE, Lei H, Muschel RJ, Stetler-Stevenson WG, et al. 92-kd type IV collagenase (matrix metalloproteinase-9) activity in human amniochorion increases with labor. Am J Pathol 1995;146:148-56.

[25] Bryant-Greenwood GD, Mamamoto SY. Control of peripartal collagenolysis in the human chorion-decidua. Am J Obstet Gynecol 1995;172:63-70.

[26] McLaren J, Taylor DJ, Bell SC. Increased incidence of apoptosis in non-labour-affected cytotrophoblast cells in term fetal membranes overlying the cervix. Hum Reprod 1999;14:2895-900.

[27] Calvin SE, Oyen ML. Microstructure and mechanics of the chorioamnion membrane with an emphasis on fracture properties. Ann N Y Acad Sci 2007;1101:166-85.

[28] Devlieger R, Millar LK, Bryant-Greenwood G, Lewi L, Deprest JA. Fetal membrane healing after spontaneous and iatrogenic membrane rupture: a review of current evidence. Am J Obstet Gynecol 2006;195:1512-20.

[29] Blencowe H, Cousens S, Oestergaard MZ, Chou D, Moller A-B, Narwal R, et al. National, regional, and worldwide estimates of preterm birth rates in the year 2010 with time trends since 1990 for selected countries: a systematic analysis and implications. The Lancet 2012;379:2162-72.

[30] Gibbs RS, Blanco JD. Premature Rupture of the Membranes. Obstet Gynecol 1982;60:671-9.

[31] Kumar D, Fung W, Moore RM, Pandey V, Fox J, Stetzer B, et al. Proinflammatory cytokines found in amniotic fluid induce collagen remodeling, apoptosis, and biophysical weakening of cultured human fetal membranes. Biol Reprod 2006;74:29-34.

[32] Kumar D, Schatz F, Moore RM, Mercer BM, Rangaswamy N, Mansour JM, et al. The effects of thrombin and cytokines upon the biomechanics and remodeling of isolated amnion membrane, in vitro. Placenta 2011;32:206-13.

[33] El Maradny E, Kanayama N, Halim A, Maehara K, Terao T. Stretching of fetal membranes increases the concentration of interleukin-8 and collagenase activity. Am J Obstet Gynecol 1996;174:843-9.

[34] Deprest JA, Flake AW, Gratacos E, Ville Y, Hecher K, Nicolaides K, et al. The making of fetal surgery. Prenat Diagn 2010;30:653-67.

[35] Gratacos E, Sanin-Blair J, Lewi L, Toran N, Verbist G, Cabero L, et al. A histological study of fetoscopic membrane defects to document membrane healing. Placenta 2006;27:452-6.

[36] Sydorak RM, Hirose S, Sandberg PL, Filly RA, Harrison MR, Farmer DL, et al. Chorioamniotic membrane separation following fetal surgery. J Perinatol 2002;22:407-10.

[37] Mallik AS, Fichter MA, Rieder S, Bilic G, Stergioula S, Henke J, et al. Fetoscopic closure of punctured fetal membranes with acellular human amnion plugs in a rabbit model. Obstet Gynecol 2007;110:1121-9.

[38] Ochsenbein-Kolble N, Jani J, Lewi L, Verbist G, Vercruysse L, Portmann-Lanz B, et al. Enhancing sealing of fetal membrane defects using tissue engineered native amniotic-scaffolds in the rabbit model. Am J Obstet Gynecol 2007;196:263-5.

[39] Gratacos E, Wu J, Yesildaglar N, Devlieger R, Pijnenborg R, Deprest JA. Successful sealing of fetoscopic access sites with collagen plugs in the rabbit model. Am J Obstet Gynecol 2000;182:142-6.

[40] Luks FI, Deprest JA, Peers KH, Steegers EA, van Der Wildt B. Gelatin sponge plug to seal fetoscopy port sites: technique in ovine and primate models. Am J Obstet Gynecol 1999;181:995-6.

[41] Harmanli OH, Wapner RJ, Lontz JF. Efficacy of fibrin glue for in vitro sealing of human chorioamniotic membranes. J Reprod Med 1998;43:986-90.

[42] Haller CM, Buerzle W, Kivelio A, Perrini M, Brubaker CE, Gubeli RJ, et al. Mussel-mimetic tissue adhesive for fetal membrane repair: an ex vivo evaluation. Acta Biomater 2012;8:4365-70.

[43] Kivelio A, Dekoninck P, Perrini M, Brubaker CE, Messersmith PB, Mazza E, et al. Mussel mimetic tissue adhesive for fetal membrane repair: initial in vivo investigation in rabbits. Eur J Obstet Gynecol Reprod Biol 2013;171:240-5.

[44] Mann LK, Papanna R, Moise KJ, Jr., Byrd RH, Popek EJ, Kaur S, et al. Fetal membrane patch and biomimetic adhesive coacervates as a sealant for fetoscopic defects. Acta Biomater 2012;8:2160-5.

[45] Al-Zaid NS, Bou-Resli MN, Goldspink G. Bursting pressure and collagen content of fetal membranes and their relation to premature rupture of the membranes. Int J Gynaecol Obstet 1980;87:227-9.

[46] Lavery JP, Miller CE. Deformation and creep in the human chorioamniotic sac. Am J Obstet Gynecol 1979;134:366-75.

[47] Oyen ML, Calvin SE, Landers DV. Premature rupture of the fetal membranes: is the amnion the major determinant? Am J Obstet Gynecol 2006;195:510-5.

[48] Oyen ML, Cook RF, Calvin SE. Mechanical failure of human fetal membrane tissues. J Mater Sci Mater Med 2004;15:651-8.

[49] Pressman EK, Cavanaugh JL, Woods JR. Physical properties of the chorioamnion throughout gestation. Am J Obstet Gynecol 2002;187:672-5.

[50] Helmig R, Oxlund H, Petersen LK, Uldbjerg N. Different biomechanical properties of human fetal membranes obtained before and after delivery. Eur J Obstet Gynecol Reprod Biol 1993;48:183-9.

[51] Lavery JP, Miller CE, Knight RD. The effect of labor on the rheologic response of chorioamniotic membranes. Obstet Gynecol 1982;60:87-92.

[52] Artal R, Sokol RJ, Neuman M, Burstein AH, Stojkov J. The mechanical properties of prematurely and non--prematurely ruptured membranes. Methods and preliminary results. Am J Obstet Gynecol 1976;125:655-9.

[53] Polishuk WZ, Kohane S, Peranio A. The physical properties of fetal membranes. Obstet Gynecol 1962;20:204-10.

[54] Arikat S, Novince RW, Mercer BM, Kumar D, Fox JM, Mansour JM, et al. Separation of amnion from choriodecidua is an integral event to the rupture of normal term fetal membranes and constitutes a significant component of the work required. Am J Obstet Gynecol 2006;194:211-7.

[55] Oxlund H, Helmig R, Halaburt JT, Uldbjerg N. Biomechanical analysis of human chorioamniotic membranes. Eur J Obstet Gynecol Reprod Biol 1990;34:247-55.

[56] Bürzle W, Mazza E, Moore JJ. About Puncture Testing Applied for Mechanical Characterization of Fetal Membranes. J Biomech Eng 2014;136.

[57] Buerzle W, Haller CM, Jabareen M, Egger J, Mallik AS, Ochsenbein-Koelble N, et al. Multiaxial mechanical behavior of human fetal membranes and its relationship to microstructure. Biomech Model Mechan 2013;12:747-62.

[58] Schober EA, Kusy RP, Savitz DA. Resistance of Fetal Membranes to Concentrated Force Applications and Reconciliation of Puncture and Burst Testing. Ann Biomed Eng 1994;22:540-8.

[59] Buerzle W, Mazza E. On the deformation behavior of human amnion. J Biomech 2013;46:1777-83.

[60] Buerzle W. Mechanical characterization and modeling of human fetal membrane tissue: Diss., Eidgenössische Technische Hochschule ETH Zürich, Nr. 21784, 2014; 2014.

[61] Lavery JP, Miller CE. The viscoelastic nature of chorioamniotic membranes. Obstet Gynecol 1977;50:467-72.

[62] Oyen ML, Calvin SE, Cook RF. Uniaxial stress-relaxation and stress-strain responses of human amnion. J Mater Sci Mater Med 2004;15:619-24.

[63] Oyen ML, Cook RF, Stylianopoulos T, Barocas VH, Calvin SE, Landers DV. Uniaxial and biaxial mechanical behavior of human amnion. J Mater Res 2005;20:2902-9.

[64] Mauri A, Perrini M, Ehret AE, De Focatiis DS, Mazza E. Time-dependent mechanical behavior of human amnion: Macroscopic and microscopic characterization. Acta Biomater 2015;11:314-23.

[65] Faturechi R, Hashemi A, Fatouraee N. Do mechanical properties of human fetal membrane depend on strain rate? J Obstet Gynaecol Res 2015;41:84-91.

[66] Toppozada MK, Sallam NA, Gaafar AA, el-Kashlan KM. Role of repeated stretching in the mechanism of timely rupture of the membranes. Am J Obstet Gynecol 1970;108:243-9.

[67] Pandey V, Jaremko K, Moore RM, Mercer BM, Stetzer B, Kumar D, et al. The force required to rupture fetal membranes paradoxically increases with acute in vitro repeated stretching. Am J Obstet Gynecol 2007;196:165 e1-7.

[68] Ockleford C, Bright N, Hubbard A, D'Lacey C, Smith J, Gardiner L, et al. Micro-trabeculae, macro-plaques or mini-basement membranes in human term fetal membranes? Philos Trans R Soc Lond B Biol Sci 1993;342:121-36.

[69] Ockleford CD, McCracken SA, Rimmington LA, Hubbard AR, Bright NA, Cockcroft N, et al. Type VII collagen associated with the basement membrane of amniotic epithelium forms giant anchoring rivets which penetrate a massive lamina reticularis. Placenta 2013;34:727-37.

[70] Smith J, Ockleford CD. Laser scanning confocal examination and comparison of nidogen (entactin) with laminin in term human amniochorion. Placenta 1994;15:95-106.

[71] Fawthrop RK, Ockleford CD. Cryofracture of Human Term Amniochorion. Cell Tissue Res 1994;277:315-23.

[72] Ockleford C, Malak T, Hubbard A, Bracken K, Burton SA, Bright N, et al. Confocal and conventional immunofluorescence and ultrastructural localisation of intracellular strength-giving components of human amniochorion. J Anat 1993;183 ( Pt 3):483-505.

[73] Cox G. Biological applications of second harmonic imaging. Biophys Rev 2011;3:131-41.

[74] Perrini M, Burzle W, Haller C, Ochsenbein-Kolble N, Deprest J, Zimmermann R, et al. Contractions, a risk for premature rupture of fetal membranes: a new protocol with cyclic biaxial tension. Med Eng Phys 2013;35:846-51.

[75] Mauri A, Perrini M, Mateos JM, Maake C, Ochsenbein-Koelble N, Zimmermann R, et al. Second harmonic generation microscopy of fetal membranes under deformation: normal and altered morphology. Placenta 2013;34:1020-6.

[76] Creasy RK. Management of labor and delivery. New York: Wiley-Blackwell 1996.

[77] Friedman EA. Labor: Clinical evaluation and management: Appleton-Century-Crofts New York; 1978.

[78] Bakker PC, Van Rijswijk S, van Geijn HP. Uterine activity monitoring during labor. J Perinat Med 2007;35:468-77.

[79] Lucovnik M, Kuon RJ, Chambliss LR, Maner WL, Shi SQ, Shi L, et al. Use of uterine electromyography to diagnose term and preterm labor. Acta Obstet Gynecol Scand 2011;90:150-7.

[80] Bastos LF, Lobo MF, van Meurs WL, Ayres-de-Campos D. An intrauterine pressure generator for educational simulation of labour and delivery. Med Eng Phys 2010;32:740-5.

[81] Joyce EM, Moore JJ, Sacks MS. Biomechanics of the fetal membrane prior to mechanical failure: review and implications. Eur J Obstet Gynecol Reprod Biol 2009;144 Suppl 1:S121-7.

[82] Schober EA, Kusy RP. Ionic Control of the Rupture of Fetal Membranes. J Mater Sci-Mater M 1995;6:569-76.

[83] Miller CE, Lavery JP, Donnelly TA. Determination of Elastic Parameters for Human Fetal Membranes. J Rheol 1979;23:57-78.

[84] Schober EA, Kusy RP, Whitley JQ, Savitz DA. Effect of Thickness on the Fracture Characteristics of Fetal Membranes. J Mater Sci-Mater M 1994;5:130-7.

[85] Hicks JB. On the contractions of the uterus throughout pregnancy: their physiological effects and their value in the diagnosis of pregnancy. Trans Obstet Soc London 1871:216-31.

[86] MATLAB. The Mathworks, Matlab Documentation, Version 7.10.0 (R2010a) The Mathworks Inc 2010.

[87] Canny J. A computational approach to edge detection. IEEE Trans Pattern Anal Mach Intell 1986;8:679–98

[88] Rubin MB, Bodner SR. A three-dimensional nonlinear model for dissipative response of soft tissue. Int J Solids Struct 2002;39:5081-99.

[89] Ogden RW. Large Deformation Isotropic Elasticity - Correlation of Theory and Experiment for Incompressible Rubberlike Solids. Proc R Soc Lon Ser-A 1972;326:565-&.

[90] Rivlin RS, Saunders DW. Large Elastic Deformations of Isotropic Materials .7. Experiments on the Deformation of Rubber. Philos Tr R Soc S-A 1951;243:251-88.

[91] Sidney S, Castellan NJ. Nonparametric statistics for the behavioral sciences. London: McGraw-Hill; 1988.

[92] Kapuscinski J. Dapi - a DNA-Specific Fluorescent-Probe. Biotech Histochem 1995;70:220-33.

[93] Cox G, Sheppard CJR. Practical limits of resolution in confocal and non-linear microscopy. Microsc Res Tech 2004;63:18-22.

[94] Gonzalez RC, Woods RE, Eddins SL. Digital image processing using MATLAB. Gatesmark Publishing 2009.

[95] Rubbens MP, Driessen-Mol A, Boerboom RA, Koppert MMJ, van Assen HC, Romeny BMT, et al. Quantification of the Temporal Evolution of Collagen Orientation in Mechanically Conditioned Engineered Cardiovascular Tissues. Ann Biomed Eng 2009;37:1263-72.

[96] Haller C. Evaluation of human fetal membrane sealing. Zurich: University of Zurich; 2012.

[97] Perrini M, Mauri A, Ehret AE, Ochsenbein-Koelble N, Zimmermann R, Ehrbar M, et al. Mechanical and microstructural investigation of the cyclic behavior of human amnion. Submitted to the Journal of Biomechanical Engineering.

[98] Zink D, Sadoni N, Stelzer E. Visualizing chromatin and chromosomes in living cells. Methods 2003;29:42-50.

[99] Emery JL, Omens JH, McCulloch AD. Strain softening in rat left ventricular myocardium. J Biomech Eng 1997;119:6-12.

[100] Zanetti EM, Perrini M, Bignardi C, Audenino AL. Bladder tissue passive response to monotonic and cyclic loading. Biorheology 2012;49:49-63.

[101] Lake SP, Barocas VH. Mechanical and structural contribution of non-fibrillar matrix in uniaxial tension: a collagen-agarose co-gel model. Ann Biomed Eng 2011;39:1891-903.

[102] Brown AE, Litvinov RI, Discher DE, Purohit PK, Weisel JW. Multiscale mechanics of fibrin polymer: gel stretching with protein unfolding and loss of water. Science 2009;325:741-4.

[103] Thorpe CT, Riley GP, Birch HL, Clegg PD, Screen HR. Effect of fatigue loading on structure and functional behaviour of fascicles from energy-storing tendons. Acta Biomater 2014;10:3217-24.

[104] Brubaker CE, Kissler H, Wang LJ, Kaufman DB, Messersmith PB. Biological performance of mussel-inspired adhesive in extrahepatic islet transplantation. Biomaterials 2010;31:420-7.

[105] Lee H, Scherer NF, Messersmith PB. Single-molecule mechanics of mussel adhesion. Proc Natl Acad Sci U S A 2006;103:12999-3003.

[106] Bilic G, Brubaker C, Messersmith PB, Mallik AS, Quinn TM, Haller C, et al. Injectable candidate sealants for fetal membrane repair: bonding and toxicity in vitro. Am J Obstet Gynecol 2010;202:85 e1-9.

[107] Haller CM, Buerzle W, Brubaker CE, Messersmith PB, Mazza E, Ochsenbein-Koelble N, et al. Mussel-mimetic tissue adhesive for fetal membrane repair: a standardized ex vivo evaluation using elastomeric membranes. Prenat Diagn 2011;31:654-60.

[108] Barrett DG, Bushnell GG, Messersmith PB. Mechanically robust, negative-swelling, mussel-inspired tissue adhesives. Adv Healthc Mater 2013;2:745-55.

[109] Alviano F, Fossati V, Marchionni C, Arpinati M, Bonsi L, Franchina M, et al. Term Amniotic membrane is a high throughput source for multipotent Mesenchymal Stem Cells with the ability to differentiate into endothelial cells in vitro. BMC Dev Biol 2007;7:11.

[110] Quintero R, Carreno C, Yelian F, Evans M. Repair kinetics of amnion cells after microsurgical injury. Fetal Diagn Ther 1996;11:348-56.

[111] Ehrbar M, Rizzi SC, Hlushchuk R, Djonov V, Zisch AH, Hubbell JA, et al. Enzymatic formation of modular cell-instructive fibrin analogs for tissue engineering. Biomaterials 2007;28:3856-66.

[112] Ehrbar M, Rizzi SC, Schoenmakers RG, Miguel BS, Hubbell JA, Weber FE, et al. Biomolecular hydrogels formed and degraded via site-specific enzymatic reactions. Biomacromolecules 2007;8:3000-7.

[113] Kivelio A, Ochsenbein-Koelble N, Zimmermann R, Ehrbar M. Engineered cell instructive matrices for fetal membrane healing. Acta Biomater 2015;15:1-10.

[114] Ehrbar M, Sala A, Lienemann P, Ranga A, Mosiewicz K, Bittermann A, et al. Elucidating the role of matrix stiffness in 3D cell migration and remodeling. Biophys J 2011;100:284-93.

[115] Bilic G, Zeisberger SM, Mallik AS, Zimmermann R, Zisch AH. Comparative characterization of cultured human term amnion epithelial and mesenchymal stromal cells for application in cell therapy. Cell Transplant 2008;17:955-68.

[116] Gilbert JA, Weinhold PS, Banes AJ, Link GW, Jones GL. Strain profiles for circular cell culture plates containing flexible surfaces employed to mechanically deform cells in vitro. J Biomech 1994;27:1169-77.

[117] Moraes C, Likhitpanichkul M, Lam CJ, Beca BM, Sun Y, Simmons CA. Microdevice array-based identification of distinct mechanobiological response profiles in layer-specific valve interstitial cells. Integr Biol (Camb) 2013;5:673-80.

[118] Williams JL, Chen JH, Belloli DM. Strain fields on cell stressing devices employing clamped circular elastic diaphragms as substrates. J Biomech Eng 1992;114:377-84.

[119] Winston FK, Macarak EJ, Gorfien SF, Thibault LE. A system to reproduce and quantify the biomechanical environment of the cell. J Appl Physiol (1985) 1989;67:397-405.

[120] Bell BJ, Nauman E, Voytik-Harbin SL. Multiscale strain analysis of tissue equivalents using a custom-designed biaxial testing device. Biophys J 2012;102:1303-12.

[121] Mi S, David AL, Chowdhury B, Jones RR, Hamley IW, Squires AM, et al. Tissue engineering a fetal membrane. Tissue Eng Part A 2011;18:373-81.

[122] Kumar D, Moore RM, Nash A, Springel E, Mercer BM, Philipson E, et al. Decidual GM-CSF is a critical common intermediate necessary for thrombin and TNF induced in-vitro fetal membrane weakening. Placenta 2014.

[123] Mauri A, Ehret AE, Perrini M, Maake C, Ochsenbein-Koelble N, Ehrbar M, et al. Deformation mechanisms of human amnion: quantitative studies based on second harmonic generation microscopy. J Biomech;In Press.

[124] Paskaleva A. Biomechanics of cervical function in pregnancy: case of cervical insufficiency: Massachusetts Institute of Technology; 2007.

[125] Fuard D, Tzvetkova-Chevolleau T, Decossas S, Tracqui P, Schiavone P. Optimization of poly-di-methyl-siloxane (PDMS) substrates for studying cellular adhesion and motility. Microelectron Eng 2008;85:1289-93.

[126] Ai H, Mills DK, Jonathan AS, Jones SA. Gelatin-glutaraldehyde cross-linking on silicone rubber to increase endothelial cell adhesion and growth. In Vitro Cell Dev Biol Anim 2002;38:487-92.

[127] Stalder AF, Russe MF, Frydrychowicz A, Bock J, Hennig J, Markl M. Quantitative 2D and 3D phase contrast MRI: optimized analysis of blood flow and vessel wall parameters. Magn Reson Med 2008;60:1218-31.

[128] Bartalena G, Loosli Y, Zambelli T, Snedeker J. Biomaterial surface modifications can dominate cell–substrate mechanics: the impact of PDMS plasma treatment on a quantitative assay of cell stiffness. Soft Matter 2012;8:673-81.

[129] Dobrin PB. Mechanical properties of arterises. Physiol Rev 1978;58:397-460.

[130] Bieler FH, Ott CE, Thompson MS, Seidel R, Ahrens S, Epari DR, et al. Biaxial cell stimulation: A mechanical validation. J Biomech 2009;42:1692-6.

[131] Franco D, Milde F, Klingauf M, Orsenigo F, Dejana E, Poulikakos D, et al. Accelerated endothelial wound healing on microstructured substrates under flow. Biomaterials 2013;34:1488-97.

## List of publications

Perrini M, Mauri A, Ehret AE, Ochsenbein-Koelble N, Zimmermann R, Ehrbar M, et al. Mechanical and microstructural investigation of the cyclic behavior of human amnion. Submitted to the Journal of Biomechanical Engineering.

Mauri A, Ehret AE, Perrini M, Maake C, Ochsenbein-Koelble N, Ehrbar M, et al. Deformation mechanisms of human amnion: quantitative studies based on second harmonic generation microscopy. Journal of Biomechanics; In Press.

Mauri A, Perrini M, Ehret AE, De Focatiis DSA, Mazza E. Time-dependent mechanical behavior of human amnion: macroscopic and microscopic characterization. Acta Biomaterialia 2015;11:314-23.

Perrini M, Mauri A, Mateos JM, Maake C, Ochsenbein-Koelble N, Zimmermann R, et al. Second harmonic generation microscopy of fetal membranes under deformation: normal and altered morphology. Placenta 2013;34:1020-6.

Perrini M, Burzle W, Haller C, Ochsenbein-Kolble N, Deprest J, Zimmermann R, et al. Contractions, a risk for premature rupture of fetal membranes: a new protocol with cyclic biaxial tension. Medical Engineering & Physics 2013;35:846-51.

Kivelio A, Dekoninck P, Perrini M, Brubaker CE, Messersmith PB, Mazza E, et al. Mussel mimetic tissue adhesive for fetal membrane repair: initial in vivo investigation in rabbits. European journal of obstetrics, gynecology, and reproductive biology 2013;171:240-5.

Haller CM, Buerzle W, Kivelio A, Perrini M, Brubaker CE, Gubeli RJ, et al. Mussel-mimetic tissue adhesive for fetal membrane repair: an ex vivo evaluation. Acta Biomaterialia 2012;8:4365-70.